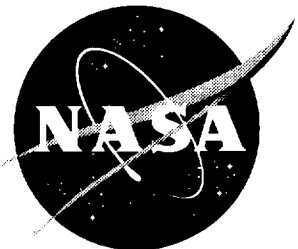


NASA/TM-97-206255



# Internal Performance of a Fixed-Shroud Nonaxisymmetric Nozzle Equipped with an Aft-Hood Exhaust Deflector

*Scott C. Asbury*  
*Langley Research Center, Hampton, Virginia*

National Aeronautics and  
Space Administration

Langley Research Center  
Hampton, Virginia 23681-2199

---

November 1997

---

**Available from the following:**

**NASA Center for AeroSpace Information (CASI)**  
800 Elkridge Landing Road  
Linthicum Heights, MD 21090-2934  
(301) 621-0390

**National Technical Information Service (NTIS)**  
5285 Port Royal Road  
Springfield, VA 22161-2171  
(703) 487-4650

## Abstract

An investigation was conducted in the model preparation area of the NASA Langley 16-Foot Transonic Tunnel to determine the internal performance of a fixed-shroud nonaxisymmetric nozzle equipped with an aft-hood exhaust deflector. Nineteen nozzle configurations were tested with primary emphasis placed on determining performance with the aft-hood deflector deployed. Model geometric parameters investigated included nozzle power setting, aft-hood deflector angle, throat area control with the aft-hood deflector deployed, and yaw vector angle. All tests were conducted with no external flow, and nozzle pressure ratio was varied during jet simulation from 1.5 to approximately 12.3. Results indicate that cruise nozzle configurations produced peak thrust ratio performance in the range consistent with previous investigations of nonaxisymmetric convergent-divergent nozzles. Deploying the aft-hood deflector produced resultant pitch vector angles that were always less than the geometric aft-hood deflector angle when the nozzle throat was positioned upstream of the deflector exit. Significant losses in resultant thrust ratio occurred when the aft-hood deflector was deployed with an upstream throat location; these losses were attributed to the inefficient process of turning supersonic flow. At each aft-hood deflector angle, repositioning the throat to the deflector exit improved pitch vectoring performance and, in some cases, substantially improved resultant thrust ratio performance. Transferring the throat to the deflector exit allowed the flow to be turned upstream of the throat at subsonic Mach numbers, thereby eliminating losses associated with turning supersonic flow. Internal throat panel deflections were largely unsuccessful in generating a significant amount of yaw vectoring. Achieving significant yaw vector angles internally in a nonaxisymmetric exhaust nozzle is difficult to accomplish, since the sidewalls tend to become pressurized and cancel any yaw vectoring produced.

## Introduction

The design of high-performance exhaust nozzles has advanced rapidly in recent years from traditional axisymmetric configurations with area ratio control to fully articulating nonaxisymmetric configurations with some or all of the following capabilities: independent throat and exit area control, multiaxis thrust vectoring, thrust reversing, and direct lift for short-takeoff and vertical-landing (STOVL) operation (refs. 1 to 4). In addition, nonaxisymmetric nozzle designs lend themselves well to reduced levels of aircraft drag and observability. Minimum boattail closure angles reduce afterbody drag, while shaping and cooling options allow reduced levels of aircraft observability (ref. 5).

Interest in multi-function exhaust nozzles has grown as designers have recognized their potential for enhancing aircraft maneuverability, survivability, and operational flexibility. Thrust vectoring capability provides large control moments that are invariant with angle of attack; thrust vectoring can offer significant flight envelope expansion, reduce the required size of conventional tail surfaces, or eliminate the need for tail surfaces altogether (refs. 5 and 6). In-flight thrust reversing can aid in air-combat maneuvering, shorten landing distances by up to 80%, and eliminate the need

for speed brakes (ref. 6). Short-takeoff and vertical-landing (STOVL) capability eliminates the need for large vulnerable airfields, thus enhancing operational flexibility by allowing aircraft to operate from austere sites and relocate closer to a changing line of battle.

The potential of multi-function exhaust nozzle designs has been proven in recent flight test programs. The F-18 High-Alpha Research Vehicle (ref. 7) and the X-31 Enhanced Fighter Maneuverability Demonstrator (ref. 8) have both demonstrated significant flight envelope expansion with the use of multiaxis thrust vectoring nozzles, including controlled flight at up to 70° angle of attack. The F-15 STOL/Maneuver Technology Demonstrator has landed in 1,500 feet and shown further benefits of pitch vectoring and thrust reversing nozzles (ref. 9). Furthermore, the YF-22 Advanced Tactical Fighter has demonstrated an exceptional amount of agility through the use of its pitch vectoring nonaxisymmetric exhaust nozzles (ref. 10).

In a continuing effort to develop high-performance, multi-function exhaust nozzles, the Pratt&Whitney, United Technologies Corporation designed a fixed-shroud nonaxisymmetric nozzle equipped with an aft-hood exhaust deflector. The fixed-shroud design simplifies propulsion/airframe integration issues,

allowing constant boattail closure angles to be maintained during variations in nozzle geometry. The nozzle design incorporates a fixed exit area, an aft-hood exhaust deflector for vertical and transitional flight (STOVL operation), and moveable throat panels for throat area control and in-flight yaw vectoring.

To evaluate the internal performance of this multi-function exhaust nozzle concept, a sub-scale model was tested at static conditions in the model preparation area of the NASA Langley 16-Foot Transonic Tunnel. Model geometric parameters investigated included nozzle power setting, aft-hood deflector angle, throat area control with the aft-hood deflector deployed, and throat panel deflection. High-pressure air was used to simulate jet-exhaust flow at nozzle pressure ratios from 1.5 to approximately 12.3.

## Acknowledgments

The research presented in this report is the result of a cooperative effort between the Pratt&Whitney, United Technologies Corporation and the National Aeronautics and Space Administration. Funding for model design and fabrication was provided by Pratt&Whitney's Government Engine Business. Model hardware was designed and fabricated by FluiDyne Engineering Corporation in Minneapolis, Minnesota. The investigation was conducted by the staffs of the Configuration Aerodynamics and Research Facilities Branches at NASA's Langley Research Center in Hampton, Virginia.

## Symbols

All forces and moments (with the exception of resultant thrust) are referenced to the model centerline (body axis). The model (balance) moment reference center was located at station 29.39. A discussion of the data reduction procedure, the definitions of the force and moment terms, and propulsion relationships used herein can be found in reference 11.

$A_e$	nozzle exit area, in <sup>2</sup>
$A_t$	nozzle throat area, in <sup>2</sup>
$F$	measured thrust along body axis, positive in forward direction, lbf
$F_i$	ideal isentropic gross thrust,
	$w_p \sqrt{\frac{R_j T_{t,j}}{g^2} \frac{2\gamma}{\gamma-1} \left[ 1 - \left( \frac{1}{NPR} \right)^{(\gamma-1)/\gamma} \right]}, \text{lbf}$
$F_N$	measured normal force, positive upward, lbf

$F_r$	resultant thrust, $\sqrt{F^2 + F_N^2 + F_S^2}, \text{lbf}$
$F_s$	measured side force, positive to right when looking upstream, lbf
$g$	acceleration due to gravity, 32.174 ft/sec <sup>2</sup>
NPR	nozzle pressure ratio, $p_i/p_a$
NPR <sub>d</sub>	design nozzle pressure ratio, NPR for fully expanded flow at the nozzle exit
$p$	local static pressure, psi
$p_a$	ambient pressure, psi
$p_{t,j}$	average jet total pressure, psi
$R_j$	gas constant (for $\gamma=1.3997$ ), 1716 ft <sup>2</sup> /sec <sup>2</sup> ·°R
$T_{t,j}$	jet total temperature, °R
$w_p$	measured weight-flow rate, lbf/sec
$x$	linear dimension measured along the model centerline from the nozzle connect station (Sta. 52.00), positive downstream, used to define the location of static pressure taps, in.
$y$	lateral distance measured from the model centerline, positive to the right when looking upstream, used to define the location of static pressure taps, in.
$z$	vertical distance measured from the model centerline, positive upwards, used to define the location of static pressure taps, in.
$\gamma$	ratio of specific heats, 1.3997 for air
$\delta_{hood}$	geometric deployment angle of aft-hood exhaust deflector, deg
$\delta_p$	resultant pitch thrust vector angle, measured from the nozzle centerline, positive deflection downward, $\tan^{-1}(F_N/F)$ , deg
$\delta_{v,p}$	geometric pitch vector angle, deg
$\delta_y$	resultant yaw thrust vector angle, measured from the nozzle centerline, positive deflection to left when looking upstream, $\tan^{-1}(F_S/F)$ , deg
<b>Abbreviations:</b>	
A/B	afterburning
C-D	convergent-divergent
PR	pressure ratio $p/p_{t,j}$ in tables 3 through 21, subscripted to indicate orifice number
R	radius, in.
Ref.	reference dimension measured from the model centerline, in.
Sta.	model station, in.

SERN single expansion ramp nozzle

STOVL short takeoff and vertical landing

## Description of Test Facility

This investigation was conducted in the model preparation area of the NASA Langley 16-Foot Transonic Tunnel. Although this facility is normally used for setup and calibration of wind-tunnel models, it can also be used for nozzle internal performance testing at static (wind-off) conditions. Testing is conducted in a 10x29 foot chamber where the jet from a single-engine propulsion simulation system exhausts to the atmosphere through an acoustically treated exhaust passage. A control room is adjacent to the test room, and offers access through a sound-proof door and observation window. The model preparation area shares an air control system with the 16-Foot Transonic Tunnel that includes valving, filters, and a heat exchanger to provide a supply of clean, dry air to the propulsion simulation system at a constant stagnation temperature of about 540°R at the nozzle. A complete description of the test facility is provided in reference 12.

## Single-Engine Propulsion Simulation System

The single-engine propulsion simulation system used in this investigation is shown in detail in figure 1. An external high-pressure air source supplied the propulsion simulation system with a continuous flow of clean, dry air at a constant stagnation temperature of about 540°R at the nozzle. This high-pressure air was varied during jet simulation up to about 180 psi total pressure in the nozzle. The high-pressure air was delivered by six air lines through a support strut into an annular high-pressure plenum. The air was then discharged radially into an annular low-pressure plenum through eight equally spaced, multiholed sonic nozzles. This flow transfer system was designed to minimize forces imposed by the transfer of axial momentum as the air passed from the non-metric high-pressure plenum to the metric (attached to the force balance) low-pressure plenum. Two flexible metal bellows functioned as seals between the non-metric and metric portions of the model and compensated for axial forces caused by pressurization. The air then passed through a multi-holed choke plate (primarily used for flow straightening), an instrumentation section, a facility to model adapter, a circular-to-rectangular transition section, and then through the nozzle, which exhausted to atmospheric back pressure. All nozzle configurations tested were attached to the downstream end of the transition section at station 52.00.

## Nozzle Concept and Models

### Nozzle Concept

The fixed-shroud nonaxisymmetric nozzle concept that was the focus of this investigation is presented in figure 2. This concept was designed to add throat area control, direct lift capability, and in-flight yaw vectoring to a fixed-shroud cruise nozzle. The fixed-shroud design greatly simplifies propulsion/airframe integration issues by allowing constant boattail closure angles to be maintained during variations in nozzle internal geometry.

Basic nozzle components consist of upper and lower convergent-divergent flaps, with the upper divergent flap slightly longer than the lower divergent flap. (Note that unequal divergent flap lengths are characteristics of single expansion ramp nozzles or SERN). Cutback sidewalls contain the exhaust flow in the lateral direction. Moveable throat panels are located within each convergent and divergent flap to provide throat area control and in-flight yaw vectoring. The throat panels employ multiple hinges to allow freedom of movement as shown in figure 2. Symmetric movement (left to right) of the throat panels provides throat area control, while asymmetric movement (left to right) provides yaw vectoring.

An aft-hood deflector is stowed during cruise within the volume created between the upper divergent flap and external boattail; this deflector is deployed to provide direct lift capability during vertical or transitional flight. The cruise nozzle can be opened for large hood deflections, thus transferring the nozzle throat to the deflector exit. This may increase performance by allowing the flow to turn the required deflection angle at lower Mach numbers, reducing losses associated with turning high Mach number flow. Downstream throat area control is available through translation of the lower divergent flap, as required, for large deflector angles to compensate for the change in flow conditions caused by deflector deployment or changes in engine cycle during vertical flight. The aft-hood deflector design was chosen based on favorable results obtained from prior investigations of an augmented deflector exhaust nozzle concept (ref. 13).

### Nozzle Models

A model of this nozzle concept was built and is shown in the photographs of figure 3 and in the sketches of figures 4 through 15. As shown in figure 4, the basic model consisted of a facility adapter (fig. 5), transition section (fig. 6), and the cruise

nozzle (figs. 7 and 8). The cruise nozzle was composed of upper (fig. 9) and lower (fig. 10) flaps and two sidewalls (fig. 11). The upper and lower flaps accepted a pair of interchangeable throat inserts (fig. 12) to simulate throat panel movement for throat area control and yaw vectoring. An aft-hood deflector, composed of a hood (fig. 13) and two hood sidewalls (fig. 14), attached to the cruise nozzle to provide geometric pitch vector angles  $\delta_{v,p}$  of either 45°, 90°, or 120°. Interchangeable throat area control blocks (fig. 15) were used to transfer the minimum (throat) area from inside the nozzle to a position at (control block #1) or near (control block #2) the deflector exit. Specifications for each nozzle configuration tested during this investigation are presented in table 1.

Six pairs of interchangeable throat inserts were tested during this investigation (fig. 12). The baseline dry, intermediate, and maximum afterburning power throat inserts simulated the effect of varying power setting. The baseline dry power throat inserts (fig. 12(a)) had a blunt contour immediately upstream of the throat location. The modified dry power throat inserts (fig. 12(b)) had a faired contour at the throat. The actual throat area for the modified dry power configuration ( $A_t = 3.913 \text{ in}^2$ ) was smaller than that of the baseline dry power configuration ( $A_t = 4.426 \text{ in}^2$ ). Pre-test performance estimates were used to oversize the throat area for the baseline dry power configuration since the blunt contour was expected to reduce nozzle discharge coefficient. Two pairs of yaw vectored throat inserts, designated the 10° yaw and maximum yaw vectoring configurations, were also tested.

## Instrumentation

All forces and moments generated by the nozzle were measured by a six-component strain-gauge balance located on the centerline of the propulsion simulation system. See figure 1(b). The weight-flow rate of high-pressure air supplied to the model was calculated from static-pressure and static-temperature measurements taken in a calibrated multiple-critical venturi system located upstream of the propulsion simulation system. The multiple-critical venturi is the standard high-pressure airflow measurement system used in the 16-Foot Transonic Tunnel and is rated to be 99.9% accurate in weight-flow measurements. Jet total pressure was determined at a fixed station in the instrumentation section by averaging measurements taken with a nine probe total-pressure rake (fig. 1(b)). Jet total temperature was determined at the same station in the instrumentation section by averaging measurements taken with two iron-constantan thermocouples. Internal (jet-flow) static pressure measurements were

made for each nozzle configuration using electronically scanned pressure modules with an accuracy of  $\pm 0.015$  psi. Model static pressure orifice locations are shown in figures 9 to 15.

## Data Reduction

Each data point is the average steady-state value computed from 50 frames of data taken at a rate of 10 frames per second. All data were taken in ascending order of  $p_{t,j}$ . With the exception of resultant thrust  $F_r$ , all data in this report are referenced to the model centerline (body axis). Four basic nozzle internal performance parameters are used in the presentation of results; they are internal thrust ratio  $F/F_i$ , resultant thrust ratio  $F/F_i$ , and two resultant thrust vector angles— $\delta_p$  for pitch and  $\delta_y$  for yaw. A detailed description of the procedures used for data reduction and analysis in this investigation can be found in reference 11.

The internal thrust ratio  $F/F_i$  is the ratio of the measured nozzle thrust along the body axis to the computed ideal nozzle thrust. Ideal thrust  $F_i$  computations are based on weight flow  $w_p$ , jet total pressure  $p_{t,j}$ , and jet total temperature  $T_{t,j}$  measurements. (See the section "Symbols".) The balance axial-force measurement, from which the measured thrust  $F$  is subsequently obtained, is initially corrected for model weight tares and isolated-balance component interactions. Although the bellows arrangement in the propulsion simulation system was designed to minimize forces on the balance caused by pressurization, small bellows tares on the six-component balance still existed. These tares resulted from a small pressure difference between the ends of the bellows when air system internal velocities were high and from small differences in the spring constant of the forward and aft bellows when the bellows were pressurized. These bellows tares were determined by testing Stratford choke calibration nozzles with known performance over a range of expected internal pressure and external forces and moments. The resulting tares were then applied to the six-component balance data to obtain corrected balance measurements. Balance axial force obtained in this manner is a direct measurement of the nozzle thrust along the body axis  $F$ . The procedure for computing the bellows tares is discussed in detail in reference 11.

Resultant thrust ratio  $F/F_i$  is the resultant thrust divided by the ideal isentropic thrust. Resultant thrust is obtained from the measured axial, normal, and side components of the jet resultant force. From the definitions of  $F$  and  $F_r$ , it is obvious that the thrust along the body axis  $F$  includes a reduction in thrust that results from turning the exhaust vector away from the axial direction, whereas the resultant thrust  $F_r$ , does

not. Losses included in both terms are the result of friction and pressure drags associated with the vectoring hardware and any changes in nozzle internal geometry.

The resultant thrust vector angles  $\delta_p$  and  $\delta_y$  are effective angles at which the thrust vectoring mechanism turns the exhaust flow from the axial direction. As indicated in the section "Symbols," determination of these angles requires the measurement of axial, normal, and side forces on the model.

## Presentation of Results

The results of this investigation are presented in both tabular and plotted forms. Table 1 is a description of the model configurations tested. Basic nozzle internal performance data for each configuration tested are presented in table 2. Nozzle internal static pressure ratios  $p/p_{t,j}$  are given in tables 3 to 21 for each model configuration tested. During discussion of the results, comparisons of nozzle internal performance are made in terms of percentage change from isentropic conditions. Graphical presentation of nozzle internal performance characteristics are presented as follows:

Figure	
Cruise nozzle configurations . . . . .	16
Pitch vectoring configurations showing the effect of—	
Aft-hood deflector angle . . . . .	17
Power setting . . . . .	18
Throat area control block . . . . .	19
Yaw vectoring configurations . . . . .	20

## Results and Discussion

Nozzle internal performance characteristics that show the effects of power setting, aft-hood deflector angle, throat area control, and yaw vectoring are presented in figures 16 to 20. Internal performance characteristics are presented in terms of internal thrust ratio  $F/F_i$ , resultant thrust ratio  $F/F_r$ , resultant pitch vector angle  $\delta_p$ , and resultant yaw vector angle  $\delta_y$ .

**Effect of power setting.** The effect of power setting on the internal performance characteristics of cruise nozzle configurations is presented in figure 16. The maximum afterburning (A/B) power configuration produced a peak  $F/F_i$  of approximately 0.982 at a nozzle pressure ratio (NPR) of about 7.5, which was near the lower end of the 0.980 to 0.992 range consistent with previous investigations of nonaxisymmetric nozzles (refs. 14 to 18). Thrust losses below peak performance were the result of exhaust flow overexpansion effects. Thrust ratios were lower for the baseline dry and modified dry power configurations because, at the NPR's shown, the maximum A/B power

configuration had lower overexpansion losses due to the lower expansion ratio of this configuration. Unfortunately, because of model balance limitations, peak performance was not reached for the dry power configurations. However, based on the available thrust ratio data and on previous studies of nonaxisymmetric nozzles (ref. 14), it is expected that any differences in peak performance would be small (less than 1%). Thrust ratios differ between the dry power configurations primarily because of differences in expansion ratio.

In general, the cruise nozzle configurations had performance trends that were consistent with previous investigations of nonaxisymmetric nozzles (refs. 14 to 18). One trend was the occurrence of a local peak in the thrust performance curves ( $F/F_i$  and  $F/F_r$ ) of the dry power configurations at low NPR's ( $NPR < 2.5$ ). This local peak in thrust performance is often observed in convergent-divergent nozzles at low NPR's and is attributed to shock-induced separation of the exhaust flow from the nozzle divergent flaps (ref. 15). When exhaust flow is separated from the divergent flaps, the nozzle effectively operates at a lower expansion ratio (below the geometric expansion ratio  $A/A_s$ ) and losses due to exhaust flow overexpansion are reduced (from a fully attached condition). As NPR increases, the flow characteristics inside the nozzle change and a point is reached where the exhaust flow fully attaches to the divergent flaps. Once the flow attaches, losses due to exhaust flow overexpansion increase and the nozzle begins operating on a performance curve characteristic of its geometric expansion ratio. As a result, the rapid change in effective expansion ratio that occurs from the separated to attached flow condition results in the local peak in performance measured in this investigation at low NPR's. Furthermore, multiple peaks in thrust performance curves usually only occur for high expansion ratio nozzles, which, because of the large divergence angle, are the most susceptible to separation. For this reason, a local peak in performance at low NPR's is less evident for the maximum A/B power configuration which had a significantly lower expansion ratio than that of the dry power configurations.

At  $NPR > 2.5$ , thrust performance for the cruise configuration increased steadily as overexpansion losses decreased. Because of the SERN geometry, it was expected that the cruise nozzle configurations might exhibit some of the thrust performance trends typical of SERN nozzles at these NPR's, which are often characterized by a tendency to have multiple performance peaks (ref. 16). These peaks are associated with the fact that a SERN design effectively has two expansion processes. The first (internal expansion) occurs as the exhaust flow expands in the region

between the nozzle throat and the nozzle exit formed by the downstream edge of the lower flap. The second (external expansion) occurs as exhaust flow expands between the upper flap and the lower-jet free boundary. This type of behavior is not evident for the nozzles of this investigation, probably because this nozzle design had a relatively short upper flap for a SERN. However, a slight discontinuity can be detected in the thrust performance curves of the cruise nozzle configurations (at  $NPR > 2.5$ ). Had the data been taken more frequently over the NPR range, the characteristic multiple peak SERN performance may have been more evident.

During nonvectoring (cruise) conditions, it would be expected that values of resultant pitch  $\delta_p$  and resultant yaw  $\delta_y$  thrust vector angle would be zero. However, at  $NPR < 2.5$  resultant pitch vector angles of as much as  $-10^\circ$  were measured for the cruise nozzle configurations. The variation in  $\delta_p$  at low  $NPR$ 's is in the same range as the performance peak discussed previously, where exhaust flow separation occurred on the divergent flaps. The separation was obviously asymmetric from the top flap to the bottom flap in order to produce nonzero values of  $\delta_p$ . This behavior has been observed in previous investigations of high-expansion-ratio convergent divergent nozzle designs (ref. 14).

Nonzero values of  $\delta_p$  continued at  $NPR > 2.5$  and resulted from unequal exhaust flow expansion on the upper and lower divergent flaps. This type of behavior is characteristic of SERN configurations (ref. 17). Since the upper flap had an unopposed normal projected area, nonzero values of normal force were generated that varied significantly with changing  $NPR$ . However, the magnitude of the resultant pitch vector angles were relatively small for a SERN. Again, this behavior is associated with the fact that the upper flap was relatively short for a SERN. An axial-force performance penalty resulted from nonzero resultant thrust vector angles, the magnitude of which can be determined by comparing the difference between internal and resultant thrust ratios at a given  $NPR$ .

### Pitch-Vectoring Performance

**Effect of aft-hood deflector angle.** The effect of aft-hood deflector angle on internal performance characteristics with the throat located upstream of the aft-hood deflector exit is presented in figure 17. Resultant pitch vector angles  $\delta_p$  typically increased with  $NPR$ , but were always less than the corresponding geometric aft-hood deflector angle  $\delta_{v,p}$ . At the modified dry power setting, for example,  $\delta_p$  increased with  $NPR$  from  $61^\circ$  to  $72^\circ$  for the  $90^\circ$  aft-hood deflector setting. This turning performance is relatively

poor in comparison to similar vectoring nozzle designs previously investigated (ref. 18). Two possible explanations exist for this behavior. First, the close proximity of the lower flap to the exhaust plume (see fig. 8(b)) may have caused some of the turning to be nullified by aspiration of the external lower flap surface. Although the external geometry of the nozzle configurations investigated do not represent realistic nozzle contours, this result could represent a potential problem regardless of external nozzle geometry. Second, because the geometric throat was positioned upstream of the aft-hood deflector, supersonic flow had to be turned downstream of the throat through a series of oblique shocks. Relying on oblique shocks to turn exhaust flow typically produces resultant vector angles that are less than the geometric vector angle (ref. 19). The alignment and 3-D nature of these oblique shocks most likely resulted in the nonzero values of resultant yaw vector angle  $\delta_y$  which were measured for these configurations.

Previous investigations have indicated that supersonic flow turning through oblique shocks is an inefficient process resulting in flow turning (resultant thrust) losses (refs. 14 and 19). In addition, any aspiration of the external lower flap, mentioned previously, would result in reduced thrust measured along the body axis (reduced  $F/F_i$ ) and also reduced normal force (reduced  $\delta_p$ ), both of which would reduce resultant thrust ratio  $F/F_i$ . Not surprisingly, significant losses in resultant thrust ratio occurred with the throat positioned upstream of the aft-hood deflector exit. Substantial improvements in performance may be possible by transferring the throat from upstream of the aft-hood deflector to the deflector exit. This would allow the flow to be turned by the aft-hood deflector at subsonic Mach numbers, thereby eliminating oblique shocks inside the nozzle and reducing turning losses of the system. The effects of transferring the throat to the deflector exit will be discussed in detail in a subsequent section of this paper.

**Effect of power setting with the aft-hood deflector deployed.** The effect of power setting on internal performance characteristics with the aft-hood deflector deployed and the throat located upstream of the aft-hood deflector exit is presented in figure 18. Superior pitch vectoring and resultant thrust ratio performance occurred at the maximum A/B power setting for each aft-hood deflector angle tested. The lower expansion ratio of the maximum A/B power setting results in a lower supersonic Mach number in the exhaust flow and weaker oblique shocks in the divergent section of the nozzle (as compared to the dry power settings), thus reducing the turning losses of the system. Peak resultant thrust ratios of the maximum

A/B power setting were 0.970, 0.952, and 0.934 at aft-hood deflector angles  $\delta_{\text{hood}}$  of  $45^\circ$ ,  $90^\circ$ , and  $120^\circ$ , respectively. This represents a maximum loss in peak performance of 4.8% for the maximum A/B power setting (with a peak resultant thrust ratio of 0.982 in the cruise configuration) as a result of deploying the aft-hood deflector. Resultant yaw vector angles remained zero at the maximum A/B power setting, supporting the hypothesis that strong oblique shocks at lower power settings were responsible for turning losses and undesirable yaw vectoring.

**Effect of throat area control block.** The effect of installing a throat area control block with the aft-hood deflector deployed at maximum A/B power is presented in figure 19. At each aft-hood deflector angle, installing the throat area control block improved pitch vectoring  $\delta_p$  performance and, in most cases, substantially improved resultant thrust ratio  $F/F_i$  performance. At each aft-hood deflector angle, the effect of installing throat area control block #1 was to relocate the throat from an upstream position ( $A/A_t \approx 1.4$ ) to the deflector exit ( $A/A_t = 1.0$ ). This allowed flow to be turned subsonically inside the nozzle, eliminating losses previously associated with supersonic flow turning. Transferring the throat to the deflector exit reduced flow Mach number inside the nozzle and likely set the minimum area closer to the desired vector angle, which improved pitch vectoring performance. This is evident in figure 19(c), where pitch vectoring performance at  $\delta_{\text{hood}} = 120^\circ$  improved from  $103^\circ$  to  $118^\circ$  at  $\text{NPR} \approx 3.0$  when throat-area control block #1 was installed.

The effect of installing throat-area control block #2 was to relocate the throat from upstream of the aft-hood deflector ( $A/A_t \approx 1.4$ ) to a location just upstream of the deflector exit ( $A/A_t \approx 1.1$ ). Since the nozzle expansion ratio  $A/A_t$  remained above 1.0 with throat-area control block #2 installed, some flow expansion still occurred inside the nozzle. This allowed higher Mach numbers and possibly weak oblique shocks inside the nozzle in comparison to throat-area control block #1, but still reduced the Mach numbers inside the nozzle below those inside configurations with no throat-area control block installed. Not surprisingly, the resultant thrust ratio and turning performance for the configurations with throat-area control block #2 installed fell between that with no throat-area control block installed and that with throat-area control block #1 installed.

### Yaw-Vectoring Performance

The effect of yaw vectored throat inserts on nozzle internal performance characteristics with the aft-hood deflector removed is presented in figure 20. Yaw-vectoring performance is measured by the ability

to generate resultant yaw vector angles  $\delta_y$  with minimum loss in resultant thrust ratio  $F/F_i$ . In the case of the yaw vectored configurations tested in this investigation, positive  $\delta_y$  denotes the intended direction of yaw vectoring. As shown in figure 20, a positive  $\delta_y$  of  $10.7^\circ$  was generated at low NPR's for the maximum yaw vectored configuration, but this value rapidly decreased to near zero by  $\text{NPR} = 5.0$ . Above  $\text{NPR} = 5.0$ ,  $\delta_y$  for the maximum yaw vectored configuration was negative, or opposite the intended direction. Achieving significant resultant yaw vector angles internally in an nonaxisymmetric exhaust nozzle with fixed sidewalls is difficult to accomplish, since the sidewalls tend to become pressurized and cancel any yaw vectoring produced. Previous investigations indicate that yaw vectoring performance would likely be improved either by increasing sidewall cutback or by outboard deflection of the sidewall (refs. 14 and 20).

### Conclusions

An investigation was conducted in the model preparation area of the Langley 16-Foot Transonic Tunnel to determine the internal performance of a fixed-shroud nonaxisymmetric nozzle equipped with an aft-hood exhaust deflector. Nineteen nozzle configurations were tested with primary emphasis placed on determining nozzle performance with the aft-hood deflector deployed. Model geometric parameters investigated included nozzle power setting, aft-hood deflector angle, throat area control with the aft-hood deflector deployed, and yaw vector angle. All tests were conducted with no external flow, and nozzle pressure ratio was varied from 1.5 to approximately 12.3. The results of this investigation indicate the following conclusions:

1. Cruise nozzle configurations produced peak thrust ratio performance near the lower end of the range consistent with previous investigations of nonaxisymmetric nozzle designs.
2. Deploying the aft-hood deflector produced resultant pitch vector angles that were less than the geometric aft-hood deflector angle when the nozzle throat was positioned upstream of the aft-hood deflector. Significant losses in resultant thrust ratio occurred with aft-hood deflector deployment that were attributed to aspiration of the lower flap external surface and the inefficient supersonic flow turning.
3. At each aft-hood deflector angle, installing the throat area control block to reposition the nozzle throat near the deflector exit improved pitch vectoring performance and, in some cases, substantially improved resultant thrust ratio performance. Transferring the throat to a location near the deflector exit

allowed the flow to be turned at lower Mach numbers, thereby reducing turning losses of the system.

4. Using internal throat panel movements to generate yaw vectoring was largely unsuccessful. Achieving significant yaw vector angles internally in a nonaxisymmetric exhaust nozzle is difficult to accomplish, since the sidewalls tend to become pressurized and cancel any yaw vectoring produced.

NASA Langley Research Center  
Hampton, VA 23681-0001  
November 25, 1997

## References

1. Capone, Francis J.: The Nonaxisymmetric Nozzle-It is for Real. AIAA-79-1810, August 1979.
2. Mello, J.F.; and Kotansky, D.R.: Aero/Propulsion Technology for STOL and Maneuver. AIAA-85-4013, October 1985.
3. Mace, J.; Smereczniak, P.; Krekeler, G; et. al.: Advanced Thrust Vectoring Nozzles for Supercruise Fighter Aircraft. AIAA-89-2816, July 1989.
4. Herrick, Paul W.: Air-to-Ground Attack Fighter Improvements Through Multi-Function Nozzles. SAE Paper No. 90-1002, April, 1990.
5. Nelson, B.D.; and Nicolai, L.M.: Application of Multi-Function Nozzles to Advanced Fighters. AIAA-81-2618, December 1981.
6. Herrick, Paul W.: Air Combat Payoffs of Vectoring/Reversing Exhaust Nozzles. AIAA-88-3239, July 1988.
7. Regenie, Victoria; Gatlin, Donald; Kempel, Robert; and Matheny, Neil: *The F-18 High Alpha Research Vehicle: A High-Angle-of-Attack Testbed Aircraft*. NASA TM-104253, 1992.
8. Knox, Fred D.: X-31 Flight Test Update. AIAA-92-1035, February 1992.
9. Bursey, R.; and Dickinson, R.: Flight Test Results of the F-15 S/MTD Thrust Vectoring/Thrust Reversing Exhaust Nozzle. AIAA-90-1906, July 1990.
10. Sweetman, Bill: Lockheed F-22: Stealth with Agility, *World Airpower Journal*, Vol. 6, Summer 1991,
11. Mercer, Charles E.; Berrier, Bobby L.; Capone, Francis J.; and Grayston, Alan M.: *Data Reduction Formulas for the 16-Foot Transonic Tunnel-NASA Langley Research Center. Revision 2*. NASA TM-107646, 1992.
12. Staff of the Propulsion Aerodynamics Branch: *A User's Guide to the Langley 16-Foot Transonic Tunnel Complex, Revision 1*. NASA TM-102750, 1990. (Supersedes NASA TM-83186, compiled by Kathryn H. Peddrew, 1981.)
13. Lander, J.A.; Nash, D.O.; and Palcza, J. L.: *Augmented Deflector Exhaust Nozzle (ADEN) Design for Future Fighters*. AIAA-75-1318, June 1975.
14. Asbury, Scott C.: *Effects of Internal Yaw-Vectoring Devices on the Static Performance of a Pitch-Vectoring Nonaxisymmetric Convergent-Divergent Nozzle*. NASA TP-3369, 1993.
15. Asbury, Scott C.; Gunther, Christopher L.; and Hunter, Craig A.: A Passive Cavity Concept for Improving the Off-Design Performance of Fixed Geometry Exhaust Nozzles. AIAA-96-2541, July 1996.
16. Berrier, Bobby L.; and Leavitt, Laurence D.: *Static Internal Performance of Single-Expansion Ramp Nozzle With Thrust-Vectoring Capability up to 60°*. NASA TP-2364, 1984.
17. Re, Richard J.; and Berrier, Bobby L.: *Static Internal Performance of Single Expansion-Ramp Nozzles with Thrust Vectoring and Reversing*. NASA TP-1962, 1982.
18. Re, Richard J.; and Leavitt, Laurence D.: *Static Internal Performance of a Thrust Vectoring and Reversing Two-Dimensional Convergent-Divergent Nozzle With an Aft Flap*. NASA TP-2549, 1986.
19. Asbury, Scott C.; and Capone, Francis J.: *Multiaxis Thrust-Vectoring Characteristics of a Model Representative of the F-18 High-Alpha Research Vehicle at Angles of Attack from 0° to 70°*. NASA TP 3531, 1995.
20. Mason, Mary L.; and Berrier, Bobby L.: *Static Investigation of Several Yaw Vectoring Concepts on Nonaxisymmetric Nozzles*. NASA TP-2432, 1985.

Table 1. Description of Model Configurations

Cruise							
Configuration	Throat insert	$A_e$ , in $^2$	$A_t$ , in $^2$	$A_e/A_t$	NPR <sub>d</sub>	Control block	$\delta_{hood}$ , deg
1	Baselinedry	8.882	4.426	2.01	10.74	None	0
2	Modifieddry	8.882	3.913	2.27	13.27	None	0
3	Maximum A/B	8.882	6.783	1.31	4.72	None	0

Pitch Vectored							
Configuration	Throat insert	$A_e$ , in $^2$	$A_t$ , in $^2$	$A_e/A_t$	NPR <sub>d</sub>	Control block	$\delta_{hood}$ , deg
4	Modifieddry	9.468	3.913	2.42	14.80	None	45
5	Modifieddry	9.175	3.913	2.35	14.08	None	90
6	Modifieddry	9.268	3.913	2.37	14.28	None	120
7	Intermediate	9.468	5.210	1.82	8.99	None	45
8	Intermediate	9.175	5.210	1.76	8.46	None	90
9	Intermediate	9.268	5.210	1.78	8.64	None	120
10	Maximum A/B	9.468	6.783	1.40	5.43	None	45
11	Maximum A/B	9.175	6.783	1.35	5.03	None	90
12	Maximum A/B	9.268	6.783	1.37	5.19	None	120
13	Maximum A/B	6.202	6.202	1.00	1.89	#1	45
14	Maximum A/B	5.459	5.459	1.00	1.89	#1	90
15	Maximum A/B	6.452	6.452	1.00	1.89	#1	120
16	Maximum A/B	7.027	6.783	1.04	2.52	#2	90
17	Maximum A/B	7.548	6.783	1.11	3.14	#2	120

YawVectored							
Configuration	Throat insert	$A_e$ , in $^2$	$A_t$ , in $^2$	$A_e/A_t$	NPR <sub>d</sub>	Control block	$\delta_{hood}$ , deg
18	10° yaw	8.882	4.163	2.08	11.40	None	0
19	Maximum yaw	8.882	4.768	1.86	9.35	None	0

Table 2. Nozzle Internal Performance Data

Configuration 1					Configuration 2				
NPR	$F_r/F_i$	$F/F_i$	$\delta_p$ , deg	$\delta_y$ , deg	NPR	$F_r/F_i$	$F/F_i$	$\delta_p$ , deg	$\delta_y$ , deg
1.56	0.811	0.802	-8.554	0.102	1.59	0.893	0.887	-6.539	-0.572
1.90	0.842	0.834	-7.769	-0.011	1.89	0.881	0.876	-6.086	0.068
2.11	0.841	0.835	-7.281	-0.044	2.10	0.864	0.861	-5.101	-0.177
2.14	0.823	0.816	-7.709	0.250	2.70	0.852	0.842	-8.900	0.290
2.69	0.856	0.851	-6.420	-0.159	3.81	0.885	0.881	-5.313	-0.058
3.79	0.911	0.910	-2.961	1.092	4.38	0.896	0.893	-4.822	0.172
4.38	0.927	0.925	-3.797	0.088	4.94	0.910	0.907	-4.631	0.096
4.97	0.943	0.940	-3.895	0.075	5.51	0.923	0.920	-4.554	0.192
5.54	0.952	0.950	-3.895	0.045	7.21	0.947	0.944	-3.825	0.159
7.20	0.965	0.964	-3.144	0.109	9.58	0.960	0.960	-2.293	0.143
9.43	0.974	0.974	-1.157	0.139	11.11	0.966	0.966	-1.267	0.114
10.27	0.976	0.976	-0.530	0.133	12.27	0.970	0.970	-0.573	0.103
Configuration 3					Configuration 4				
NPR	$F_r/F_i$	$F/F_i$	$\delta_p$ , deg	$\delta_y$ , deg	NPR	$F_r/F_i$	$F/F_i$	$\delta_p$ , deg	$\delta_y$ , deg
1.58	0.905	0.899	-6.181	-0.128	1.50	0.755	0.745	9.415	-0.124
1.92	0.915	0.902	-9.330	-0.130	1.81	0.782	0.766	11.542	0.003
2.14	0.923	0.911	-9.480	-0.065	2.00	0.788	0.769	12.769	0.107
2.71	0.941	0.937	-5.309	0.029	2.48	0.780	0.748	16.394	-0.022
3.25	0.954	0.950	-5.508	0.076	2.99	0.760	0.689	24.926	0.129
3.81	0.963	0.960	-5.139	0.078	3.50	0.788	0.713	25.239	0.321
4.96	0.975	0.974	-1.963	0.018	3.99	0.811	0.730	25.838	0.409
6.64	0.981	0.980	1.042	0.081	4.53	0.833	0.741	27.152	0.404
7.56	0.982	0.981	1.996	0.063	4.97	0.846	0.746	28.158	0.432
					5.49	0.858	0.749	29.138	0.430
					6.01	0.863	0.748	29.849	0.483
					6.51	0.869	0.750	30.307	0.456
					8.48	0.887	0.753	31.853	0.446
Configuration 5					Configuration 6				
NPR	$F_r/F_i$	$F/F_i$	$\delta_p$ , deg	$\delta_y$ , deg	NPR	$F_r/F_i$	$F/F_i$	$\delta_p$ , deg	$\delta_y$ , deg
1.50	0.767	0.375	60.742	-0.197	1.51	0.754	-0.131	99.996	-5.887
1.80	0.789	0.384	60.901	0.375	1.83	0.785	-0.125	99.192	-3.399
2.02	0.799	0.382	61.424	0.202	1.98	0.789	-0.127	99.249	-2.784
2.51	0.805	0.348	64.374	4.071	2.49	0.788	-0.166	102.180	8.725
3.01	0.811	0.330	66.014	4.526	2.99	0.798	-0.192	103.930	9.300
3.51	0.827	0.323	67.041	4.431	3.51	0.819	-0.199	104.090	7.361
4.00	0.833	0.310	68.186	3.850	3.99	0.830	-0.199	103.850	6.071
4.51	0.846	0.299	69.312	3.410	4.49	0.818	-0.218	105.430	4.495
5.02	0.858	0.294	69.954	3.035	4.98	0.816	-0.226	106.080	1.993
5.49	0.861	0.281	70.965	2.401	5.52	0.820	-0.234	106.620	1.004
5.87	0.862	0.270	71.738	2.505	5.86	0.824	-0.232	106.330	1.668

Table 2. Continued

Configuration 7				Configuration 8					
NPR	$F_r/F_i$	$F/F_i$	$\delta_p$ , deg	$\delta_y$ , deg	NPR	$F_r/F_i$	$F/F_i$	$\delta_p$ , deg	$\delta_y$ , deg
1.49	0.837	0.753	25.767	0.171	1.51	0.875	0.334	67.570	0.645
1.80	0.832	0.750	25.664	0.005	1.81	0.882	0.336	67.582	0.745
1.99	0.815	0.719	28.067	-0.204	2.00	0.888	0.334	67.934	0.687
2.50	0.860	0.763	27.568	0.045	2.51	0.902	0.318	69.328	0.891
3.00	0.892	0.791	27.548	0.073	2.99	0.912	0.305	70.443	0.989
3.49	0.912	0.804	28.146	0.071	3.49	0.918	0.295	71.280	1.136
4.00	0.928	0.808	29.425	0.087	3.98	0.919	0.281	72.184	1.213
4.53	0.940	0.810	30.499	0.178	4.21	0.924	0.279	72.408	1.081
5.01	0.948	0.811	31.174	0.220					
5.51	0.953	0.812	31.606	0.222					
6.05	0.955	0.812	31.836	0.188					
Configuration 9				Configuration 10					
NPR	$F_r/F_i$	$F/F_i$	$\delta_p$ , deg	$\delta_y$ , deg	NPR	$F_r/F_i$	$F/F_i$	$\delta_p$ , deg	$\delta_y$ , deg
1.51	0.867	-0.131	98.662	0.400	1.50	0.898	0.765	31.661	0.195
1.81	0.883	-0.132	98.603	0.140	1.81	0.899	0.774	30.548	0.243
2.01	0.891	-0.140	99.060	0.600	2.00	0.905	0.792	28.985	0.214
2.53	0.906	-0.166	100.570	0.850	2.52	0.926	0.805	29.634	0.171
3.03	0.908	-0.186	101.810	0.930	3.00	0.936	0.798	31.488	0.235
3.50	0.907	-0.197	102.540	1.060	3.50	0.951	0.802	32.513	0.280
4.00	0.907	-0.204	103.000	0.930	4.00	0.960	0.799	33.648	0.303
4.25	0.912	-0.206	103.070	1.160	4.51	0.966	0.798	34.308	0.332
					5.00	0.968	0.797	34.648	0.334
					5.50	0.970	0.793	35.124	0.371
Configuration 11				Configuration 12					
NPR	$F_r/F_i$	$F/F_i$	$\delta_p$ , deg	$\delta_y$ , deg	NPR	$F_r/F_i$	$F/F_i$	$\delta_p$ , deg	$\delta_y$ , deg
1.51	0.903	0.317	69.475	0.039	1.50	0.902	-0.126	98.021	-0.480
1.80	0.904	0.301	70.546	0.643	1.81	0.913	-0.141	98.919	0.194
2.01	0.910	0.291	71.323	0.908	2.01	0.913	-0.158	99.961	0.555
2.03	0.911	0.297	70.983	0.653	2.51	0.927	-0.186	101.560	1.127
2.50	0.926	0.271	72.963	1.458	3.02	0.931	-0.201	102.490	1.222
3.02	0.948	0.257	74.277	1.988	3.50	0.930	-0.208	102.950	1.292
3.51	0.951	0.250	74.740	1.990	3.89	0.934	-0.214	103.220	1.551
3.78	0.952	0.250	74.764	1.651					

Table 2. Continued

Configuration 13				Configuration 14					
NPR	$F_r/F_i$	$F/F_i$	$\delta_p$ , deg	$\delta_y$ , deg	NPR	$F_r/F_i$	$F/F_i$	$\delta_p$ , deg	$\delta_y$ , deg
1.50	0.946	0.788	33.611	0.168	1.50	0.937	0.168	79.684	-1.016
1.79	0.958	0.791	34.258	0.236	1.80	0.947	0.157	80.482	-0.366
1.99	0.961	0.788	34.900	0.265	2.00	0.952	0.148	81.070	0.025
2.52	0.966	0.781	36.001	0.314	2.50	0.964	0.126	82.485	1.759
3.00	0.970	0.777	36.768	0.394	2.65	0.966	0.119	82.927	1.339
3.52	0.973	0.774	37.359	0.351	3.02	0.969	0.110	83.504	1.964
4.00	0.971	0.769	37.624	0.376	3.53	0.975	0.108	83.655	1.931
4.51	0.973	0.768	37.869	0.369	3.99	0.967	0.102	83.960	1.970
5.01	0.974	0.766	38.108	0.394	4.52	0.975	0.102	83.975	3.131
5.26	0.976	0.765	38.361	0.445	4.71	0.979	0.100	84.112	2.825

Configuration 15				Configuration 16					
NPR	$F_r/F_i$	$F/F_i$	$\delta_p$ , deg	$\delta_y$ , deg	NPR	$F_r/F_i$	$F/F_i$	$\delta_p$ , deg	$\delta_y$ , deg
1.51	0.908	-0.359	113.280	0.620	1.49	0.928	0.252	74.273	0.171
1.81	0.910	-0.368	113.870	0.770	1.80	0.938	0.245	74.890	0.465
2.01	0.917	-0.384	114.760	1.050	2.00	0.946	0.235	75.652	0.508
2.49	0.920	-0.410	116.490	1.320	2.50	0.960	0.213	77.184	0.902
2.99	0.925	-0.424	117.260	1.240	3.00	0.964	0.199	78.114	1.072
3.50	0.930	-0.432	117.690	1.230	3.50	0.966	0.191	78.574	1.144
4.00	0.929	-0.437	118.060	1.460	3.94	0.977	0.190	78.809	1.624
5.29	0.905	-0.448	119.660	1.410					

Configuration 17				Configuration 18					
NPR	$F_r/F_i$	$F/F_i$	$\delta_p$ , deg	$\delta_y$ , deg	NPR	$F_r/F_i$	$F/F_i$	$\delta_p$ , deg	$\delta_y$ , deg
1.51	0.937	-0.251	105.540	-0.723	1.57	0.905	0.887	5.096	10.313
1.78	0.938	-0.273	106.950	-0.495	1.89	0.905	0.891	4.106	9.056
1.99	0.942	-0.291	108.000	0.234	2.13	0.910	0.899	3.305	8.208
2.51	0.949	-0.318	109.540	0.705	2.71	0.920	0.915	1.370	6.004
2.98	0.956	-0.330	110.180	0.693	3.81	0.927	0.924	-2.753	3.028
3.50	0.955	-0.337	110.660	0.748	4.38	0.935	0.932	-3.459	2.210
4.00	0.957	-0.340	110.780	0.853	4.93	0.942	0.940	-2.983	1.523
4.40	0.959	-0.340	110.760	0.917	5.50	0.948	0.946	-3.043	0.766
					7.19	0.959	0.959	-1.410	-0.095
					9.45	0.964	0.963	0.016	-0.842
					11.01	0.966	0.966	0.796	-1.140

Table 2. Concluded

## Configuration 19

NPR	$F_r/F_i$	$F/F_i$	$\delta_p$ , deg	$\delta_y$ , deg
1.55	0.925	0.905	5.294	10.714
1.91	0.925	0.912	4.353	8.670
2.13	0.930	0.921	3.089	7.543
2.70	0.936	0.932	0.936	4.774
3.83	0.935	0.933	-3.007	1.323
4.37	0.942	0.941	-2.452	0.496
4.93	0.950	0.950	-1.719	-0.096
5.49	0.955	0.955	-1.246	-0.578
7.20	0.963	0.962	-0.069	-1.504
8.89	0.965	0.965	1.007	-2.076
9.40	0.966	0.965	1.161	-2.220
10.33	0.965	0.964	1.753	-2.377

Table 3. Nozzle Internal Static Pressure Ratios for Configuration 1

NPR	Upper flap										Lower flap			
	PR <sub>54</sub>	PR <sub>55</sub>	PR <sub>56</sub>	PR <sub>57</sub>	PR <sub>58</sub>	PR <sub>59</sub>	PR <sub>60</sub>	PR <sub>61</sub>	PR <sub>62</sub>	PR <sub>63</sub>	PR <sub>46</sub>	PR <sub>47</sub>	PR <sub>48</sub>	PR <sub>49</sub>
1.57	0.600	0.604	0.607	0.594	0.657	0.649	0.644	0.638	0.644	0.660	0.614	0.609	0.605	0.615
1.90	0.486	0.504	0.499	0.425	0.559	0.542	0.534	0.533	0.537	0.545	0.502	0.491	0.482	0.499
2.11	0.384	0.387	0.440	0.380	0.510	0.492	0.496	0.487	0.488	0.511	0.448	0.435	0.430	0.448
2.14	0.375	0.373	0.430	0.376	0.505	0.484	0.488	0.471	0.480	0.506	0.432	0.428	0.424	0.441
2.69	0.334	0.251	0.170	0.248	0.416	0.379	0.330	0.336	0.339	0.373	0.345	0.308	0.305	0.342
3.79	0.168	0.170	0.170	0.170	0.269	0.243	0.251	0.251	0.199	0.269	0.172	0.173	0.174	0.232
4.38	0.168	0.170	0.170	0.141	0.238	0.207	0.214	0.215	0.171	0.217	0.172	0.176	0.174	0.193
4.97	0.168	0.170	0.171	0.140	0.214	0.181	0.181	0.184	0.091	0.166	0.172	0.176	0.175	0.186
5.54	0.168	0.170	0.171	0.140	0.164	0.158	0.137	0.148	0.091	0.116	0.172	0.176	0.175	0.177
7.20	0.169	0.170	0.171	0.141	0.091	0.067	0.073	0.073	0.091	0.116	0.172	0.175	0.175	0.140
9.43	0.169	0.170	0.170	0.142	0.091	0.068	0.073	0.073	0.091	0.114	0.172	0.174	0.176	0.132
10.27	0.169	0.170	0.170	0.142	0.091	0.068	0.073	0.073	0.092	0.114	0.172	0.174	0.176	0.131
Right sidewall														
NPR	PR <sub>26</sub>	PR <sub>27</sub>	PR <sub>28</sub>	PR <sub>29</sub>	PR <sub>30</sub>	PR <sub>31</sub>	PR <sub>32</sub>	PR <sub>33</sub>	PR <sub>34</sub>	PR <sub>35</sub>	PR <sub>21</sub>	PR <sub>22</sub>	PR <sub>23</sub>	PR <sub>24</sub>
1.57	0.645	0.523	0.611	0.649	0.565	0.591	0.614	0.783	0.570	0.602	0.776	0.517	0.650	0.568
1.90	0.533	0.416	0.451	0.533	0.483	0.486	0.490	0.770	0.450	0.481	0.766	0.405	0.533	0.446
2.11	0.480	0.298	0.417	0.496	0.455	0.398	0.453	0.768	0.396	0.430	0.764	0.288	0.492	0.392
2.14	0.473	0.271	0.409	0.489	0.454	0.375	0.449	0.770	0.388	0.423	0.765	0.245	0.490	0.384
2.69	0.377	0.188	0.297	0.371	0.442	0.098	0.300	0.766	0.173	0.341	0.764	0.173	0.355	0.170
3.79	0.267	0.189	0.243	0.255	0.444	0.235	0.239	0.765	0.169	0.228	0.763	0.174	0.252	0.167
4.38	0.231	0.188	0.199	0.223	0.444	0.089	0.192	0.764	0.169	0.111	0.762	0.174	0.222	0.166
4.97	0.203	0.188	0.115	0.196	0.444	0.089	0.095	0.764	0.169	0.104	0.762	0.173	0.196	0.166
5.54	0.182	0.189	0.094	0.176	0.444	0.089	0.089	0.763	0.169	0.104	0.762	0.174	0.177	0.166
7.20	0.140	0.187	0.095	0.117	0.445	0.089	0.090	0.763	0.170	0.103	0.762	0.173	0.114	0.164
9.43	0.106	0.187	0.095	0.116	0.444	0.089	0.090	0.764	0.168	0.103	0.761	0.173	0.113	0.164
10.27	0.097	0.186	0.096	0.116	0.444	0.089	0.090	0.763	0.168	0.103	0.761	0.173	0.113	0.164
Lower throat insert														
NPR	PR <sub>36</sub>	PR <sub>37</sub>	PR <sub>38</sub>	PR <sub>39</sub>	PR <sub>40</sub>	PR <sub>41</sub>	PR <sub>42</sub>	PR <sub>43</sub>	PR <sub>44</sub>	PR <sub>45</sub>				
1.57	0.890	0.477	0.547	0.916	0.925	0.477	0.561	0.967	0.476	0.543				
1.90	0.886	0.332	0.412	0.912	0.923	0.353	0.430	0.966	0.358	0.419				
2.11	0.885	0.253	0.350	0.910	0.923	0.270	0.380	0.966	0.296	0.370				
2.14	0.885	0.241	0.344	0.911	0.924	0.254	0.375	0.967	0.285	0.364				
2.69	0.884	0.144	0.324	0.909	0.924	0.153	0.305	0.967	0.166	0.191				
3.79	0.884	0.144	0.322	0.909	0.927	0.153	0.289	0.967	0.168	0.167				
4.38	0.884	0.144	0.322	0.908	0.928	0.152	0.288	0.966	0.168	0.166				
4.97	0.885	0.145	0.321	0.908	0.929	0.152	0.287	0.967	0.169	0.166				
5.54	0.886	0.145	0.321	0.908	0.930	0.152	0.288	0.966	0.169	0.165				
7.20	0.888	0.144	0.321	0.908	0.932	0.151	0.291	0.967	0.170	0.162				
9.43	0.886	0.144	0.318	0.905	0.936	0.151	0.293	0.967	0.170	0.161				
10.27	0.886	0.144	0.315	0.905	0.936	0.151	0.293	0.966	0.170	0.161				

Table 4. Nozzle Internal Static Pressure Ratios for Configuration 2

NPR	Upper flap										Lower flap			
	PR <sub>54</sub>	PR <sub>55</sub>	PR <sub>56</sub>	PR <sub>57</sub>	PR <sub>58</sub>	PR <sub>59</sub>	PR <sub>60</sub>	PR <sub>61</sub>	PR <sub>62</sub>	PR <sub>63</sub>	PR <sub>46</sub>	PR <sub>47</sub>	PR <sub>48</sub>	PR <sub>49</sub>
1.59	0.619	0.636	0.653	0.683	0.636	0.644	0.638	0.635	0.652	0.645	0.606	0.611	0.610	0.614
1.89	0.507	0.524	0.535	0.524	0.551	0.553	0.545	0.540	0.563	0.550	0.519	0.501	0.503	0.508
2.10	0.465	0.461	0.485	0.430	0.510	0.503	0.495	0.493	0.516	0.519	0.454	0.449	0.449	0.454
2.70	0.238	0.159	0.233	0.261	0.435	0.391	0.397	0.328	0.385	0.416	0.335	0.333	0.334	0.350
3.81	0.152	0.154	0.147	0.166	0.273	0.238	0.240	0.249	0.221	0.215	0.155	0.160	0.174	0.238
4.38	0.152	0.154	0.146	0.114	0.281	0.205	0.217	0.219	0.194	0.238	0.155	0.160	0.156	0.190
4.94	0.152	0.154	0.146	0.111	0.216	0.186	0.190	0.192	0.169	0.193	0.155	0.161	0.151	0.166
5.51	0.153	0.155	0.147	0.109	0.224	0.165	0.167	0.170	0.078	0.171	0.155	0.161	0.151	0.165
7.21	0.153	0.154	0.148	0.110	0.132	0.058	0.063	0.063	0.078	0.092	0.155	0.160	0.150	0.135
9.58	0.153	0.155	0.149	0.111	0.088	0.058	0.063	0.063	0.079	0.091	0.155	0.160	0.150	0.108
11.11	0.153	0.155	0.149	0.111	0.087	0.058	0.063	0.063	0.079	0.091	0.155	0.160	0.150	0.098
12.27	0.153	0.155	0.149	0.112	0.087	0.058	0.063	0.063	0.079	0.090	0.155	0.160	0.151	0.096
Right sidewall														
NPR	PR <sub>26</sub>	PR <sub>27</sub>	PR <sub>28</sub>	PR <sub>29</sub>	PR <sub>30</sub>	PR <sub>31</sub>	PR <sub>32</sub>	PR <sub>33</sub>	PR <sub>34</sub>	PR <sub>35</sub>	PR <sub>21</sub>	PR <sub>22</sub>	PR <sub>23</sub>	PR <sub>24</sub>
1.59	0.637	0.587	0.653	0.641	0.570	0.603	0.624	0.704	0.604	0.603	0.680	0.581	0.642	0.608
1.89	0.535	0.453	0.559	0.547	0.396	0.499	0.526	0.671	0.504	0.499	0.664	0.435	0.556	0.503
2.10	0.482	0.387	0.493	0.498	0.331	0.431	0.466	0.662	0.437	0.445	0.659	0.381	0.508	0.446
2.70	0.375	0.239	0.283	0.392	0.242	0.323	0.358	0.660	0.342	0.340	0.658	0.248	0.385	0.337
3.81	0.266	0.107	0.190	0.228	0.245	0.072	0.257	0.659	0.154	0.241	0.657	0.107	0.226	0.179
4.38	0.232	0.106	0.138	0.231	0.245	0.070	0.112	0.659	0.111	0.199	0.656	0.106	0.246	0.105
4.94	0.205	0.107	0.095	0.193	0.245	0.070	0.090	0.660	0.108	0.147	0.656	0.107	0.191	0.105
5.51	0.184	0.107	0.123	0.173	0.246	0.069	0.066	0.661	0.108	0.112	0.655	0.107	0.172	0.106
7.21	0.141	0.108	0.080	0.138	0.246	0.069	0.068	0.661	0.108	0.101	0.654	0.107	0.141	0.106
9.58	0.106	0.108	0.080	0.089	0.246	0.070	0.065	0.661	0.107	0.068	0.654	0.106	0.099	0.105
11.11	0.091	0.108	0.080	0.089	0.246	0.070	0.065	0.661	0.108	0.068	0.654	0.106	0.099	0.105
12.27	0.083	0.108	0.079	0.088	0.246	0.070	0.065	0.661	0.107	0.068	0.654	0.106	0.099	0.105
Lower throat insert														
NPR	PR <sub>36</sub>	PR <sub>37</sub>	PR <sub>38</sub>	PR <sub>39</sub>	PR <sub>40</sub>	PR <sub>41</sub>	PR <sub>42</sub>	PR <sub>43</sub>	PR <sub>44</sub>	PR <sub>45</sub>				
1.59	0.882	0.601	0.608	0.614	0.955	0.615	0.615	0.927	0.603	0.608				
1.89	0.868	0.468	0.325	0.510	0.951	0.512	0.509	0.921	0.480	0.500				
2.10	0.865	0.371	0.238	0.460	0.949	0.456	0.454	0.919	0.406	0.441				
2.70	0.864	0.331	0.218	0.292	0.947	0.166	0.322	0.919	0.215	0.323				
3.81	0.864	0.330	0.125	0.329	0.947	0.166	0.290	0.919	0.215	0.193				
4.38	0.865	0.330	0.125	0.327	0.947	0.166	0.278	0.919	0.214	0.118				
4.94	0.864	0.330	0.125	0.324	0.947	0.166	0.279	0.919	0.214	0.114				
5.51	0.864	0.330	0.125	0.324	0.947	0.166	0.282	0.919	0.214	0.114				
7.21	0.863	0.329	0.125	0.323	0.946	0.166	0.292	0.919	0.215	0.114				
9.58	0.862	0.328	0.124	0.323	0.946	0.167	0.301	0.919	0.217	0.113				
11.11	0.862	0.327	0.124	0.323	0.946	0.166	0.301	0.919	0.217	0.113				
12.27	0.862	0.326	0.124	0.323	0.946	0.165	0.300	0.919	0.217	0.113				

Table 5. Nozzle Internal Static Pressure Ratios for Configuration 3

NPR	Upper flap										Lower flap			
	PR <sub>54</sub>	PR <sub>55</sub>	PR <sub>56</sub>	PR <sub>57</sub>	PR <sub>58</sub>	PR <sub>59</sub>	PR <sub>60</sub>	PR <sub>61</sub>	PR <sub>62</sub>	PR <sub>63</sub>	PR <sub>46</sub>	PR <sub>47</sub>	PR <sub>48</sub>	PR <sub>49</sub>
1.58	0.593	0.590	0.559	0.557	0.640	0.639	0.638	0.640	0.635	0.633	0.597	0.599	0.612	0.612
1.92	0.393	0.363	0.349	0.277	0.542	0.509	0.503	0.492	0.450	0.523	0.502	0.503	0.498	0.487
2.14	0.215	0.222	0.230	0.276	0.495	0.420	0.419	0.412	0.377	0.468	0.447	0.442	0.435	0.425
2.71	0.211	0.223	0.231	0.276	0.394	0.333	0.335	0.338	0.318	0.370	0.215	0.225	0.232	0.337
3.25	0.211	0.224	0.232	0.277	0.167	0.272	0.248	0.181	0.157	0.308	0.216	0.225	0.232	0.288
3.81	0.212	0.224	0.232	0.276	0.164	0.127	0.175	0.181	0.158	0.262	0.216	0.225	0.233	0.260
4.96	0.212	0.225	0.232	0.276	0.164	0.127	0.175	0.181	0.159	0.202	0.215	0.225	0.233	0.242
6.64	0.212	0.225	0.232	0.276	0.165	0.128	0.175	0.180	0.159	0.151	0.215	0.225	0.234	0.234
7.56	0.212	0.225	0.232	0.276	0.165	0.127	0.175	0.180	0.158	0.132	0.215	0.225	0.234	0.235
Right sidewall										Left sidewall				
NPR	PR <sub>26</sub>	PR <sub>27</sub>	PR <sub>28</sub>	PR <sub>29</sub>	PR <sub>30</sub>	PR <sub>31</sub>	PR <sub>32</sub>	PR <sub>33</sub>	PR <sub>34</sub>	PR <sub>35</sub>	PR <sub>21</sub>	PR <sub>22</sub>	PR <sub>23</sub>	PR <sub>24</sub>
1.58	0.661	0.494	0.596	0.641	0.616	0.421	0.619	0.686	0.492	0.621	0.684	0.487	0.642	0.489
1.92	0.545	0.493	0.273	0.535	0.614	0.393	0.401	0.683	0.489	0.485	0.681	0.488	0.540	0.487
2.14	0.489	0.494	0.271	0.452	0.614	0.392	0.322	0.684	0.489	0.426	0.682	0.486	0.456	0.490
2.71	0.387	0.492	0.272	0.317	0.615	0.390	0.298	0.683	0.490	0.366	0.682	0.485	0.305	0.486
3.25	0.323	0.493	0.273	0.201	0.616	0.390	0.297	0.682	0.490	0.357	0.682	0.485	0.205	0.486
3.81	0.276	0.493	0.273	0.201	0.617	0.390	0.296	0.682	0.490	0.357	0.682	0.485	0.206	0.485
4.96	0.212	0.494	0.272	0.201	0.618	0.391	0.296	0.684	0.489	0.354	0.682	0.484	0.205	0.485
6.64	0.158	0.492	0.272	0.199	0.618	0.394	0.295	0.684	0.488	0.354	0.682	0.482	0.205	0.484
7.56	0.139	0.490	0.273	0.199	0.618	0.393	0.294	0.684	0.488	0.354	0.681	0.482	0.204	0.484
Lower throat insert														
NPR	PR <sub>36</sub>	PR <sub>37</sub>	PR <sub>38</sub>	PR <sub>39</sub>	PR <sub>40</sub>	PR <sub>41</sub>	PR <sub>42</sub>	PR <sub>43</sub>	PR <sub>44</sub>	PR <sub>45</sub>				
1.58	0.760	0.511	0.524	0.314	0.541	0.642	0.322	0.783	0.478	0.569				
1.92	0.762	0.381	0.520	0.310	0.335	0.639	0.322	0.781	0.480	0.437				
2.14	0.762	0.382	0.516	0.308	0.335	0.644	0.324	0.798	0.480	0.319				
2.71	0.762	0.381	0.523	0.307	0.336	0.659	0.325	0.798	0.483	0.273				
3.25	0.762	0.382	0.520	0.309	0.336	0.659	0.326	0.798	0.485	0.272				
3.81	0.762	0.383	0.523	0.311	0.335	0.684	0.324	0.782	0.485	0.270				
4.96	0.762	0.384	0.527	0.311	0.333	0.666	0.325	0.787	0.485	0.268				
6.64	0.762	0.383	0.543	0.310	0.333	0.684	0.325	0.786	0.481	0.267				
7.56	0.761	0.383	0.553	0.309	0.333	0.692	0.324	0.792	0.483	0.267				

**Table 6. Nozzle Internal Static Pressure Ratios for Configuration 4**

Upper flap										Lower flap				
NPR	PR <sub>54</sub>	PR <sub>55</sub>	PR <sub>56</sub>	PR <sub>57</sub>	PR <sub>58</sub>	PR <sub>59</sub>	PR <sub>60</sub>	PR <sub>61</sub>	PR <sub>62</sub>	PR <sub>63</sub>	PR <sub>46</sub>	PR <sub>47</sub>	PR <sub>48</sub>	PR <sub>49</sub>
1.50	0.665	0.647	0.639	0.651	0.664	0.643	0.637	0.637	0.634	0.666	0.653	0.665	0.679	0.722
1.81	0.559	0.538	0.525	0.538	0.552	0.527	0.521	0.524	0.518	0.553	0.534	0.544	0.547	0.626
2.00	0.518	0.494	0.473	0.487	0.499	0.477	0.473	0.478	0.470	0.501	0.485	0.486	0.496	0.563
2.48	0.444	0.415	0.390	0.390	0.402	0.390	0.391	0.397	0.398	0.404	0.369	0.397	0.393	0.479
2.99	0.421	0.411	0.369	0.314	0.334	0.395	0.401	0.400	0.421	0.335	0.304	0.255	0.308	0.432
3.50	0.391	0.375	0.326	0.276	0.285	0.358	0.361	0.360	0.379	0.286	0.155	0.159	0.189	0.303
3.99	0.368	0.355	0.308	0.252	0.250	0.336	0.337	0.337	0.355	0.250	0.152	0.158	0.155	0.226
4.53	0.357	0.343	0.298	0.237	0.220	0.321	0.322	0.325	0.342	0.221	0.152	0.158	0.149	0.186
4.97	0.353	0.337	0.294	0.232	0.201	0.314	0.314	0.321	0.336	0.201	0.152	0.158	0.149	0.166
5.49	0.348	0.333	0.293	0.228	0.182	0.309	0.310	0.319	0.333	0.182	0.152	0.158	0.148	0.153
6.01	0.345	0.328	0.283	0.218	0.166	0.301	0.305	0.319	0.329	0.166	0.152	0.158	0.149	0.172
6.51	0.340	0.324	0.265	0.210	0.153	0.296	0.301	0.316	0.325	0.154	0.152	0.158	0.149	0.177
8.48	0.326	0.297	0.222	0.202	0.118	0.288	0.286	0.308	0.313	0.118	0.152	0.158	0.147	0.143
Right sidewall										Left sidewall				
NPR	PR <sub>26</sub>	PR <sub>27</sub>	PR <sub>28</sub>	PR <sub>29</sub>	PR <sub>30</sub>	PR <sub>31</sub>	PR <sub>32</sub>	PR <sub>33</sub>	PR <sub>34</sub>	PR <sub>35</sub>	PR <sub>21</sub>	PR <sub>22</sub>	PR <sub>23</sub>	PR <sub>24</sub>
1.50	0.691	0.663	0.654	0.656	0.627	0.663	0.662	0.698	0.639	0.692	0.720	0.656	0.658	0.634
1.81	0.575	0.550	0.542	0.545	0.452	0.556	0.552	0.675	0.475	0.577	0.665	0.544	0.544	0.466
2.00	0.520	0.501	0.491	0.494	0.369	0.506	0.504	0.669	0.426	0.529	0.655	0.493	0.494	0.424
2.48	0.419	0.402	0.395	0.414	0.262	0.409	0.415	0.666	0.307	0.393	0.650	0.400	0.409	0.308
2.99	0.347	0.378	0.357	0.377	0.249	0.365	0.392	0.664	0.247	0.345	0.650	0.373	0.375	0.223
3.50	0.297	0.351	0.329	0.329	0.243	0.279	0.358	0.664	0.175	0.286	0.651	0.346	0.330	0.139
3.99	0.260	0.330	0.311	0.304	0.243	0.220	0.340	0.663	0.122	0.280	0.651	0.323	0.306	0.113
4.53	0.229	0.299	0.300	0.294	0.243	0.177	0.327	0.662	0.106	0.250	0.650	0.304	0.291	0.106
4.97	0.208	0.270	0.297	0.291	0.244	0.157	0.305	0.662	0.106	0.212	0.649	0.293	0.283	0.105
5.49	0.189	0.271	0.281	0.288	0.245	0.168	0.296	0.660	0.109	0.194	0.648	0.279	0.276	0.104
6.01	0.172	0.279	0.265	0.280	0.246	0.174	0.295	0.660	0.109	0.188	0.648	0.280	0.277	0.105
6.51	0.159	0.290	0.263	0.271	0.246	0.175	0.301	0.660	0.109	0.184	0.648	0.292	0.268	0.104
8.48	0.122	0.287	0.263	0.258	0.246	0.159	0.282	0.661	0.105	0.164	0.648	0.286	0.254	0.104
Lower throat insert										Aft-hood deflector				
NPR	PR <sub>36</sub>	PR <sub>37</sub>	PR <sub>38</sub>	PR <sub>39</sub>	PR <sub>40</sub>	PR <sub>41</sub>	PR <sub>42</sub>	PR <sub>43</sub>	PR <sub>44</sub>	PR <sub>45</sub>	PR <sub>64</sub>	PR <sub>65</sub>	PR <sub>66</sub>	PR <sub>67</sub>
1.50	0.880	0.581	0.539	0.566	0.954	0.667	0.581	0.924	0.337	0.604	0.677	0.715	0.842	0.650
1.81	0.867	0.435	0.402	0.428	0.948	0.555	0.439	0.919	0.252	0.458	0.570	0.619	0.769	0.537
2.00	0.864	0.380	0.343	0.371	0.947	0.501	0.392	0.919	0.239	0.425	0.534	0.588	0.712	0.489
2.48	0.861	0.341	0.189	0.322	0.945	0.404	0.318	0.918	0.231	0.276	0.466	0.551	0.624	0.395
2.99	0.861	0.330	0.147	0.320	0.946	0.336	0.288	0.918	0.231	0.215	0.481	0.636	0.564	0.326
3.50	0.862	0.327	0.124	0.327	0.946	0.287	0.280	0.918	0.231	0.156	0.455	0.619	0.499	0.307
3.99	0.862	0.327	0.123	0.325	0.946	0.251	0.276	0.918	0.232	0.124	0.435	0.601	0.472	0.299
4.53	0.862	0.326	0.123	0.325	0.946	0.222	0.274	0.918	0.232	0.111	0.432	0.599	0.453	0.286
4.97	0.862	0.325	0.123	0.325	0.946	0.202	0.275	0.918	0.231	0.109	0.436	0.606	0.436	0.279
5.49	0.861	0.324	0.122	0.324	0.946	0.183	0.276	0.917	0.231	0.110	0.434	0.608	0.411	0.276
6.01	0.861	0.324	0.121	0.324	0.946	0.167	0.278	0.917	0.231	0.110	0.439	0.622	0.383	0.238
6.51	0.861	0.324	0.121	0.324	0.946	0.155	0.279	0.917	0.231	0.110	0.444	0.634	0.367	0.224
8.48	0.861	0.323	0.120	0.321	0.945	0.119	0.287	0.917	0.231	0.109	0.491	0.669	0.312	0.240

Table 7. Nozzle Internal Static Pressure Ratios for Configuration 5

Upper flap										Lower flap					
NPR	PR <sub>54</sub>	PR <sub>55</sub>	PR <sub>56</sub>	PR <sub>57</sub>	PR <sub>58</sub>	PR <sub>59</sub>	PR <sub>60</sub>	PR <sub>61</sub>	PR <sub>62</sub>	PR <sub>63</sub>	PR <sub>46</sub>	PR <sub>47</sub>	PR <sub>48</sub>	PR <sub>49</sub>	
1.50	0.781	0.767	0.761	0.768	0.667	0.754	0.752	0.752	0.745	0.668	0.730	0.746	0.773	0.803	
1.80	0.711	0.694	0.684	0.693	0.553	0.672	0.672	0.673	0.664	0.555	0.646	0.666	0.703	0.741	
2.02	0.674	0.657	0.646	0.655	0.494	0.632	0.631	0.633	0.623	0.495	0.607	0.628	0.666	0.711	
2.51	0.579	0.590	0.570	0.532	0.397	0.630	0.621	0.584	0.568	0.397	0.531	0.533	0.568	0.621	
3.01	0.533	0.551	0.535	0.490	0.331	0.583	0.603	0.560	0.534	0.331	0.488	0.477	0.529	0.584	
3.51	0.511	0.526	0.508	0.464	0.284	0.560	0.578	0.537	0.509	0.285	0.467	0.450	0.487	0.567	
4.00	0.509	0.509	0.494	0.449	0.250	0.547	0.543	0.514	0.495	0.250	0.465	0.439	0.457	0.551	
4.51	0.505	0.495	0.478	0.448	0.221	0.522	0.515	0.499	0.485	0.222	0.468	0.436	0.436	0.534	
5.02	0.501	0.486	0.469	0.447	0.199	0.501	0.497	0.487	0.476	0.199	0.464	0.432	0.423	0.528	
5.49	0.487	0.470	0.451	0.435	0.181	0.486	0.493	0.488	0.463	0.182	0.427	0.417	0.412	0.515	
5.87	0.478	0.461	0.443	0.426	0.170	0.480	0.493	0.490	0.454	0.170	0.394	0.407	0.406	0.505	
Right sidewall										Left sidewall					
NPR	PR <sub>26</sub>	PR <sub>27</sub>	PR <sub>28</sub>	PR <sub>29</sub>	PR <sub>30</sub>	PR <sub>31</sub>	PR <sub>32</sub>	PR <sub>33</sub>	PR <sub>34</sub>	PR <sub>35</sub>	PR <sub>21</sub>	PR <sub>22</sub>	PR <sub>23</sub>	PR <sub>24</sub>	
1.50	0.702	0.778	0.770	0.774	0.770	0.781	0.781	0.751	0.770	0.795	0.805	0.777	0.776	0.762	
1.80	0.582	0.707	0.696	0.700	0.688	0.709	0.709	0.706	0.693	0.729	0.746	0.704	0.700	0.683	
2.02	0.519	0.672	0.661	0.665	0.644	0.675	0.674	0.694	0.656	0.697	0.719	0.668	0.663	0.642	
2.51	0.418	0.620	0.614	0.615	0.565	0.628	0.624	0.679	0.588	0.649	0.680	0.596	0.565	0.528	
3.01	0.348	0.582	0.579	0.581	0.504	0.593	0.589	0.673	0.527	0.613	0.666	0.564	0.497	0.479	
3.51	0.299	0.557	0.554	0.556	0.452	0.565	0.563	0.669	0.490	0.583	0.658	0.537	0.471	0.448	
4.00	0.263	0.525	0.521	0.528	0.393	0.532	0.533	0.666	0.452	0.553	0.654	0.504	0.480	0.423	
4.51	0.233	0.501	0.498	0.509	0.377	0.500	0.511	0.664	0.403	0.513	0.651	0.480	0.493	0.403	
5.02	0.209	0.485	0.489	0.500	0.349	0.476	0.498	0.663	0.382	0.481	0.650	0.471	0.491	0.396	
5.49	0.190	0.465	0.467	0.486	0.295	0.458	0.477	0.662	0.359	0.467	0.649	0.450	0.487	0.379	
5.87	0.178	0.459	0.457	0.479	0.279	0.450	0.470	0.662	0.349	0.459	0.648	0.440	0.483	0.372	
Lower throat insert										Aft-hood deflector					
NPR	PR <sub>36</sub>	PR <sub>37</sub>	PR <sub>38</sub>	PR <sub>39</sub>	PR <sub>40</sub>	PR <sub>41</sub>	PR <sub>42</sub>	PR <sub>43</sub>	PR <sub>44</sub>	PR <sub>45</sub>	PR <sub>64</sub>	PR <sub>65</sub>	PR <sub>66</sub>	PR <sub>67</sub>	PR <sub>68</sub>
1.50	0.906	0.733	0.680	0.722	0.964	0.672	0.774	0.939	0.565	0.746	0.839	0.765	0.930	0.830	0.753
1.80	0.885	0.639	0.577	0.626	0.957	0.558	0.658	0.929	0.401	0.660	0.784	0.688	0.909	0.786	0.673
2.02	0.880	0.590	0.528	0.577	0.954	0.498	0.603	0.927	0.326	0.614	0.757	0.651	0.898	0.768	0.629
2.51	0.870	0.498	0.424	0.454	0.949	0.399	0.453	0.920	0.255	0.506	0.753	0.620	0.829	0.709	0.530
3.01	0.866	0.447	0.381	0.402	0.948	0.334	0.399	0.919	0.244	0.469	0.728	0.588	0.810	0.690	0.483
3.51	0.866	0.413	0.348	0.372	0.947	0.287	0.376	0.918	0.238	0.449	0.709	0.565	0.789	0.673	0.442
4.00	0.864	0.377	0.312	0.350	0.947	0.252	0.367	0.918	0.236	0.418	0.685	0.543	0.763	0.649	0.405
4.51	0.863	0.357	0.280	0.340	0.947	0.223	0.356	0.918	0.234	0.378	0.652	0.513	0.748	0.635	0.380
5.02	0.863	0.350	0.262	0.336	0.946	0.200	0.355	0.918	0.232	0.361	0.633	0.497	0.750	0.636	0.353
5.49	0.862	0.341	0.240	0.324	0.946	0.183	0.349	0.918	0.233	0.335	0.596	0.464	0.755	0.636	0.345
5.87	0.862	0.337	0.226	0.320	0.947	0.171	0.345	0.918	0.232	0.325	0.579	0.448	0.749	0.630	0.342

**Table 8. Nozzle Internal Static Pressure Ratios for Configuration 6**

NPR	Upper flap										Lower flap			
	PR <sub>54</sub>	PR <sub>55</sub>	PR <sub>56</sub>	PR <sub>57</sub>	PR <sub>58</sub>	PR <sub>59</sub>	PR <sub>60</sub>	PR <sub>61</sub>	PR <sub>62</sub>	PR <sub>63</sub>	PR <sub>46</sub>	PR <sub>47</sub>	PR <sub>48</sub>	PR <sub>49</sub>
1.51	0.815	0.805	0.802	0.809	0.662	0.793	0.794	0.794	0.790	0.664	0.759	0.775	0.799	0.830
1.83	0.756	0.743	0.739	0.747	0.544	0.728	0.729	0.729	0.724	0.546	0.686	0.707	0.740	0.777
1.98	0.734	0.721	0.716	0.725	0.502	0.705	0.706	0.706	0.702	0.504	0.662	0.684	0.719	0.758
2.49	0.658	0.659	0.641	0.617	0.401	0.687	0.663	0.658	0.650	0.402	0.599	0.602	0.616	0.685
2.99	0.616	0.623	0.598	0.567	0.334	0.668	0.641	0.629	0.621	0.335	0.568	0.557	0.560	0.644
3.51	0.590	0.607	0.583	0.552	0.285	0.642	0.642	0.613	0.601	0.286	0.547	0.535	0.557	0.628
3.99	0.576	0.594	0.575	0.549	0.250	0.625	0.637	0.601	0.587	0.251	0.534	0.527	0.551	0.618
4.49	0.564	0.569	0.554	0.541	0.222	0.602	0.598	0.583	0.570	0.223	0.515	0.512	0.520	0.604
4.98	0.558	0.557	0.542	0.543	0.200	0.576	0.579	0.575	0.555	0.201	0.500	0.506	0.520	0.594
5.52	0.544	0.542	0.528	0.523	0.181	0.562	0.566	0.578	0.529	0.182	0.485	0.493	0.506	0.586
5.86	0.546	0.543	0.526	0.524	0.170	0.560	0.564	0.571	0.534	0.171	0.486	0.497	0.510	0.580
Right sidewall										Left sidewall				
NPR	PR <sub>26</sub>	PR <sub>27</sub>	PR <sub>28</sub>	PR <sub>29</sub>	PR <sub>30</sub>	PR <sub>31</sub>	PR <sub>32</sub>	PR <sub>33</sub>	PR <sub>34</sub>	PR <sub>35</sub>	PR <sub>21</sub>	PR <sub>22</sub>	PR <sub>23</sub>	PR <sub>24</sub>
1.50	0.702	0.811	0.801	0.812	0.808	0.818	0.817	0.783	0.806	0.828	0.836	0.816	0.814	0.802
1.80	0.576	0.753	0.742	0.750	0.745	0.758	0.757	0.732	0.744	0.772	0.781	0.753	0.753	0.738
2.02	0.530	0.732	0.722	0.729	0.722	0.736	0.736	0.718	0.722	0.753	0.762	0.733	0.732	0.716
2.51	0.423	0.685	0.678	0.682	0.660	0.693	0.691	0.694	0.671	0.710	0.700	0.654	0.664	0.630
3.01	0.352	0.655	0.651	0.654	0.617	0.665	0.662	0.685	0.634	0.681	0.677	0.613	0.623	0.576
3.51	0.299	0.638	0.636	0.639	0.590	0.648	0.646	0.678	0.602	0.665	0.672	0.606	0.584	0.555
4.00	0.264	0.624	0.625	0.629	0.567	0.633	0.635	0.674	0.569	0.647	0.662	0.595	0.572	0.522
4.51	0.234	0.586	0.591	0.599	0.517	0.589	0.593	0.668	0.508	0.600	0.655	0.558	0.582	0.484
5.02	0.211	0.548	0.566	0.583	0.471	0.548	0.559	0.665	0.459	0.563	0.652	0.547	0.580	0.464
5.49	0.191	0.506	0.551	0.569	0.422	0.499	0.532	0.663	0.420	0.518	0.651	0.522	0.571	0.448
5.87	0.180	0.524	0.544	0.568	0.441	0.507	0.536	0.663	0.424	0.527	0.650	0.513	0.570	0.442
Lower throat insert										Aft-hood deflector				
NPR	PR <sub>36</sub>	PR <sub>37</sub>	PR <sub>38</sub>	PR <sub>39</sub>	PR <sub>40</sub>	PR <sub>41</sub>	PR <sub>42</sub>	PR <sub>43</sub>	PR <sub>44</sub>	PR <sub>45</sub>	PR <sub>64</sub>	PR <sub>65</sub>	PR <sub>66</sub>	PR <sub>67</sub>
1.50	0.913	0.776	0.730	0.769	0.968	0.665	0.828	0.947	0.641	0.789	0.812	0.830	0.871	0.875
1.80	0.896	0.700	0.642	0.687	0.961	0.548	0.761	0.937	0.501	0.717	0.751	0.774	0.823	0.827
2.02	0.892	0.672	0.613	0.659	0.959	0.505	0.733	0.933	0.451	0.693	0.731	0.755	0.807	0.810
2.51	0.878	0.595	0.500	0.543	0.952	0.403	0.560	0.924	0.323	0.596	0.736	0.765	0.803	0.799
3.01	0.872	0.546	0.447	0.485	0.949	0.336	0.498	0.922	0.270	0.541	0.738	0.760	0.802	0.796
3.51	0.870	0.518	0.430	0.465	0.948	0.286	0.485	0.921	0.252	0.525	0.719	0.738	0.783	0.776
4.00	0.869	0.503	0.409	0.450	0.948	0.252	0.468	0.920	0.244	0.498	0.692	0.716	0.756	0.746
4.51	0.866	0.455	0.369	0.424	0.948	0.224	0.440	0.919	0.236	0.464	0.645	0.684	0.723	0.713
5.02	0.864	0.418	0.343	0.411	0.947	0.202	0.429	0.918	0.235	0.452	0.608	0.652	0.690	0.682
5.49	0.863	0.389	0.314	0.394	0.946	0.182	0.412	0.919	0.235	0.440	0.592	0.627	0.662	0.653
5.87	0.863	0.388	0.306	0.396	0.947	0.171	0.409	0.918	0.235	0.438	0.587	0.622	0.656	0.648

Table 9. Nozzle Internal Static Pressure Ratios for Configuration 7

Upper flap											Lower flap			
NPR	PR <sub>54</sub>	PR <sub>55</sub>	PR <sub>56</sub>	PR <sub>57</sub>	PR <sub>58</sub>	PR <sub>59</sub>	PR <sub>60</sub>	PR <sub>61</sub>	PR <sub>62</sub>	PR <sub>63</sub>	PR <sub>46</sub>	PR <sub>47</sub>	PR <sub>48</sub>	PR <sub>49</sub>
1.49	0.712	0.697	0.693	0.722	0.766	0.744	0.749	0.751	0.712	0.670	0.676	0.680	0.688	0.711
1.80	0.600	0.573	0.575	0.594	0.680	0.627	0.629	0.651	0.616	0.557	0.580	0.586	0.593	0.606
1.99	0.550	0.551	0.573	0.506	0.632	0.604	0.574	0.579	0.633	0.503	0.548	0.556	0.561	0.569
2.50	0.512	0.512	0.510	0.461	0.514	0.483	0.488	0.500	0.508	0.399	0.371	0.373	0.368	0.411
3.00	0.472	0.468	0.461	0.427	0.463	0.436	0.437	0.458	0.451	0.334	0.261	0.233	0.187	0.300
3.49	0.445	0.440	0.434	0.398	0.435	0.407	0.410	0.430	0.422	0.287	0.172	0.175	0.177	0.195
4.00	0.433	0.429	0.423	0.386	0.421	0.394	0.397	0.419	0.410	0.250	0.173	0.175	0.177	0.181
4.53	0.427	0.423	0.417	0.380	0.414	0.388	0.391	0.414	0.404	0.221	0.173	0.175	0.177	0.175
5.01	0.423	0.419	0.412	0.376	0.409	0.384	0.388	0.411	0.401	0.200	0.173	0.175	0.178	0.172
5.51	0.418	0.414	0.406	0.372	0.405	0.381	0.384	0.408	0.398	0.182	0.173	0.175	0.177	0.170
6.06	0.412	0.408	0.399	0.366	0.401	0.378	0.381	0.403	0.395	0.166	0.172	0.175	0.177	0.168
Right sidewall											Left sidewall			
NPR	PR <sub>26</sub>	PR <sub>27</sub>	PR <sub>28</sub>	PR <sub>29</sub>	PR <sub>30</sub>	PR <sub>31</sub>	PR <sub>32</sub>	PR <sub>33</sub>	PR <sub>34</sub>	PR <sub>35</sub>	PR <sub>21</sub>	PR <sub>22</sub>	PR <sub>23</sub>	PR <sub>24</sub>
1.49	0.714	0.687	0.721	0.737	0.644	0.718	0.719	0.689	0.663	0.739	0.696	0.654	0.764	0.635
1.80	0.595	0.562	0.620	0.646	0.477	0.608	0.621	0.657	0.543	0.638	0.658	0.543	0.671	0.498
1.99	0.536	0.532	0.508	0.585	0.472	0.535	0.555	0.654	0.415	0.586	0.655	0.531	0.584	0.456
2.50	0.427	0.402	0.452	0.502	0.420	0.396	0.498	0.652	0.281	0.448	0.647	0.342	0.513	0.272
3.00	0.356	0.283	0.454	0.471	0.414	0.227	0.399	0.651	0.276	0.305	0.647	0.277	0.470	0.271
3.49	0.308	0.278	0.432	0.433	0.415	0.207	0.350	0.650	0.274	0.243	0.647	0.276	0.433	0.270
4.00	0.269	0.278	0.421	0.416	0.415	0.207	0.336	0.650	0.274	0.229	0.647	0.274	0.416	0.268
4.53	0.237	0.277	0.416	0.410	0.416	0.207	0.328	0.650	0.274	0.223	0.647	0.274	0.408	0.268
5.01	0.213	0.277	0.412	0.405	0.416	0.207	0.321	0.650	0.274	0.219	0.646	0.275	0.403	0.269
5.51	0.194	0.277	0.408	0.402	0.416	0.206	0.313	0.650	0.274	0.215	0.646	0.274	0.399	0.269
6.06	0.176	0.276	0.403	0.398	0.415	0.206	0.305	0.649	0.274	0.212	0.646	0.274	0.396	0.268
Lower throat insert											Aft-hood deflector			
NPR	PR <sub>36</sub>	PR <sub>37</sub>	PR <sub>38</sub>	PR <sub>39</sub>	PR <sub>40</sub>	PR <sub>41</sub>	PR <sub>42</sub>	PR <sub>43</sub>	PR <sub>44</sub>	PR <sub>45</sub>	PR <sub>64</sub>	PR <sub>65</sub>	PR <sub>66</sub>	PR <sub>67</sub>
1.49	0.820	0.596	0.432	0.636	0.869	0.673	0.658	0.841	0.364	0.601	0.779	0.746	0.791	0.721
1.80	0.810	0.468	0.219	0.555	0.865	0.559	0.578	0.834	0.230	0.475	0.684	0.654	0.715	0.616
1.99	0.810	0.333	0.210	0.399	0.864	0.505	0.462	0.833	0.217	0.419	0.725	0.717	0.582	0.539
2.50	0.810	0.323	0.208	0.337	0.864	0.402	0.319	0.834	0.217	0.274	0.643	0.734	0.500	0.483
3.00	0.811	0.323	0.207	0.336	0.866	0.335	0.320	0.833	0.216	0.271	0.601	0.735	0.447	0.441
3.49	0.812	0.322	0.207	0.336	0.866	0.288	0.320	0.834	0.216	0.268	0.544	0.698	0.429	0.370
4.00	0.811	0.324	0.206	0.335	0.866	0.252	0.319	0.834	0.216	0.269	0.515	0.674	0.424	0.326
4.53	0.812	0.324	0.206	0.334	0.865	0.222	0.319	0.834	0.215	0.268	0.499	0.663	0.420	0.326
5.01	0.812	0.324	0.205	0.334	0.866	0.201	0.319	0.834	0.214	0.268	0.489	0.662	0.417	0.343
5.51	0.811	0.324	0.204	0.334	0.866	0.183	0.319	0.834	0.214	0.267	0.482	0.659	0.413	0.371
6.06	0.811	0.324	0.204	0.334	0.865	0.166	0.318	0.833	0.214	0.266	0.476	0.653	0.409	0.387

Table 10. Nozzle Internal Static Pressure Ratios for Configuration 8

Upper flap											Lower flap			
NPR	PR <sub>54</sub>	PR <sub>55</sub>	PR <sub>56</sub>	PR <sub>57</sub>	PR <sub>58</sub>	PR <sub>59</sub>	PR <sub>60</sub>	PR <sub>61</sub>	PR <sub>62</sub>	PR <sub>63</sub>	PR <sub>46</sub>	PR <sub>47</sub>	PR <sub>48</sub>	PR <sub>49</sub>
1.51	0.832	0.831	0.832	0.841	0.863	0.851	0.848	0.850	0.835	0.663	0.770	0.769	0.773	0.801
1.81	0.777	0.774	0.775	0.782	0.813	0.798	0.795	0.797	0.785	0.554	0.701	0.701	0.708	0.743
2.00	0.752	0.745	0.745	0.753	0.789	0.772	0.769	0.773	0.763	0.499	0.670	0.672	0.680	0.715
2.51	0.701	0.692	0.696	0.702	0.745	0.725	0.722	0.729	0.720	0.399	0.621	0.627	0.636	0.671
2.99	0.677	0.666	0.666	0.670	0.721	0.694	0.697	0.703	0.696	0.334	0.600	0.608	0.616	0.646
3.49	0.662	0.652	0.651	0.643	0.706	0.678	0.682	0.687	0.681	0.287	0.589	0.597	0.606	0.632
3.98	0.651	0.643	0.644	0.620	0.694	0.672	0.673	0.677	0.667	0.251	0.584	0.590	0.602	0.628
4.21	0.646	0.639	0.643	0.612	0.691	0.670	0.670	0.674	0.664	0.238	0.582	0.588	0.600	0.628
Right sidewall											Left sidewall			
NPR	PR <sub>26</sub>	PR <sub>27</sub>	PR <sub>28</sub>	PR <sub>29</sub>	PR <sub>30</sub>	PR <sub>31</sub>	PR <sub>32</sub>	PR <sub>33</sub>	PR <sub>34</sub>	PR <sub>35</sub>	PR <sub>21</sub>	PR <sub>22</sub>	PR <sub>23</sub>	PR <sub>24</sub>
1.51	0.693	0.811	0.846	0.858	0.784	0.830	0.831	0.778	0.790	0.834	0.787	0.811	0.861	0.788
1.81	0.579	0.747	0.792	0.803	0.712	0.775	0.774	0.717	0.722	0.779	0.740	0.741	0.808	0.721
2.00	0.525	0.717	0.765	0.776	0.674	0.748	0.749	0.693	0.689	0.754	0.716	0.704	0.783	0.685
2.51	0.418	0.661	0.719	0.730	0.606	0.697	0.703	0.668	0.618	0.708	0.687	0.643	0.738	0.610
2.99	0.351	0.629	0.697	0.707	0.566	0.670	0.680	0.660	0.579	0.679	0.674	0.610	0.715	0.564
3.49	0.302	0.604	0.682	0.694	0.531	0.649	0.663	0.655	0.562	0.662	0.669	0.592	0.700	0.541
3.98	0.264	0.588	0.664	0.685	0.522	0.631	0.650	0.654	0.579	0.661	0.670	0.596	0.679	0.540
4.21	0.250	0.584	0.657	0.681	0.521	0.625	0.644	0.654	0.579	0.658	0.671	0.598	0.672	0.540
Lower throat insert											Aft-hood deflector			
NPR	PR <sub>36</sub>	PR <sub>37</sub>	PR <sub>38</sub>	PR <sub>39</sub>	PR <sub>40</sub>	PR <sub>41</sub>	PR <sub>42</sub>	PR <sub>43</sub>	PR <sub>44</sub>	PR <sub>45</sub>	PR <sub>64</sub>	PR <sub>65</sub>	PR <sub>66</sub>	PR <sub>67</sub>
1.51	0.860	0.770	0.544	0.792	0.897	0.668	0.795	0.874	0.588	0.763	0.860	0.748	0.832	0.754
1.81	0.835	0.687	0.464	0.714	0.879	0.556	0.728	0.852	0.451	0.687	0.812	0.672	0.790	0.693
2.00	0.827	0.637	0.439	0.671	0.875	0.502	0.695	0.846	0.388	0.647	0.792	0.641	0.769	0.664
2.51	0.818	0.553	0.382	0.598	0.869	0.401	0.627	0.839	0.310	0.567	0.765	0.608	0.739	0.627
2.99	0.815	0.514	0.293	0.573	0.868	0.337	0.609	0.837	0.268	0.525	0.736	0.579	0.727	0.614
3.49	0.814	0.495	0.244	0.561	0.867	0.289	0.606	0.836	0.246	0.505	0.726	0.568	0.709	0.597
3.98	0.813	0.489	0.223	0.564	0.867	0.253	0.597	0.836	0.238	0.500	0.723	0.564	0.701	0.589
4.21	0.814	0.490	0.218	0.566	0.867	0.239	0.593	0.836	0.236	0.498	0.726	0.565	0.699	0.587

Table 11. Nozzle Internal Static Pressure Ratios for Configuration 9

NPR	Upper flap										Lower flap					
	PR <sub>54</sub>	PR <sub>55</sub>	PR <sub>56</sub>	PR <sub>57</sub>	PR <sub>58</sub>	PR <sub>59</sub>	PR <sub>60</sub>	PR <sub>61</sub>	PR <sub>62</sub>	PR <sub>63</sub>	PR <sub>46</sub>	PR <sub>47</sub>	PR <sub>48</sub>	PR <sub>49</sub>		
1.51	0.874	0.877	0.880	0.878	0.893	0.886	0.885	0.886	0.874	0.664	0.810	0.809	0.813	0.842		
1.81	0.838	0.842	0.842	0.841	0.859	0.851	0.852	0.853	0.833	0.553	0.757	0.757	0.762	0.793		
2.01	0.820	0.824	0.822	0.823	0.844	0.835	0.836	0.838	0.817	0.499	0.735	0.735	0.740	0.769		
2.53	0.792	0.793	0.791	0.793	0.812	0.800	0.803	0.807	0.789	0.395	0.697	0.699	0.703	0.734		
3.03	0.768	0.766	0.767	0.774	0.794	0.778	0.779	0.784	0.775	0.330	0.676	0.681	0.683	0.714		
3.50	0.744	0.741	0.745	0.763	0.783	0.762	0.761	0.765	0.769	0.286	0.666	0.671	0.670	0.700		
4.00	0.728	0.726	0.728	0.756	0.773	0.747	0.751	0.753	0.764	0.251	0.658	0.664	0.662	0.690		
4.25	0.722	0.720	0.720	0.752	0.770	0.741	0.745	0.747	0.762	0.236	0.655	0.662	0.659	0.685		
Right sidewall										Left sidewall						
NPR	PR <sub>26</sub>	PR <sub>27</sub>	PR <sub>28</sub>	PR <sub>29</sub>	PR <sub>30</sub>	PR <sub>31</sub>	PR <sub>32</sub>	PR <sub>33</sub>	PR <sub>34</sub>	PR <sub>35</sub>	PR <sub>21</sub>	PR <sub>22</sub>	PR <sub>23</sub>	PR <sub>24</sub>		
1.51	0.691	0.856	0.881	0.890	0.834	0.869	0.870	0.831	0.839	0.865	0.840	0.863	0.889	0.842		
1.81	0.575	0.812	0.845	0.854	0.781	0.828	0.826	0.777	0.789	0.824	0.791	0.816	0.854	0.792		
2.01	0.519	0.789	0.831	0.838	0.756	0.809	0.809	0.750	0.764	0.806	0.765	0.794	0.839	0.765		
2.53	0.411	0.749	0.803	0.809	0.708	0.775	0.779	0.706	0.724	0.776	0.730	0.751	0.807	0.724		
3.03	0.344	0.726	0.781	0.789	0.688	0.753	0.761	0.690	0.702	0.759	0.713	0.720	0.787	0.695		
3.50	0.299	0.711	0.768	0.777	0.673	0.738	0.749	0.681	0.684	0.747	0.700	0.700	0.776	0.670		
4.00	0.261	0.701	0.760	0.769	0.661	0.729	0.740	0.676	0.671	0.737	0.689	0.686	0.766	0.643		
4.25	0.246	0.697	0.757	0.766	0.656	0.725	0.736	0.674	0.665	0.734	0.683	0.679	0.764	0.630		
Lower throat insert										Aft-hood deflector						
NPR	PR <sub>36</sub>	PR <sub>37</sub>	PR <sub>38</sub>	PR <sub>39</sub>	PR <sub>40</sub>	PR <sub>41</sub>	PR <sub>42</sub>	PR <sub>43</sub>	PR <sub>44</sub>	PR <sub>45</sub>	PR <sub>64</sub>	PR <sub>65</sub>	PR <sub>66</sub>	PR <sub>67</sub>	PR <sub>68</sub>	PR <sub>69</sub>
1.51	0.887	0.824	0.597	0.834	0.916	0.615	0.841	0.899	0.688	0.822	0.904	0.928	0.931	0.919	0.891	0.768
1.81	0.862	0.771	0.544	0.786	0.898	0.492	0.795	0.875	0.580	0.766	0.866	0.891	0.902	0.889	0.854	0.703
2.01	0.853	0.747	0.515	0.765	0.891	0.452	0.774	0.865	0.527	0.737	0.848	0.871	0.884	0.871	0.834	0.674
2.53	0.838	0.702	0.462	0.722	0.881	0.405	0.736	0.853	0.442	0.690	0.815	0.842	0.859	0.846	0.808	0.643
3.03	0.831	0.675	0.413	0.699	0.876	0.377	0.711	0.846	0.399	0.655	0.797	0.827	0.842	0.829	0.791	0.629
3.50	0.828	0.663	0.385	0.686	0.874	0.350	0.698	0.843	0.382	0.627	0.785	0.819	0.827	0.813	0.775	0.617
4.00	0.827	0.656	0.364	0.681	0.874	0.251	0.692	0.842	0.390	0.601	0.773	0.805	0.809	0.795	0.757	0.600
4.25	0.826	0.652	0.353	0.678	0.873	0.236	0.688	0.841	0.400	0.590	0.768	0.798	0.803	0.788	0.751	0.595

Table 12. Nozzle Internal Static Pressure Ratios for Configuration 10

NPR	Upper flap										Lower flap			
	PR <sub>54</sub>	PR <sub>55</sub>	PR <sub>56</sub>	PR <sub>57</sub>	PR <sub>58</sub>	PR <sub>59</sub>	PR <sub>60</sub>	PR <sub>61</sub>	PR <sub>62</sub>	PR <sub>63</sub>	PR <sub>46</sub>	PR <sub>47</sub>	PR <sub>48</sub>	PR <sub>49</sub>
1.50	0.764	0.753	0.763	0.788	0.829	0.765	0.750	0.785	0.766	0.667	0.710	0.701	0.697	0.715
1.81	0.653	0.643	0.673	0.711	0.736	0.683	0.653	0.690	0.692	0.553	0.620	0.606	0.603	0.614
2.00	0.595	0.595	0.631	0.623	0.652	0.623	0.608	0.624	0.643	0.499	0.564	0.557	0.543	0.507
2.52	0.547	0.549	0.543	0.527	0.557	0.546	0.549	0.554	0.553	0.397	0.354	0.317	0.243	0.322
3.00	0.528	0.527	0.520	0.492	0.531	0.520	0.527	0.533	0.524	0.333	0.290	0.268	0.233	0.292
3.50	0.511	0.512	0.505	0.489	0.518	0.514	0.515	0.516	0.520	0.286	0.214	0.223	0.230	0.275
4.00	0.506	0.506	0.500	0.483	0.513	0.510	0.510	0.511	0.516	0.250	0.214	0.224	0.231	0.272
4.51	0.501	0.501	0.495	0.476	0.507	0.506	0.507	0.507	0.511	0.222	0.214	0.223	0.231	0.272
5.00	0.496	0.496	0.491	0.470	0.503	0.502	0.503	0.502	0.507	0.201	0.214	0.223	0.231	0.271
5.50	0.492	0.491	0.485	0.463	0.497	0.497	0.499	0.498	0.503	0.182	0.214	0.223	0.231	0.271
Right sidewall										Left sidewall				
NPR	PR <sub>26</sub>	PR <sub>27</sub>	PR <sub>28</sub>	PR <sub>29</sub>	PR <sub>30</sub>	PR <sub>31</sub>	PR <sub>32</sub>	PR <sub>33</sub>	PR <sub>34</sub>	PR <sub>35</sub>	PR <sub>21</sub>	PR <sub>22</sub>	PR <sub>23</sub>	PR <sub>24</sub>
1.50	0.719	0.696	0.787	0.836	0.711	0.740	0.760	0.743	0.684	0.750	0.742	0.684	0.835	0.678
1.81	0.597	0.538	0.714	0.755	0.620	0.637	0.679	0.686	0.509	0.661	0.684	0.514	0.757	0.508
2.00	0.538	0.490	0.637	0.660	0.616	0.485	0.604	0.683	0.490	0.576	0.682	0.482	0.662	0.491
2.52	0.427	0.488	0.530	0.563	0.616	0.395	0.426	0.681	0.489	0.385	0.682	0.478	0.565	0.486
3.00	0.359	0.496	0.494	0.532	0.618	0.399	0.390	0.682	0.490	0.379	0.682	0.478	0.533	0.486
3.50	0.309	0.495	0.480	0.528	0.618	0.394	0.372	0.682	0.490	0.360	0.682	0.477	0.529	0.486
4.00	0.270	0.493	0.473	0.523	0.618	0.393	0.364	0.681	0.489	0.359	0.682	0.477	0.523	0.486
4.51	0.239	0.493	0.466	0.519	0.618	0.394	0.356	0.682	0.489	0.357	0.681	0.476	0.519	0.486
5.00	0.216	0.493	0.459	0.514	0.618	0.393	0.347	0.682	0.489	0.357	0.681	0.476	0.512	0.486
5.50	0.196	0.492	0.451	0.508	0.618	0.393	0.337	0.682	0.488	0.356	0.681	0.475	0.505	0.485
Lower throat insert										Aft-hood deflector				
NPR	PR <sub>36</sub>	PR <sub>37</sub>	PR <sub>38</sub>	PR <sub>39</sub>	PR <sub>40</sub>	PR <sub>41</sub>	PR <sub>42</sub>	PR <sub>43</sub>	PR <sub>44</sub>	PR <sub>45</sub>	PR <sub>64</sub>	PR <sub>65</sub>	PR <sub>66</sub>	PR <sub>67</sub>
1.50	0.781	0.686	0.612	0.584	0.687	0.719	0.632	0.811	0.620	0.687	0.862	0.838	0.725	0.761
1.81	0.762	0.531	0.529	0.323	0.575	0.643	0.362	0.780	0.479	0.557	0.798	0.798	0.638	0.669
2.00	0.761	0.395	0.517	0.310	0.351	0.640	0.318	0.778	0.472	0.383	0.724	0.758	0.594	0.601
2.52	0.761	0.381	0.514	0.310	0.331	0.645	0.319	0.779	0.470	0.278	0.597	0.620	0.562	0.519
3.00	0.762	0.379	0.514	0.310	0.330	0.668	0.320	0.779	0.470	0.273	0.570	0.569	0.551	0.489
3.50	0.762	0.381	0.515	0.312	0.329	0.714	0.321	0.781	0.471	0.269	0.554	0.556	0.534	0.411
4.00	0.762	0.380	0.518	0.313	0.329	0.717	0.320	0.781	0.472	0.268	0.546	0.544	0.529	0.442
4.51	0.762	0.380	0.522	0.315	0.329	0.679	0.321	0.781	0.473	0.267	0.538	0.535	0.534	0.477
5.00	0.762	0.381	0.525	0.311	0.329	0.674	0.322	0.782	0.474	0.266	0.532	0.528	0.534	0.488
5.50	0.762	0.381	0.541	0.310	0.328	0.684	0.321	0.782	0.474	0.266	0.524	0.520	0.533	0.422

Table 13. Nozzle Internal Static Pressure Ratios for Configuration 11

Upper flap											Lower flap				
NPR	PR <sub>54</sub>	PR <sub>55</sub>	PR <sub>56</sub>	PR <sub>57</sub>	PR <sub>58</sub>	PR <sub>59</sub>	PR <sub>60</sub>	PR <sub>61</sub>	PR <sub>62</sub>	PR <sub>63</sub>	PR <sub>46</sub>	PR <sub>47</sub>	PR <sub>48</sub>	PR <sub>49</sub>	
1.51	0.869	0.860	0.862	0.877	0.887	0.851	0.855	0.876	0.860	0.663	0.797	0.791	0.784	0.796	
1.80	0.834	0.822	0.822	0.840	0.859	0.809	0.814	0.844	0.820	0.556	0.747	0.737	0.729	0.741	
2.01	0.816	0.803	0.802	0.822	0.845	0.788	0.794	0.827	0.799	0.497	0.724	0.714	0.703	0.716	
2.03	0.814	0.802	0.803	0.822	0.843	0.788	0.793	0.826	0.798	0.494	0.723	0.712	0.702	0.715	
2.50	0.782	0.767	0.771	0.795	0.826	0.755	0.760	0.800	0.768	0.400	0.696	0.682	0.670	0.683	
3.02	0.760	0.746	0.753	0.780	0.815	0.739	0.742	0.785	0.752	0.331	0.682	0.667	0.653	0.666	
3.51	0.746	0.733	0.742	0.770	0.809	0.730	0.732	0.774	0.743	0.286	0.674	0.659	0.645	0.657	
3.78	0.741	0.728	0.738	0.767	0.806	0.726	0.728	0.770	0.739	0.265	0.670	0.654	0.641	0.654	
Right sidewall											Left sidewall				
NPR	PR <sub>26</sub>	PR <sub>27</sub>	PR <sub>28</sub>	PR <sub>29</sub>	PR <sub>30</sub>	PR <sub>31</sub>	PR <sub>32</sub>	PR <sub>33</sub>	PR <sub>34</sub>	PR <sub>35</sub>	PR <sub>21</sub>	PR <sub>22</sub>	PR <sub>23</sub>	PR <sub>24</sub>	
1.51	0.674	0.824	0.869	0.898	0.831	0.844	0.847	0.844	0.814	0.835	0.840	0.822	0.900	0.810	
1.80	0.566	0.772	0.837	0.873	0.783	0.800	0.807	0.800	0.759	0.790	0.796	0.767	0.872	0.755	
2.01	0.507	0.746	0.819	0.861	0.760	0.777	0.786	0.778	0.732	0.767	0.776	0.738	0.860	0.727	
2.03	0.502	0.744	0.818	0.861	0.758	0.776	0.783	0.778	0.731	0.766	0.774	0.737	0.858	0.724	
2.50	0.407	0.706	0.795	0.843	0.726	0.745	0.757	0.752	0.692	0.737	0.748	0.697	0.842	0.684	
3.02	0.338	0.682	0.780	0.833	0.706	0.726	0.739	0.736	0.666	0.720	0.734	0.670	0.829	0.657	
3.51	0.292	0.664	0.771	0.826	0.694	0.714	0.729	0.728	0.650	0.709	0.725	0.653	0.822	0.641	
3.78	0.271	0.657	0.768	0.824	0.689	0.709	0.725	0.725	0.642	0.705	0.722	0.645	0.818	0.634	
Lower throat insert											Aft-hood deflector				
NPR	PR <sub>36</sub>	PR <sub>37</sub>	PR <sub>38</sub>	PR <sub>39</sub>	PR <sub>40</sub>	PR <sub>41</sub>	PR <sub>42</sub>	PR <sub>43</sub>	PR <sub>44</sub>	PR <sub>45</sub>	PR <sub>64</sub>	PR <sub>65</sub>	PR <sub>66</sub>	PR <sub>67</sub>	PR <sub>68</sub>
1.51	0.855	0.811	0.792	0.763	0.807	0.855	0.783	0.885	0.772	0.797	0.897	0.772	0.819	0.734	0.802
1.80	0.821	0.763	0.726	0.694	0.757	0.804	0.722	0.857	0.707	0.740	0.870	0.716	0.769	0.660	0.747
2.01	0.807	0.738	0.689	0.662	0.733	0.780	0.692	0.846	0.674	0.713	0.857	0.691	0.745	0.623	0.721
2.03	0.806	0.736	0.687	0.659	0.731	0.778	0.690	0.845	0.673	0.712	0.858	0.691	0.745	0.622	0.720
2.50	0.792	0.708	0.643	0.617	0.701	0.747	0.651	0.831	0.627	0.675	0.843	0.665	0.714	0.578	0.687
3.02	0.786	0.690	0.617	0.593	0.683	0.731	0.628	0.823	0.599	0.654	0.834	0.651	0.699	0.560	0.669
3.51	0.784	0.679	0.605	0.577	0.674	0.725	0.614	0.820	0.583	0.642	0.827	0.644	0.690	0.551	0.658
3.78	0.782	0.674	0.598	0.568	0.669	0.723	0.607	0.818	0.574	0.637	0.824	0.640	0.687	0.548	0.653

Table 14. Nozzle Internal Static Pressure Ratios for Configuration 12

NPR	Upper flap										Lower flap			
	PR <sub>54</sub>	PR <sub>55</sub>	PR <sub>56</sub>	PR <sub>57</sub>	PR <sub>58</sub>	PR <sub>59</sub>	PR <sub>60</sub>	PR <sub>61</sub>	PR <sub>62</sub>	PR <sub>63</sub>	PR <sub>46</sub>	PR <sub>47</sub>	PR <sub>48</sub>	PR <sub>49</sub>
1.50	0.903	0.898	0.897	0.906	0.914	0.887	0.893	0.908	0.894	0.665	0.835	0.829	0.823	0.832
1.81	0.876	0.869	0.866	0.878	0.890	0.855	0.861	0.882	0.861	0.552	0.791	0.783	0.775	0.785
2.01	0.865	0.856	0.853	0.865	0.881	0.842	0.847	0.871	0.847	0.499	0.773	0.764	0.755	0.766
2.51	0.844	0.832	0.829	0.843	0.870	0.819	0.822	0.852	0.821	0.399	0.747	0.735	0.723	0.736
3.02	0.831	0.817	0.815	0.829	0.863	0.806	0.806	0.840	0.805	0.332	0.732	0.719	0.707	0.720
3.50	0.820	0.804	0.804	0.821	0.860	0.797	0.794	0.832	0.797	0.286	0.725	0.710	0.697	0.710
3.89	0.810	0.794	0.797	0.815	0.858	0.791	0.786	0.826	0.791	0.257	0.721	0.705	0.691	0.705
Right sidewall														
NPR	PR <sub>26</sub>	PR <sub>27</sub>	PR <sub>28</sub>	PR <sub>29</sub>	PR <sub>30</sub>	PR <sub>31</sub>	PR <sub>32</sub>	PR <sub>33</sub>	PR <sub>34</sub>	PR <sub>35</sub>	PR <sub>21</sub>	PR <sub>22</sub>	PR <sub>23</sub>	PR <sub>24</sub>
1.50	0.689	0.869	0.899	0.920	0.872	0.881	0.881	0.882	0.860	0.870	0.882	0.863	0.925	0.854
1.81	0.572	0.826	0.872	0.899	0.833	0.844	0.847	0.845	0.817	0.832	0.846	0.822	0.903	0.807
2.01	0.517	0.809	0.861	0.890	0.817	0.827	0.831	0.831	0.797	0.816	0.830	0.803	0.893	0.790
2.51	0.414	0.778	0.840	0.876	0.791	0.802	0.808	0.806	0.765	0.791	0.803	0.769	0.879	0.756
3.02	0.345	0.760	0.829	0.867	0.776	0.787	0.793	0.792	0.746	0.776	0.787	0.749	0.871	0.736
3.50	0.298	0.749	0.822	0.862	0.766	0.777	0.785	0.784	0.735	0.767	0.779	0.735	0.866	0.723
3.89	0.268	0.741	0.817	0.859	0.761	0.771	0.779	0.780	0.727	0.761	0.773	0.727	0.862	0.714
Lower throat insert														
NPR	PR <sub>36</sub>	PR <sub>37</sub>	PR <sub>38</sub>	PR <sub>39</sub>	PR <sub>40</sub>	PR <sub>41</sub>	PR <sub>42</sub>	PR <sub>43</sub>	PR <sub>44</sub>	PR <sub>45</sub>	PR <sub>64</sub>	PR <sub>65</sub>	PR <sub>66</sub>	PR <sub>67</sub>
1.50	0.881	0.855	0.845	0.822	0.851	0.891	0.831	0.910	0.832	0.839	0.917	0.938	0.938	0.928
1.81	0.851	0.815	0.793	0.766	0.809	0.855	0.784	0.883	0.784	0.791	0.893	0.920	0.919	0.905
2.01	0.839	0.797	0.771	0.743	0.791	0.838	0.762	0.871	0.762	0.773	0.884	0.914	0.912	0.897
2.51	0.821	0.771	0.730	0.703	0.762	0.809	0.727	0.853	0.724	0.738	0.871	0.908	0.903	0.885
3.02	0.811	0.755	0.708	0.680	0.746	0.796	0.706	0.842	0.703	0.720	0.864	0.903	0.897	0.879
3.50	0.808	0.746	0.694	0.667	0.736	0.789	0.693	0.835	0.689	0.708	0.863	0.904	0.894	0.875
3.89	0.805	0.741	0.688	0.660	0.730	0.786	0.685	0.832	0.679	0.701	0.861	0.904	0.893	0.873
Aft-hood deflector														
NPR	PR <sub>68</sub>	PR <sub>69</sub>	PR <sub>64</sub>	PR <sub>65</sub>	PR <sub>66</sub>	PR <sub>67</sub>	PR <sub>68</sub>	PR <sub>69</sub>	PR <sub>64</sub>	PR <sub>65</sub>	PR <sub>66</sub>	PR <sub>67</sub>	PR <sub>68</sub>	PR <sub>69</sub>

Table 15. Nozzle Internal Static Pressure Ratios for Configuration 13

NPR	Upper flap										Lower flap					
	PR <sub>54</sub>	PR <sub>55</sub>	PR <sub>56</sub>	PR <sub>57</sub>	PR <sub>58</sub>	PR <sub>59</sub>	PR <sub>60</sub>	PR <sub>61</sub>	PR <sub>62</sub>	PR <sub>63</sub>	PR <sub>46</sub>	PR <sub>47</sub>	PR <sub>48</sub>	PR <sub>49</sub>		
1.50	0.867	0.865	0.865	0.866	0.901	0.874	0.861	0.877	0.877	0.666	0.839	0.837	0.838	0.849		
1.79	0.837	0.833	0.833	0.835	0.881	0.847	0.831	0.848	0.844	0.558	0.802	0.800	0.800	0.814		
1.99	0.824	0.819	0.819	0.822	0.873	0.838	0.819	0.837	0.830	0.502	0.786	0.785	0.785	0.800		
2.52	0.796	0.793	0.799	0.806	0.861	0.825	0.796	0.816	0.811	0.397	0.766	0.765	0.766	0.781		
3.00	0.779	0.777	0.788	0.800	0.858	0.817	0.784	0.806	0.801	0.333	0.758	0.757	0.758	0.775		
3.52	0.768	0.766	0.782	0.795	0.857	0.813	0.776	0.800	0.794	0.285	0.753	0.752	0.753	0.771		
4.01	0.762	0.761	0.778	0.793	0.856	0.811	0.774	0.797	0.792	0.250	0.751	0.750	0.751	0.769		
4.51	0.759	0.758	0.777	0.792	0.856	0.810	0.772	0.795	0.792	0.222	0.749	0.749	0.750	0.768		
5.01	0.759	0.758	0.777	0.792	0.856	0.809	0.772	0.795	0.791	0.200	0.749	0.748	0.750	0.768		
5.26	0.757	0.756	0.777	0.792	0.856	0.809	0.773	0.794	0.792	0.191	0.748	0.748	0.750	0.768		
Right sidewall										Left sidewall						
NPR	PR <sub>26</sub>	PR <sub>27</sub>	PR <sub>28</sub>	PR <sub>29</sub>	PR <sub>30</sub>	PR <sub>31</sub>	PR <sub>32</sub>	PR <sub>33</sub>	PR <sub>34</sub>	PR <sub>35</sub>	PR <sub>21</sub>	PR <sub>22</sub>	PR <sub>23</sub>	PR <sub>24</sub>		
1.50	0.727	0.822	0.864	0.894	0.831	0.847	0.857	0.838	0.820	0.853	0.834	0.815	0.898	0.815		
1.79	0.609	0.775	0.834	0.870	0.786	0.809	0.825	0.797	0.773	0.819	0.794	0.767	0.875	0.767		
1.99	0.547	0.754	0.823	0.860	0.767	0.792	0.811	0.778	0.751	0.806	0.776	0.747	0.864	0.746		
2.52	0.434	0.726	0.806	0.849	0.744	0.771	0.794	0.759	0.723	0.787	0.756	0.720	0.853	0.720		
3.00	0.364	0.717	0.800	0.843	0.735	0.764	0.787	0.751	0.712	0.779	0.751	0.709	0.849	0.709		
3.52	0.310	0.709	0.796	0.841	0.730	0.758	0.783	0.747	0.705	0.774	0.746	0.703	0.845	0.702		
4.01	0.274	0.705	0.794	0.840	0.727	0.756	0.782	0.745	0.702	0.773	0.745	0.700	0.844	0.698		
4.51	0.242	0.703	0.794	0.839	0.725	0.754	0.781	0.744	0.700	0.771	0.744	0.698	0.844	0.697		
5.01	0.218	0.703	0.793	0.839	0.725	0.754	0.780	0.743	0.699	0.771	0.743	0.697	0.843	0.696		
5.26	0.208	0.702	0.793	0.839	0.724	0.753	0.780	0.744	0.698	0.771	0.743	0.697	0.843	0.695		
Lower throat insert										Aft-hood deflector						
NPR	PR <sub>36</sub>	PR <sub>37</sub>	PR <sub>38</sub>	PR <sub>39</sub>	PR <sub>40</sub>	PR <sub>41</sub>	PR <sub>42</sub>	PR <sub>43</sub>	PR <sub>44</sub>	PR <sub>45</sub>	PR <sub>64</sub>	PR <sub>65</sub>	PR <sub>66</sub>	PR <sub>67</sub>	PR <sub>68</sub>	PR <sub>69</sub>
1.50	0.838	0.805	0.773	0.751	0.805	0.844	0.780	0.880	0.786	0.818	0.929	0.848	0.764	0.810	0.667	0.665
1.79	0.807	0.756	0.699	0.678	0.760	0.795	0.722	0.854	0.732	0.775	0.910	0.813	0.697	0.760	0.557	0.557
1.99	0.796	0.737	0.666	0.649	0.739	0.772	0.698	0.843	0.706	0.758	0.903	0.800	0.667	0.738	0.501	0.501
2.52	0.786	0.710	0.626	0.612	0.715	0.746	0.669	0.831	0.675	0.734	0.903	0.787	0.624	0.707	0.397	0.396
3.00	0.784	0.703	0.618	0.603	0.707	0.742	0.659	0.829	0.665	0.726	0.904	0.783	0.610	0.694	0.333	0.332
3.52	0.784	0.697	0.615	0.597	0.702	0.744	0.653	0.827	0.657	0.720	0.905	0.779	0.604	0.685	0.284	0.284
4.01	0.784	0.695	0.617	0.594	0.699	0.745	0.650	0.827	0.654	0.717	0.905	0.777	0.602	0.680	0.250	0.250
4.51	0.783	0.692	0.622	0.592	0.698	0.747	0.648	0.827	0.652	0.716	0.906	0.775	0.602	0.678	0.222	0.221
5.01	0.783	0.691	0.631	0.591	0.698	0.751	0.647	0.825	0.651	0.715	0.906	0.774	0.601	0.679	0.200	0.200
5.26	0.783	0.691	0.636	0.590	0.698	0.753	0.647	0.825	0.651	0.715	0.906	0.774	0.602	0.679	0.191	0.190
Throat area control block																
NPR	PR <sub>70</sub>	PR <sub>71</sub>	PR <sub>72</sub>	PR <sub>73</sub>												
1.50	0.827	0.823	0.824	0.831												
1.79	0.789	0.785	0.786	0.794												
1.99	0.773	0.769	0.770	0.779												
2.52	0.755	0.749	0.751	0.761												
3.00	0.749	0.742	0.744	0.755												
3.52	0.746	0.738	0.740	0.751												
4.01	0.744	0.736	0.738	0.750												
4.51	0.743	0.736	0.738	0.749												
5.01	0.743	0.736	0.738	0.749												
5.26	0.743	0.736	0.737	0.749												

**Table 16. Nozzle Internal Static Pressure Ratios for Configuration 14**

NPR	Upper flap										Lower flap			
	PR <sub>54</sub>	PR <sub>55</sub>	PR <sub>56</sub>	PR <sub>57</sub>	PR <sub>58</sub>	PR <sub>59</sub>	PR <sub>60</sub>	PR <sub>61</sub>	PR <sub>62</sub>	PR <sub>63</sub>	PR <sub>46</sub>	PR <sub>47</sub>	PR <sub>48</sub>	PR <sub>49</sub>
1.50	0.948	0.948	0.947	0.947	0.956	0.946	0.943	0.951	0.948	0.665	0.933	0.931	0.931	0.937
1.80	0.936	0.935	0.935	0.936	0.947	0.932	0.930	0.940	0.936	0.555	0.917	0.915	0.915	0.921
2.00	0.932	0.930	0.930	0.931	0.943	0.927	0.925	0.936	0.931	0.500	0.910	0.909	0.908	0.915
2.50	0.926	0.925	0.924	0.924	0.938	0.920	0.918	0.930	0.926	0.400	0.901	0.900	0.899	0.907
2.65	0.925	0.924	0.923	0.923	0.937	0.920	0.917	0.930	0.925	0.378	0.900	0.899	0.898	0.905
3.02	0.923	0.922	0.921	0.921	0.936	0.918	0.916	0.928	0.923	0.332	0.897	0.896	0.895	0.902
3.53	0.923	0.922	0.920	0.919	0.936	0.917	0.916	0.926	0.921	0.284	0.894	0.893	0.892	0.900
3.99	0.922	0.921	0.919	0.918	0.935	0.917	0.914	0.926	0.920	0.252	0.892	0.892	0.891	0.898
4.52	0.921	0.921	0.919	0.917	0.934	0.917	0.915	0.925	0.918	0.222	0.891	0.890	0.889	0.897
4.71	0.921	0.921	0.918	0.917	0.934	0.916	0.914	0.925	0.918	0.213	0.890	0.890	0.889	0.897

NPR	Right sidewall										Left sidewall			
	PR <sub>26</sub>	PR <sub>27</sub>	PR <sub>28</sub>	PR <sub>29</sub>	PR <sub>30</sub>	PR <sub>31</sub>	PR <sub>32</sub>	PR <sub>33</sub>	PR <sub>34</sub>	PR <sub>35</sub>	PR <sub>21</sub>	PR <sub>22</sub>	PR <sub>23</sub>	PR <sub>24</sub>
1.50	0.708	0.932	0.944	0.957	0.931	0.940	0.941	0.938	0.930	0.940	0.934	0.930	0.959	0.925
1.80	0.591	0.915	0.933	0.948	0.917	0.926	0.928	0.922	0.914	0.926	0.918	0.912	0.949	0.909
2.00	0.533	0.909	0.929	0.945	0.911	0.921	0.922	0.916	0.906	0.922	0.912	0.906	0.947	0.903
2.50	0.427	0.899	0.923	0.941	0.902	0.912	0.915	0.906	0.896	0.912	0.903	0.896	0.941	0.893
2.65	0.403	0.897	0.921	0.941	0.900	0.910	0.913	0.904	0.894	0.911	0.903	0.894	0.941	0.892
3.02	0.354	0.894	0.919	0.939	0.898	0.908	0.911	0.902	0.890	0.908	0.900	0.891	0.940	0.889
3.53	0.304	0.891	0.917	0.939	0.895	0.905	0.909	0.899	0.888	0.906	0.897	0.888	0.938	0.886
3.99	0.268	0.888	0.916	0.937	0.893	0.903	0.908	0.897	0.885	0.904	0.895	0.886	0.937	0.884
4.52	0.237	0.887	0.916	0.937	0.891	0.902	0.907	0.895	0.883	0.903	0.894	0.884	0.937	0.883
4.71	0.227	0.887	0.915	0.937	0.892	0.902	0.906	0.895	0.883	0.902	0.894	0.884	0.937	0.883

NPR	Lower throat insert										Aft-hood deflector					
	PR <sub>36</sub>	PR <sub>37</sub>	PR <sub>38</sub>	PR <sub>39</sub>	PR <sub>40</sub>	PR <sub>41</sub>	PR <sub>42</sub>	PR <sub>43</sub>	PR <sub>44</sub>	PR <sub>45</sub>	PR <sub>64</sub>	PR <sub>65</sub>	PR <sub>66</sub>	PR <sub>67</sub>	PR <sub>68</sub>	PR <sub>69</sub>
1.50	0.932	0.922	0.919	0.903	0.923	0.940	0.914	0.953	0.909	0.924	0.896	0.750	0.862	0.753	0.753	0.664
1.80	0.918	0.905	0.899	0.877	0.906	0.928	0.893	0.942	0.890	0.907	0.870	0.687	0.828	0.689	0.682	0.555
2.00	0.911	0.898	0.891	0.869	0.898	0.922	0.884	0.937	0.881	0.901	0.860	0.665	0.815	0.665	0.650	0.499
2.50	0.904	0.887	0.881	0.854	0.887	0.915	0.873	0.931	0.871	0.891	0.847	0.643	0.799	0.642	0.597	0.399
2.65	0.901	0.884	0.878	0.852	0.885	0.914	0.870	0.931	0.869	0.889	0.845	0.640	0.796	0.638	0.587	0.377
3.02	0.899	0.880	0.875	0.846	0.882	0.911	0.867	0.928	0.865	0.886	0.841	0.634	0.791	0.632	0.566	0.331
3.53	0.896	0.877	0.875	0.842	0.879	0.910	0.863	0.927	0.862	0.884	0.837	0.628	0.788	0.629	0.542	0.283
3.99	0.894	0.875	0.875	0.839	0.877	0.909	0.861	0.926	0.860	0.881	0.834	0.625	0.786	0.626	0.531	0.251
4.52	0.893	0.873	0.876	0.836	0.875	0.908	0.859	0.925	0.859	0.880	0.831	0.622	0.785	0.625	0.526	0.221
4.71	0.892	0.873	0.876	0.835	0.875	0.907	0.858	0.924	0.858	0.879	0.831	0.621	0.784	0.625	0.524	0.212

#### Throat area control block

NPR	PR <sub>70</sub>	PR <sub>71</sub>	PR <sub>72</sub>	PR <sub>73</sub>
1.50	0.915	0.911	0.909	0.914
1.80	0.896	0.891	0.889	0.896
2.00	0.887	0.884	0.881	0.889
2.50	0.881	0.873	0.871	0.879
2.65	0.859	0.871	0.869	0.877
3.02	0.812	0.869	0.866	0.874
3.53	0.818	0.866	0.864	0.871
3.99	0.823	0.864	0.862	0.869
4.52	0.828	0.863	0.861	0.868
4.71	0.828	0.863	0.861	0.868

Table 17. Nozzle Internal Static Pressure Ratios for Configuration 15

Upper flap											Lower flap								
NPR	PR <sub>54</sub>	PR <sub>55</sub>	PR <sub>56</sub>	PR <sub>57</sub>	PR <sub>58</sub>	PR <sub>59</sub>	PR <sub>60</sub>	PR <sub>61</sub>	PR <sub>62</sub>	PR <sub>63</sub>	PR <sub>46</sub>	PR <sub>47</sub>	PR <sub>48</sub>	PR <sub>49</sub>					
1.51	0.960	0.959	0.958	0.957	0.661	0.954	0.956	0.961	0.957	0.668	0.664	0.665	0.666	0.664					
1.81	0.948	0.948	0.946	0.945	0.551	0.941	0.942	0.950	0.946	0.556	0.553	0.554	0.554	0.553					
2.01	0.943	0.943	0.942	0.940	0.496	0.935	0.937	0.945	0.941	0.501	0.498	0.498	0.499	0.498					
2.49	0.936	0.936	0.935	0.933	0.400	0.928	0.929	0.939	0.934	0.403	0.401	0.401	0.402	0.401					
2.99	0.932	0.932	0.931	0.929	0.333	0.924	0.924	0.936	0.932	0.337	0.334	0.335	0.335	0.334					
3.50	0.930	0.930	0.929	0.926	0.285	0.921	0.922	0.933	0.930	0.288	0.286	0.286	0.287	0.286					
4.00	0.929	0.929	0.928	0.924	0.249	0.919	0.921	0.933	0.929	0.252	0.250	0.250	0.250	0.250					
5.29	0.928	0.927	0.925	0.921	0.189	0.917	0.919	0.931	0.928	0.191	0.189	0.189	0.189	0.189					
Right sidewall											Left sidewall								
NPR	PR <sub>26</sub>	PR <sub>27</sub>	PR <sub>28</sub>	PR <sub>29</sub>	PR <sub>30</sub>	PR <sub>31</sub>	PR <sub>32</sub>	PR <sub>33</sub>	PR <sub>34</sub>	PR <sub>35</sub>	PR <sub>21</sub>	PR <sub>22</sub>	PR <sub>23</sub>	PR <sub>24</sub>					
1.51	0.683	0.954	0.954	0.971	0.948	0.954	0.952	0.950	0.944	0.956	0.952	0.950	0.972	0.954					
1.81	0.569	0.936	0.943	0.962	0.934	0.940	0.940	0.935	0.928	0.941	0.938	0.932	0.961	0.936					
2.01	0.512	0.930	0.940	0.959	0.929	0.934	0.934	0.930	0.921	0.935	0.931	0.925	0.959	0.929					
2.49	0.413	0.918	0.933	0.953	0.918	0.925	0.926	0.921	0.910	0.926	0.922	0.914	0.952	0.917					
2.99	0.344	0.911	0.929	0.950	0.913	0.920	0.922	0.914	0.904	0.921	0.916	0.907	0.949	0.910					
3.50	0.294	0.907	0.927	0.947	0.909	0.916	0.918	0.910	0.900	0.918	0.911	0.902	0.947	0.905					
4.00	0.258	0.903	0.926	0.946	0.906	0.914	0.917	0.908	0.898	0.915	0.909	0.900	0.945	0.901					
5.29	0.195	0.899	0.924	0.944	0.902	0.910	0.913	0.904	0.893	0.911	0.904	0.895	0.942	0.896					
Lower throat insert											Aft-hood deflector								
NPR	PR <sub>36</sub>	PR <sub>37</sub>	PR <sub>38</sub>	PR <sub>39</sub>	PR <sub>40</sub>	PR <sub>41</sub>	PR <sub>42</sub>	PR <sub>43</sub>	PR <sub>44</sub>	PR <sub>45</sub>	PR <sub>64</sub>	PR <sub>65</sub>	PR <sub>66</sub>	PR <sub>67</sub>	PR <sub>68</sub>	PR <sub>69</sub>			
1.51	0.669	0.668	0.676	0.929	0.667	0.668	0.670	0.793	0.669	0.945	0.972	0.981	0.941	0.911	0.858	0.732			
1.81	0.558	0.555	0.562	0.905	0.557	0.556	0.556	0.749	0.557	0.928	0.966	0.976	0.923	0.885	0.817	0.661			
2.01	0.502	0.499	0.507	0.896	0.501	0.500	0.501	0.729	0.502	0.920	0.963	0.975	0.915	0.873	0.801	0.638			
2.49	0.405	0.402	0.407	0.879	0.403	0.404	0.404	0.702	0.404	0.909	0.959	0.972	0.902	0.855	0.777	0.617			
2.99	0.338	0.335	0.340	0.870	0.337	0.336	0.336	0.676	0.338	0.901	0.957	0.970	0.892	0.844	0.762	0.607			
3.50	0.289	0.287	0.291	0.863	0.288	0.288	0.288	0.674	0.288	0.896	0.954	0.967	0.884	0.835	0.750	0.599			
4.00	0.253	0.251	0.254	0.858	0.252	0.252	0.251	0.684	0.252	0.893	0.952	0.965	0.883	0.829	0.742	0.595			
5.29	0.191	0.190	0.192	0.851	0.191	0.190	0.190	0.741	0.190	0.888	0.949	0.961	0.886	0.817	0.726	0.585			
Throat area control block																			
NPR	PR <sub>70</sub>	PR <sub>71</sub>	PR <sub>72</sub>	PR <sub>73</sub>															
1.51	0.934	0.930	0.926	0.932															
1.81	0.917	0.912	0.908	0.915															
2.01	0.909	0.904	0.900	0.908															
2.49	0.898	0.892	0.888	0.897															
2.99	0.892	0.886	0.882	0.891															
3.50	0.888	0.883	0.878	0.887															
4.00	0.885	0.880	0.876	0.885															
5.29	0.880	0.876	0.873	0.880															

**Table 18. Nozzle Internal Static Pressure Ratios for Configuration 16**

NPR	Upper flap										Lower flap			
	PR <sub>54</sub>	PR <sub>55</sub>	PR <sub>56</sub>	PR <sub>57</sub>	PR <sub>58</sub>	PR <sub>59</sub>	PR <sub>60</sub>	PR <sub>61</sub>	PR <sub>62</sub>	PR <sub>63</sub>	PR <sub>46</sub>	PR <sub>47</sub>	PR <sub>48</sub>	PR <sub>49</sub>
1.49	0.916	0.912	0.913	0.919	0.928	0.909	0.907	0.921	0.914	0.670	0.886	0.884	0.882	0.889
1.80	0.895	0.891	0.891	0.898	0.912	0.884	0.883	0.902	0.892	0.555	0.858	0.855	0.851	0.861
2.00	0.887	0.882	0.882	0.889	0.906	0.875	0.873	0.895	0.883	0.499	0.846	0.842	0.839	0.849
2.50	0.875	0.870	0.871	0.877	0.897	0.863	0.861	0.883	0.871	0.400	0.829	0.826	0.823	0.833
3.00	0.870	0.865	0.866	0.871	0.892	0.857	0.855	0.878	0.864	0.334	0.821	0.818	0.814	0.825
3.50	0.866	0.863	0.863	0.868	0.890	0.855	0.852	0.875	0.860	0.286	0.816	0.813	0.810	0.820
3.94	0.864	0.861	0.861	0.866	0.888	0.855	0.851	0.873	0.858	0.254	0.814	0.810	0.807	0.818
Right sidewall														
NPR	PR <sub>26</sub>	PR <sub>27</sub>	PR <sub>28</sub>	PR <sub>29</sub>	PR <sub>30</sub>	PR <sub>31</sub>	PR <sub>32</sub>	PR <sub>33</sub>	PR <sub>34</sub>	PR <sub>35</sub>	PR <sub>21</sub>	PR <sub>22</sub>	PR <sub>23</sub>	PR <sub>24</sub>
1.49	0.737	0.891	0.915	0.937	0.891	0.903	0.904	0.898	0.886	0.901	0.896	0.889	0.936	0.881
1.80	0.611	0.861	0.894	0.920	0.865	0.877	0.879	0.871	0.855	0.874	0.871	0.857	0.920	0.851
2.00	0.551	0.848	0.887	0.914	0.853	0.867	0.871	0.860	0.843	0.865	0.860	0.843	0.915	0.837
2.50	0.440	0.828	0.875	0.905	0.836	0.850	0.856	0.842	0.822	0.849	0.844	0.825	0.904	0.819
3.00	0.368	0.819	0.869	0.901	0.828	0.842	0.850	0.834	0.812	0.842	0.835	0.814	0.900	0.810
3.50	0.315	0.812	0.866	0.898	0.821	0.836	0.845	0.829	0.806	0.836	0.830	0.808	0.897	0.803
3.94	0.281	0.809	0.864	0.896	0.819	0.833	0.843	0.826	0.802	0.834	0.827	0.804	0.897	0.800
Lower throat insert														
NPR	PR <sub>36</sub>	PR <sub>37</sub>	PR <sub>38</sub>	PR <sub>39</sub>	PR <sub>40</sub>	PR <sub>41</sub>	PR <sub>42</sub>	PR <sub>43</sub>	PR <sub>44</sub>	PR <sub>45</sub>	PR <sub>64</sub>	PR <sub>65</sub>	PR <sub>66</sub>	PR <sub>67</sub>
1.49	0.899	0.880	0.870	0.847	0.876	0.910	0.860	0.928	0.860	0.878	0.900	0.763	0.846	0.749
1.80	0.874	0.847	0.831	0.805	0.844	0.884	0.824	0.908	0.822	0.846	0.874	0.700	0.804	0.677
2.00	0.865	0.834	0.815	0.787	0.831	0.874	0.809	0.902	0.807	0.833	0.863	0.677	0.788	0.648
2.50	0.848	0.815	0.790	0.761	0.814	0.857	0.788	0.889	0.784	0.814	0.850	0.653	0.766	0.614
3.00	0.841	0.805	0.778	0.747	0.804	0.848	0.776	0.883	0.772	0.804	0.844	0.644	0.756	0.602
3.50	0.836	0.799	0.772	0.739	0.798	0.846	0.769	0.880	0.766	0.798	0.840	0.639	0.751	0.597
3.94	0.833	0.795	0.771	0.733	0.794	0.844	0.765	0.878	0.761	0.794	0.837	0.636	0.748	0.594
Throat area control block														
NPR	PR <sub>70</sub>	PR <sub>71</sub>	PR <sub>72</sub>	PR <sub>73</sub>							PR <sub>68</sub>	PR <sub>69</sub>		
1.49	0.873	0.867	0.860	0.873							0.900	0.763	0.846	0.749
1.80	0.842	0.834	0.826	0.842							0.874	0.700	0.804	0.677
2.00	0.830	0.822	0.813	0.830							0.863	0.677	0.788	0.648
2.50	0.812	0.805	0.795	0.813							0.850	0.653	0.766	0.614
3.00	0.808	0.797	0.786	0.805							0.844	0.644	0.756	0.602
3.50	0.799	0.793	0.781	0.801							0.840	0.639	0.751	0.597
3.94	0.841	0.790	0.779	0.799							0.837	0.636	0.748	0.594

Table 19. Nozzle Internal Static Pressure Ratios for Configuration 17

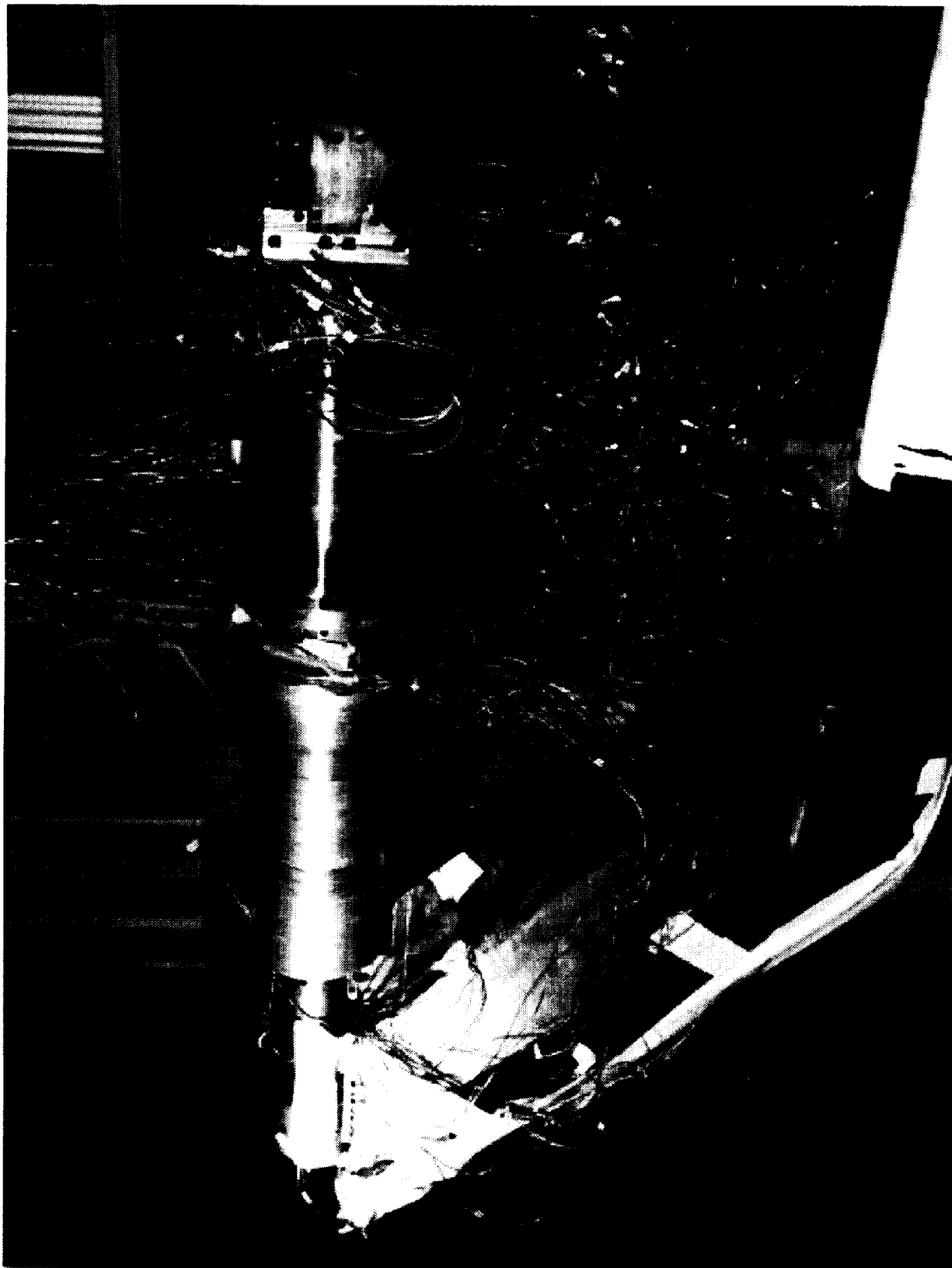
NPR	Upper flap										Lower flap					
	PR <sub>54</sub>	PR <sub>55</sub>	PR <sub>56</sub>	PR <sub>57</sub>	PR <sub>58</sub>	PR <sub>59</sub>	PR <sub>60</sub>	PR <sub>61</sub>	PR <sub>62</sub>	PR <sub>63</sub>	PR <sub>46</sub>	PR <sub>47</sub>	PR <sub>48</sub>	PR <sub>49</sub>		
1.51	0.937	0.936	0.935	0.936	0.661	0.927	0.931	0.940	0.933	0.667	0.664	0.664	0.665	0.663		
1.78	0.921	0.918	0.917	0.920	0.560	0.908	0.911	0.924	0.916	0.566	0.562	0.563	0.564	0.562		
1.99	0.912	0.908	0.909	0.912	0.500	0.898	0.901	0.917	0.907	0.505	0.502	0.502	0.503	0.502		
2.51	0.899	0.896	0.897	0.900	0.396	0.886	0.887	0.905	0.896	0.401	0.398	0.398	0.399	0.398		
2.98	0.894	0.890	0.890	0.892	0.335	0.880	0.879	0.900	0.890	0.338	0.336	0.336	0.337	0.336		
3.50	0.890	0.885	0.886	0.888	0.285	0.876	0.874	0.896	0.886	0.288	0.286	0.286	0.286	0.286		
4.00	0.887	0.883	0.883	0.885	0.249	0.873	0.871	0.893	0.884	0.251	0.250	0.250	0.250	0.249		
4.40	0.886	0.882	0.882	0.883	0.227	0.872	0.869	0.892	0.883	0.229	0.227	0.227	0.227	0.227		
Right sidewall										Left sidewall						
NPR	PR <sub>26</sub>	PR <sub>27</sub>	PR <sub>28</sub>	PR <sub>29</sub>	PR <sub>30</sub>	PR <sub>31</sub>	PR <sub>32</sub>	PR <sub>33</sub>	PR <sub>34</sub>	PR <sub>35</sub>	PR <sub>21</sub>	PR <sub>22</sub>	PR <sub>23</sub>	PR <sub>24</sub>		
1.51	0.688	0.922	0.933	0.955	0.921	0.926	0.925	0.922	0.911	0.925	0.926	0.918	0.956	0.920		
1.78	0.585	0.899	0.918	0.943	0.900	0.907	0.906	0.903	0.889	0.906	0.905	0.893	0.944	0.896		
1.99	0.522	0.886	0.911	0.937	0.889	0.897	0.898	0.892	0.876	0.894	0.894	0.882	0.938	0.884		
2.51	0.414	0.869	0.900	0.928	0.872	0.881	0.883	0.877	0.857	0.879	0.877	0.863	0.927	0.863		
2.98	0.349	0.859	0.894	0.922	0.864	0.873	0.876	0.868	0.848	0.871	0.868	0.851	0.922	0.852		
3.50	0.297	0.851	0.890	0.919	0.857	0.866	0.870	0.862	0.840	0.864	0.861	0.844	0.920	0.844		
4.00	0.260	0.845	0.887	0.916	0.853	0.862	0.867	0.857	0.836	0.861	0.856	0.839	0.917	0.838		
4.40	0.236	0.843	0.885	0.915	0.850	0.860	0.865	0.855	0.833	0.858	0.854	0.836	0.916	0.835		
Lower throat insert										Aft-hood deflector						
NPR	PR <sub>36</sub>	PR <sub>37</sub>	PR <sub>38</sub>	PR <sub>39</sub>	PR <sub>40</sub>	PR <sub>41</sub>	PR <sub>42</sub>	PR <sub>43</sub>	PR <sub>44</sub>	PR <sub>45</sub>	PR <sub>64</sub>	PR <sub>65</sub>	PR <sub>66</sub>	PR <sub>67</sub>	PR <sub>68</sub>	PR <sub>69</sub>
1.51	0.667	0.665	0.674	0.886	0.667	0.667	0.667	0.676	0.670	0.907	0.954	0.970	0.955	0.928	0.885	0.752
1.78	0.567	0.564	0.571	0.855	0.565	0.565	0.567	0.570	0.568	0.884	0.944	0.964	0.943	0.909	0.856	0.695
1.99	0.506	0.505	0.509	0.838	0.504	0.505	0.506	0.508	0.506	0.870	0.939	0.960	0.912	0.899	0.843	0.670
2.51	0.401	0.400	0.404	0.812	0.401	0.400	0.401	0.402	0.401	0.851	0.932	0.957	0.913	0.885	0.824	0.649
2.98	0.339	0.338	0.341	0.798	0.338	0.338	0.339	0.339	0.338	0.841	0.929	0.954	0.908	0.878	0.815	0.642
3.50	0.288	0.287	0.290	0.788	0.288	0.287	0.287	0.289	0.288	0.834	0.928	0.953	0.903	0.872	0.808	0.637
4.00	0.252	0.251	0.254	0.780	0.252	0.251	0.251	0.252	0.252	0.829	0.927	0.953	0.902	0.868	0.802	0.636
4.40	0.229	0.228	0.231	0.776	0.229	0.229	0.228	0.229	0.229	0.826	0.926	0.953	0.894	0.866	0.800	0.634
Throat area control block																
NPR	PR <sub>70</sub>	PR <sub>71</sub>	PR <sub>72</sub>	PR <sub>73</sub>	PR <sub>74</sub>	PR <sub>75</sub>	PR <sub>76</sub>	PR <sub>77</sub>	PR <sub>78</sub>	PR <sub>79</sub>	PR <sub>80</sub>	PR <sub>81</sub>				
1.51	0.667	0.665	0.674	0.886	0.667	0.667	0.667	0.676	0.670	0.907	0.670	0.907				
1.78	0.567	0.564	0.571	0.855	0.565	0.565	0.567	0.570	0.568	0.884	0.568	0.884				
1.99	0.506	0.505	0.509	0.838	0.504	0.505	0.506	0.508	0.506	0.870	0.506	0.870				
2.51	0.401	0.400	0.404	0.812	0.401	0.400	0.401	0.402	0.401	0.851	0.401	0.851				
2.98	0.339	0.338	0.341	0.798	0.338	0.338	0.339	0.339	0.338	0.841	0.338	0.841				
3.50	0.288	0.287	0.290	0.788	0.288	0.287	0.287	0.289	0.288	0.834	0.288	0.834				
4.00	0.252	0.251	0.254	0.780	0.252	0.251	0.251	0.252	0.252	0.829	0.252	0.829				
4.40	0.229	0.228	0.231	0.776	0.229	0.229	0.228	0.229	0.229	0.826	0.229	0.826				

**Table 20. Nozzle Internal Static Pressure Ratios for Configuration 18**

NPR	Upper flap										Lower flap							
	PR54	PR55	PR56	PR57	PR58	PR59	PR60	PR61	PR62	PR63	PR46	PR47	PR48	PR49				
1.57	0.626	0.627	0.645	0.634	0.655	0.632	0.625	0.626	0.631	0.636	0.611	0.627	0.629	0.626				
1.89	0.519	0.518	0.531	0.438	0.554	0.533	0.517	0.518	0.523	0.529	0.499	0.524	0.545	0.498				
2.13	0.458	0.450	0.306	0.359	0.494	0.482	0.457	0.459	0.464	0.470	0.437	0.426	0.320	0.433				
2.71	0.359	0.258	0.226	0.241	0.390	0.419	0.357	0.360	0.364	0.369	0.347	0.215	0.226	0.355				
3.81	0.166	0.192	0.219	0.241	0.148	0.235	0.213	0.245	0.254	0.262	0.169	0.196	0.220	0.257				
4.38	0.161	0.191	0.217	0.240	0.148	0.151	0.107	0.138	0.225	0.228	0.164	0.195	0.220	0.240				
4.93	0.160	0.191	0.216	0.240	0.148	0.097	0.138	0.148	0.203	0.202	0.163	0.194	0.220	0.224				
5.50	0.160	0.190	0.216	0.240	0.148	0.097	0.093	0.145	0.181	0.182	0.163	0.194	0.220	0.212				
7.19	0.160	0.190	0.217	0.240	0.148	0.097	0.091	0.070	0.107	0.139	0.162	0.193	0.220	0.200				
9.45	0.160	0.190	0.217	0.238	0.149	0.097	0.090	0.071	0.058	0.106	0.161	0.193	0.221	0.192				
11.01	0.160	0.190	0.217	0.238	0.149	0.097	0.089	0.071	0.055	0.091	0.161	0.193	0.221	0.192				
Right sidewall										Left sidewall								
NPR	PR26	PR27	PR28	PR29	PR30	PR31	PR32	PR33	PR34	PR35	PR21	PR22	PR23	PR24				
1.57	0.661	0.640	0.622	0.618	0.631	0.625	0.620	0.867	0.638	0.626	0.709	0.408	0.664	0.543				
1.89	0.550	0.539	0.513	0.508	0.523	0.517	0.512	0.833	0.534	0.516	0.702	0.367	0.549	0.354				
2.13	0.488	0.486	0.455	0.451	0.464	0.458	0.455	0.812	0.478	0.458	0.702	0.368	0.476	0.354				
2.71	0.384	0.400	0.357	0.353	0.366	0.359	0.357	0.770	0.382	0.358	0.703	0.364	0.386	0.354				
3.81	0.273	0.309	0.252	0.248	0.260	0.251	0.248	0.708	0.280	0.247	0.702	0.364	0.205	0.351				
4.38	0.238	0.286	0.219	0.217	0.226	0.218	0.215	0.685	0.250	0.216	0.702	0.364	0.190	0.351				
4.93	0.211	0.270	0.195	0.193	0.201	0.190	0.188	0.670	0.224	0.190	0.701	0.365	0.190	0.350				
5.50	0.189	0.275	0.174	0.172	0.179	0.169	0.165	0.657	0.204	0.169	0.701	0.363	0.189	0.349				
7.19	0.145	0.253	0.132	0.130	0.136	0.128	0.125	0.615	0.168	0.128	0.700	0.362	0.188	0.350				
9.45	0.110	0.240	0.096	0.097	0.095	0.093	0.096	0.581	0.156	0.096	0.699	0.362	0.189	0.361				
11.01	0.094	0.240	0.080	0.082	0.079	0.078	0.081	0.557	0.152	0.081	0.699	0.362	0.189	0.360				
Lower throat insert																		
NPR	PR38	PR39	PR40	PR41	PR42	PR43	PR44	PR45										
1.57	0.564	0.375	0.434	0.606	0.412	0.447	0.412	0.542										
1.89	0.452	0.347	0.326	0.597	0.405	0.290	0.408	0.399										
2.13	0.414	0.344	0.294	0.596	0.398	0.244	0.409	0.330										
2.71	0.304	0.341	0.216	0.595	0.404	0.250	0.409	0.262										
3.81	0.187	0.337	0.219	0.593	0.404	0.267	0.410	0.233										
4.38	0.168	0.338	0.234	0.594	0.405	0.267	0.410	0.231										
4.93	0.162	0.337	0.242	0.593	0.405	0.267	0.410	0.231										
5.50	0.158	0.337	0.247	0.592	0.405	0.266	0.410	0.230										
7.19	0.156	0.335	0.253	0.590	0.404	0.264	0.409	0.228										
9.45	0.158	0.334	0.253	0.588	0.403	0.261	0.409	0.219										
11.01	0.158	0.334	0.252	0.587	0.403	0.259	0.408	0.217										

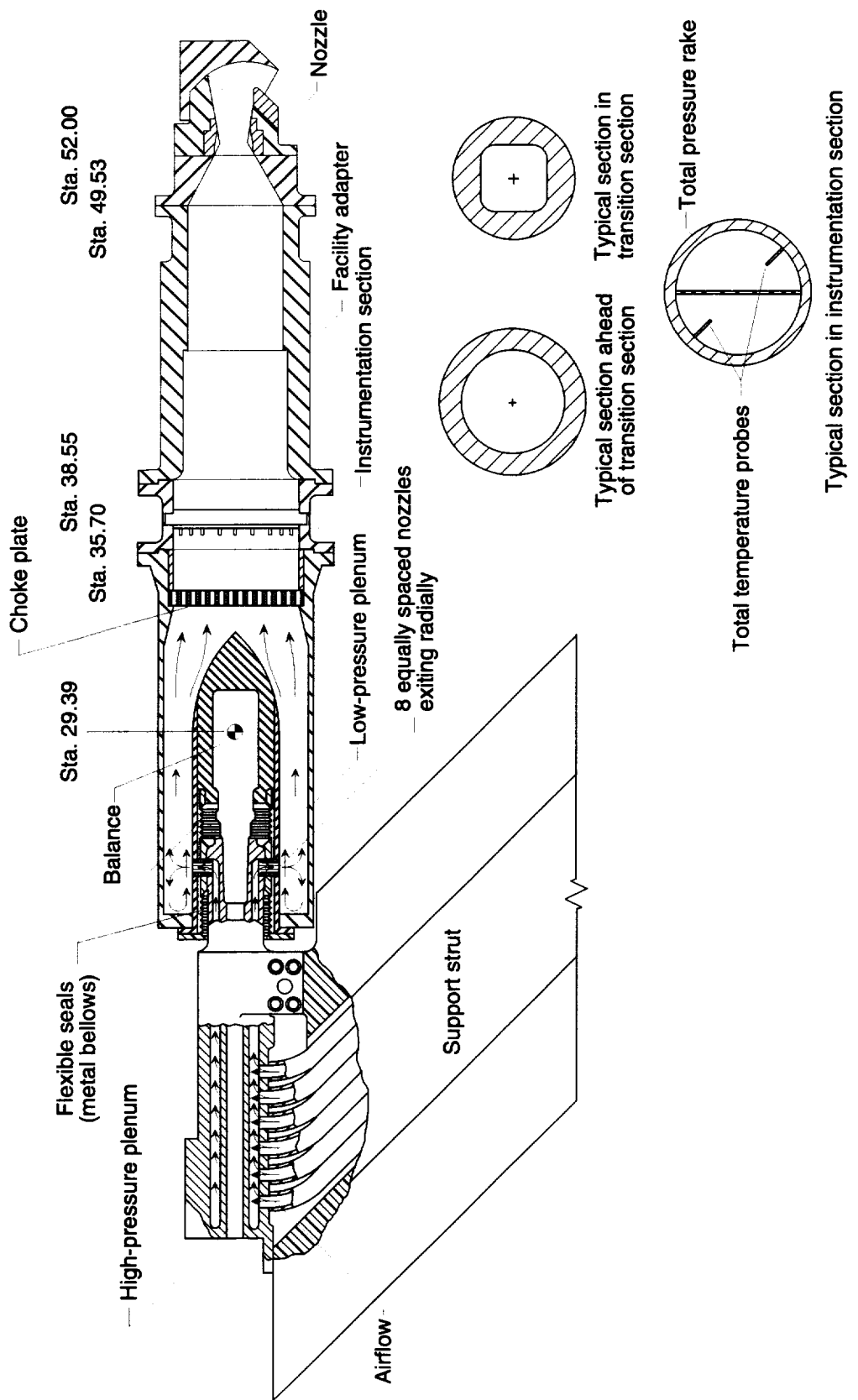
Table 21. Nozzle Internal Static Pressure Ratios for Configuration 19

NPR	Upper flap										Lower flap			
	PR54	PR55	PR56	PR57	PR58	PR59	PR60	PR61	PR62	PR63	PR46	PR47	PR48	PR49
1.55	0.634	0.634	0.644	0.658	0.662	0.639	0.633	0.634	0.639	0.645	0.620	0.630	0.628	0.640
1.91	0.514	0.506	0.432	0.424	0.558	0.528	0.512	0.514	0.518	0.524	0.497	0.487	0.376	0.499
2.13	0.460	0.452	0.316	0.299	0.503	0.487	0.457	0.461	0.465	0.470	0.441	0.425	0.298	0.431
2.70	0.362	0.274	0.258	0.295	0.386	0.362	0.362	0.362	0.365	0.370	0.354	0.250	0.262	0.344
3.83	0.171	0.213	0.249	0.293	0.175	0.150	0.147	0.257	0.256	0.261	0.176	0.217	0.253	0.274
4.37	0.168	0.213	0.247	0.293	0.175	0.146	0.134	0.184	0.221	0.229	0.172	0.216	0.252	0.264
4.94	0.168	0.213	0.246	0.293	0.175	0.146	0.132	0.113	0.198	0.203	0.171	0.215	0.252	0.260
5.49	0.167	0.212	0.246	0.293	0.175	0.145	0.131	0.089	0.180	0.182	0.170	0.215	0.252	0.257
7.20	0.167	0.212	0.246	0.293	0.176	0.145	0.129	0.086	0.115	0.139	0.169	0.214	0.252	0.255
8.89	0.167	0.212	0.246	0.294	0.176	0.145	0.128	0.085	0.063	0.112	0.169	0.214	0.253	0.254
9.40	0.167	0.213	0.246	0.294	0.176	0.145	0.128	0.085	0.058	0.106	0.169	0.214	0.253	0.254
10.33	0.167	0.213	0.246	0.294	0.176	0.145	0.128	0.085	0.055	0.097	0.168	0.213	0.252	0.254
Right sidewall														
NPR	PR26	PR27	PR28	PR29	PR30	PR31	PR32	PR33	PR34	PR35	PR21	PR22	PR23	PR24
1.55	0.660	0.640	0.629	0.628	0.636	0.633	0.626	0.815	0.642	0.635	0.727	0.524	0.668	0.522
1.91	0.537	0.521	0.508	0.505	0.517	0.512	0.507	0.767	0.525	0.512	0.710	0.507	0.547	0.504
2.13	0.482	0.470	0.457	0.453	0.463	0.458	0.455	0.746	0.475	0.461	0.709	0.502	0.495	0.501
2.70	0.379	0.374	0.359	0.355	0.364	0.360	0.355	0.705	0.380	0.362	0.708	0.501	0.278	0.500
3.83	0.267	0.276	0.250	0.246	0.255	0.249	0.244	0.655	0.279	0.249	0.708	0.499	0.217	0.499
4.37	0.235	0.251	0.219	0.217	0.223	0.218	0.213	0.640	0.251	0.218	0.708	0.498	0.217	0.498
4.94	0.207	0.231	0.195	0.193	0.198	0.191	0.188	0.626	0.228	0.193	0.708	0.498	0.216	0.498
5.49	0.187	0.217	0.175	0.174	0.177	0.172	0.169	0.616	0.211	0.173	0.708	0.498	0.216	0.497
7.20	0.142	0.195	0.133	0.133	0.133	0.130	0.127	0.600	0.176	0.131	0.707	0.496	0.216	0.497
8.89	0.115	0.179	0.104	0.105	0.106	0.104	0.102	0.578	0.160	0.105	0.706	0.495	0.216	0.496
9.40	0.109	0.169	0.097	0.099	0.097	0.097	0.096	0.568	0.157	0.099	0.706	0.495	0.216	0.496
10.33	0.099	0.173	0.087	0.088	0.086	0.087	0.087	0.556	0.152	0.089	0.706	0.494	0.216	0.496
Lower throat insert														
NPR	PR38	PR39	PR40	PR41	PR42	PR43	PR44	PR45						
1.55	0.576	0.558	0.554	0.513	0.566	0.550	0.661	0.661						
1.91	0.443	0.413	0.384	0.349	0.542	0.304	0.537	0.537						
2.13	0.408	0.368	0.357	0.346	0.540	0.305	0.483	0.483						
2.70	0.306	0.332	0.348	0.344	0.536	0.305	0.380	0.380						
3.83	0.164	0.328	0.347	0.342	0.535	0.306	0.268	0.268						
4.37	0.144	0.326	0.348	0.342	0.534	0.306	0.235	0.235						
4.94	0.135	0.327	0.348	0.341	0.534	0.306	0.208	0.207						
5.49	0.131	0.327	0.348	0.341	0.533	0.306	0.187	0.186						
7.20	0.125	0.327	0.348	0.340	0.532	0.306	0.142	0.142						
8.89	0.124	0.327	0.347	0.340	0.531	0.306	0.115	0.115						
9.40	0.124	0.326	0.346	0.340	0.531	0.305	0.109	0.109						
10.33	0.124	0.326	0.346	0.340	0.530	0.305	0.099	0.099						



(a) Photograph of the propulsion simulation system with a typical nozzle configuration installed. L-91-07470

Figure 1. Single-engine propulsion simulation system.



(b) Cutaway side view of propulsion simulation system. Station numbers are in inches.

Figure 1. Concluded.

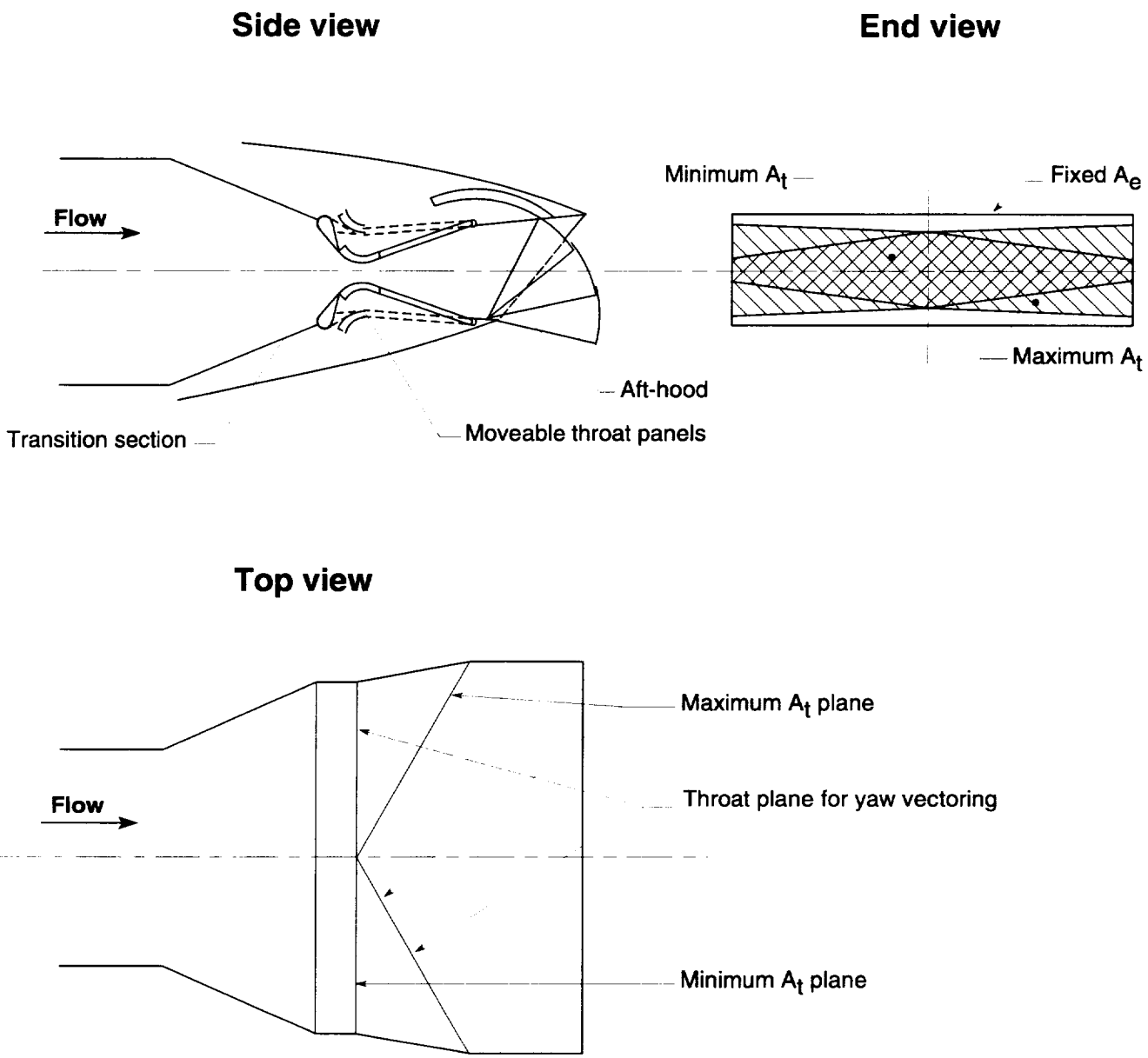
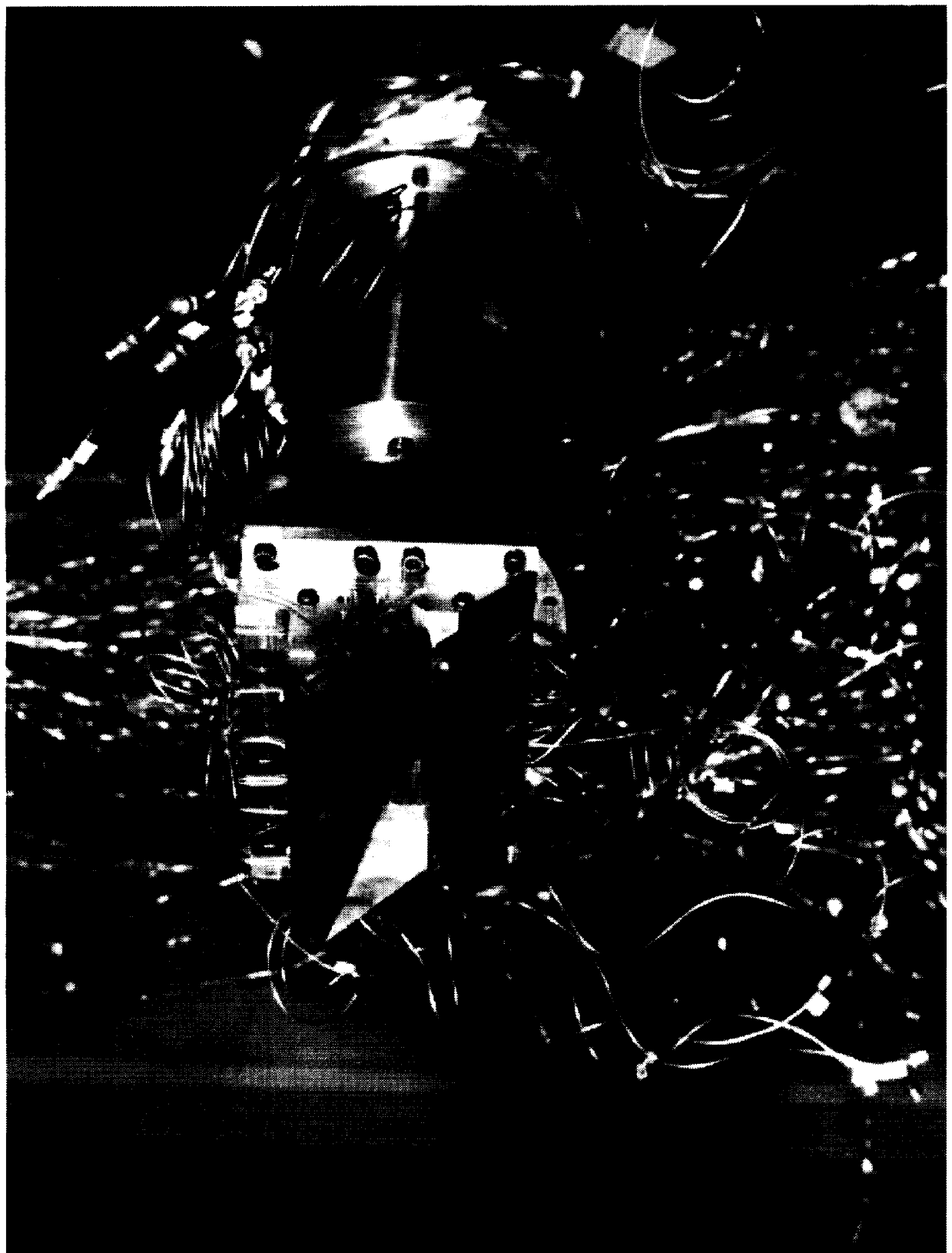


Figure 2. Sketch showing fixed-shroud nonaxisymmetric nozzle concept.



L-91-07468

(a) Cruise configuration.

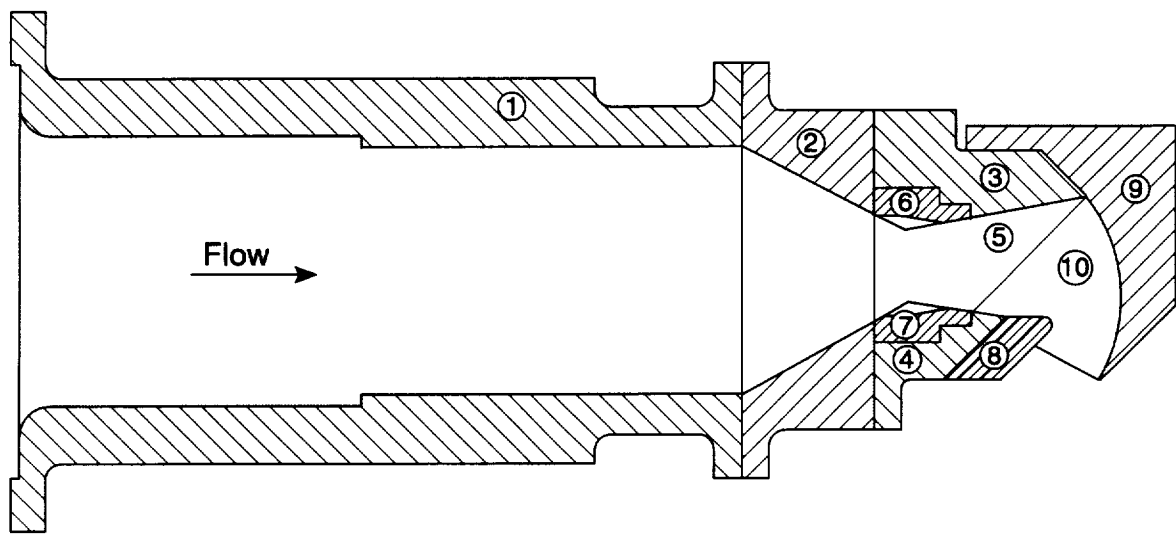
Figure 3. Photographs of typical nozzle configurations installed on the propulsion simulation system.



L-91-07466

(b) STOVL configuration (hood sidewalls removed).

Figure 3. Concluded.



Part number	Designation
1	Facility adapter
2	Transition section
3	Upper flap
4	Lower flap
5	Nozzle sidewall
6	Upper throat insert
7	Lower throat insert
8	Throat area control block
9	Hood
10	Hood sidewall

Figure 4. Sketch defining model parts.

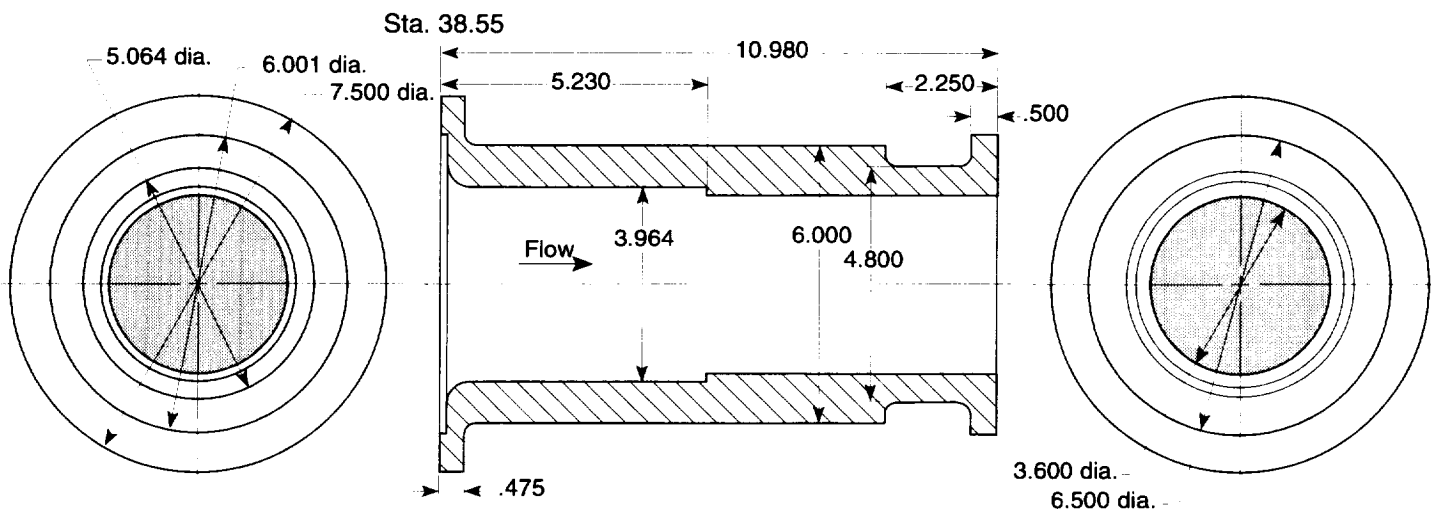


Figure 5. Sketch showing facility adapter details. Dimensions are in inches.

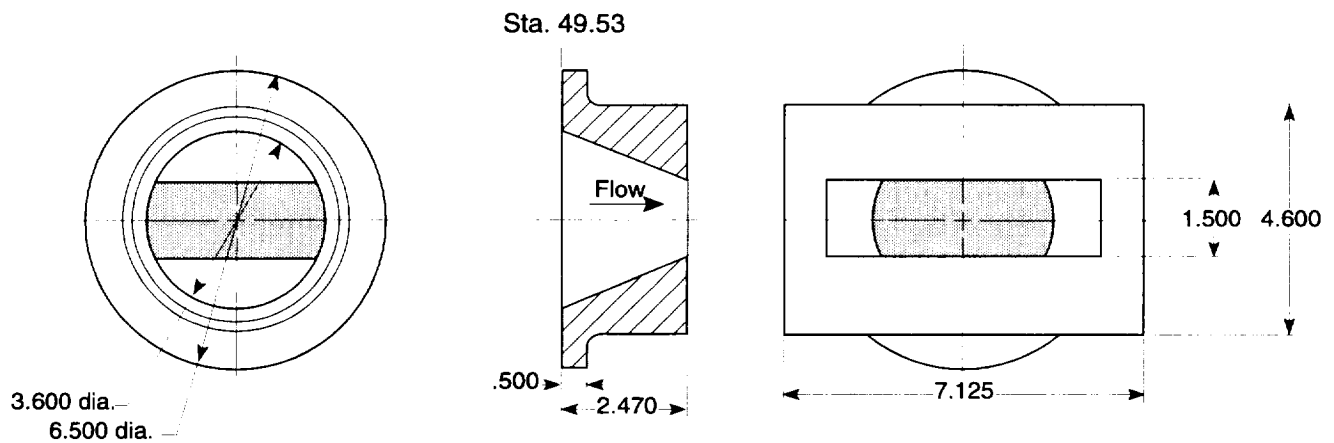
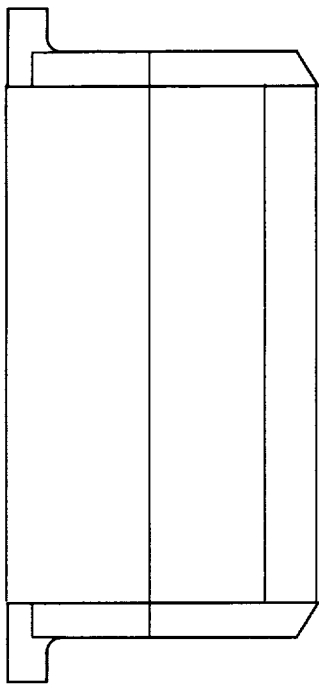
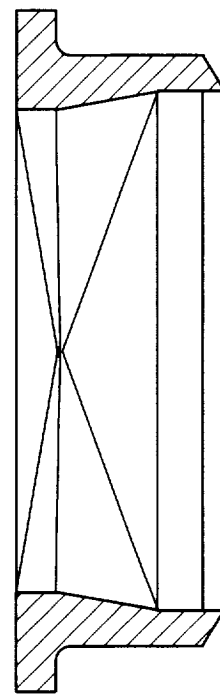


Figure 6. Sketch showing transition section details. Dimensions are in inches.

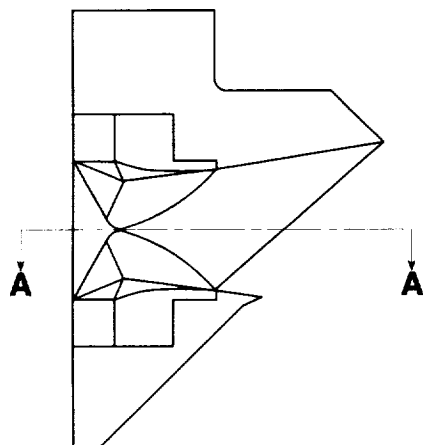
**Top view**



**Section A-A**



**Side view  
(left sidewall removed)**



**End view  
(looking upstream)**

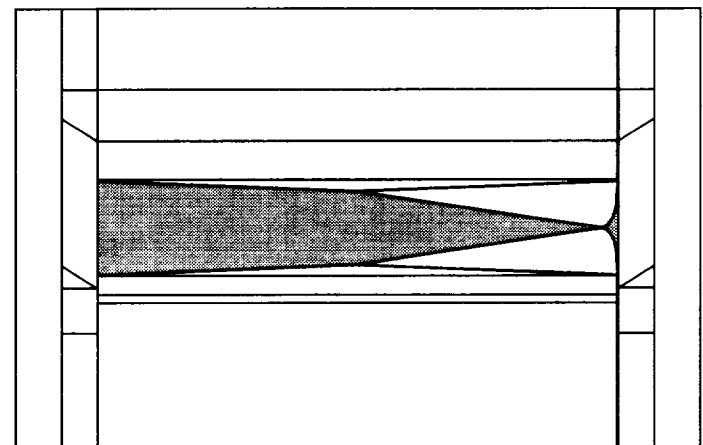
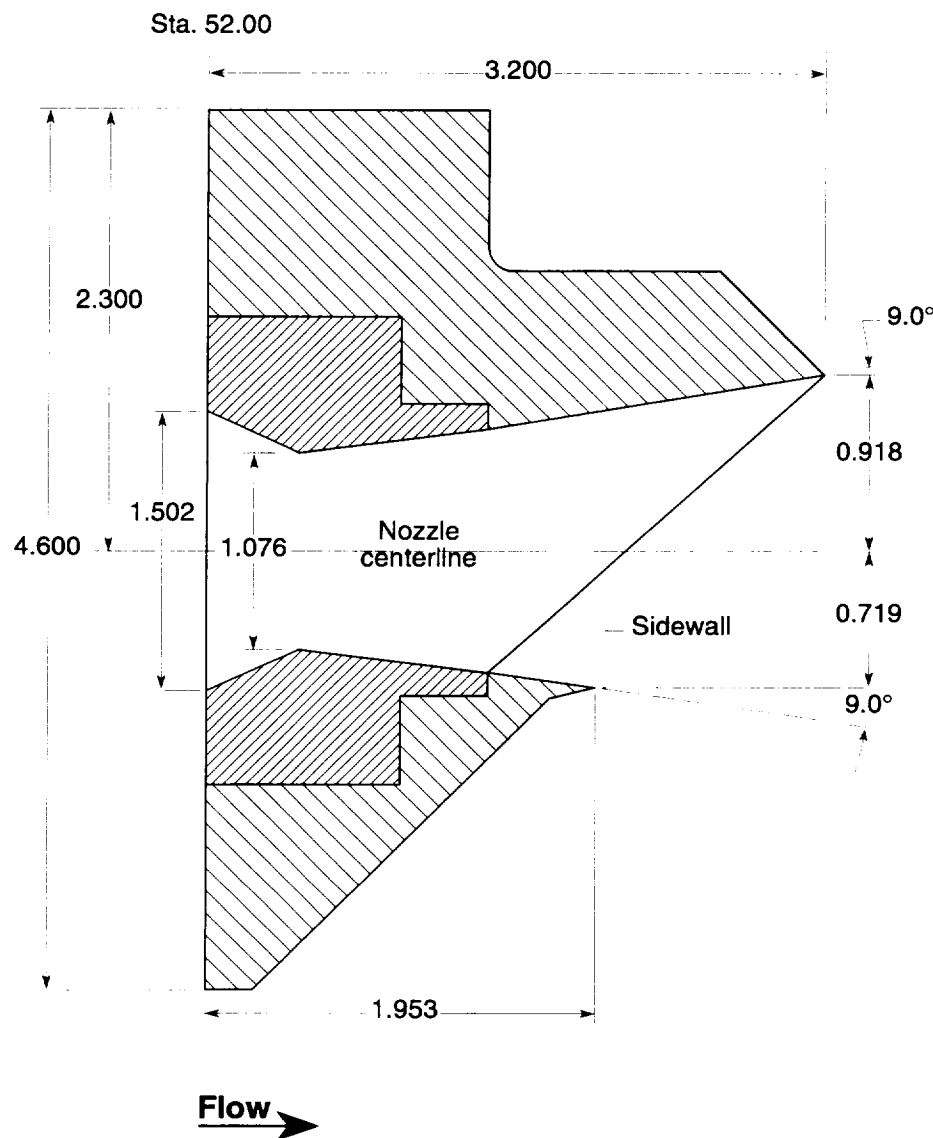
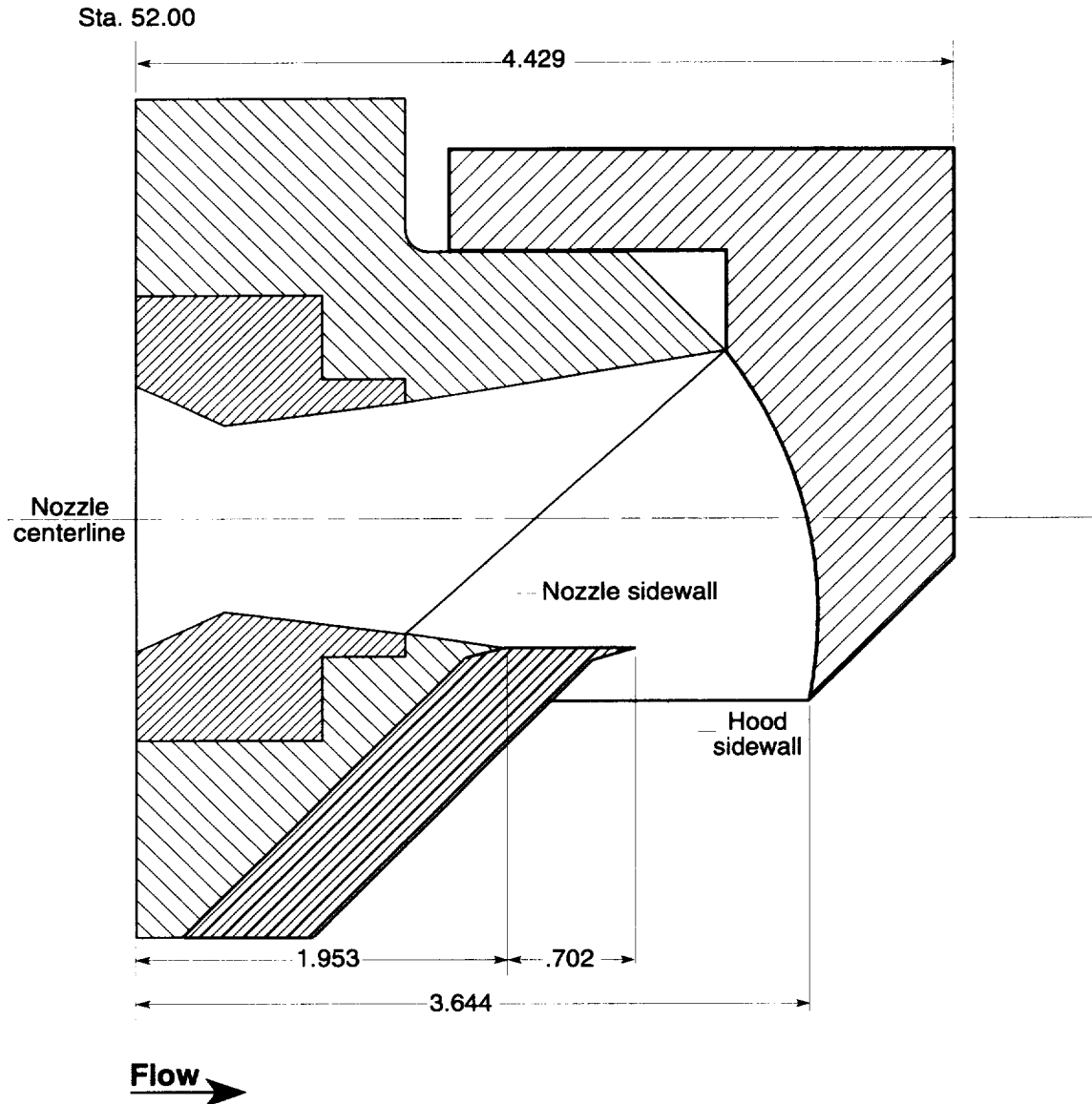


Figure 7. Sketch showing static test nozzle model with maximum yaw vectored throat inserts installed.



(a) Unvectored nozzle.

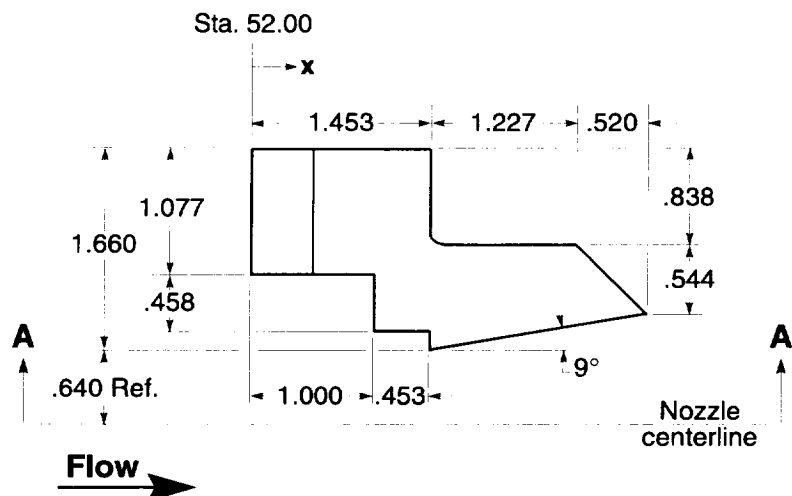
Figure 8. Sketches showing nozzle geometry details for A/B power configuration. Dimensions are in inches.



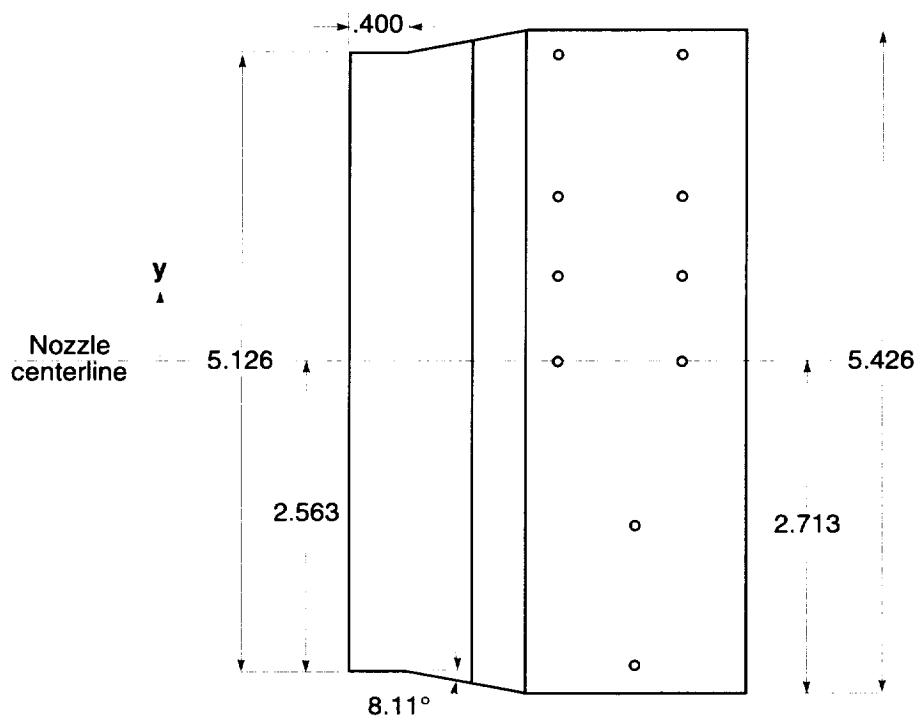
(b) Pitch-vectorized nozzle  $\delta_{v,p} = 90^\circ$  with throat area control block #1 installed.

Figure 8. Concluded.

### Side view



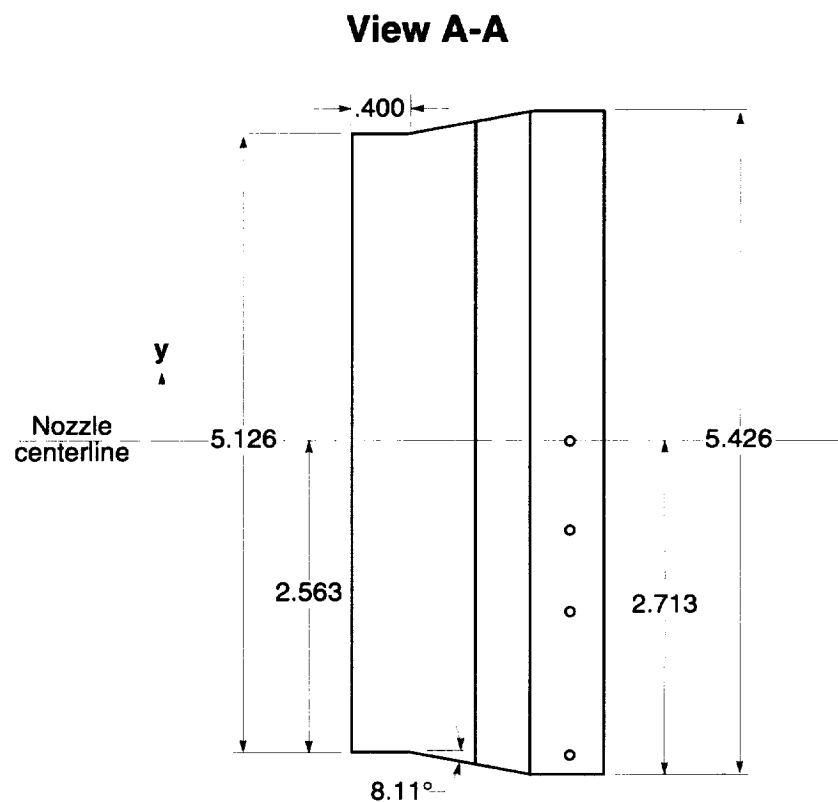
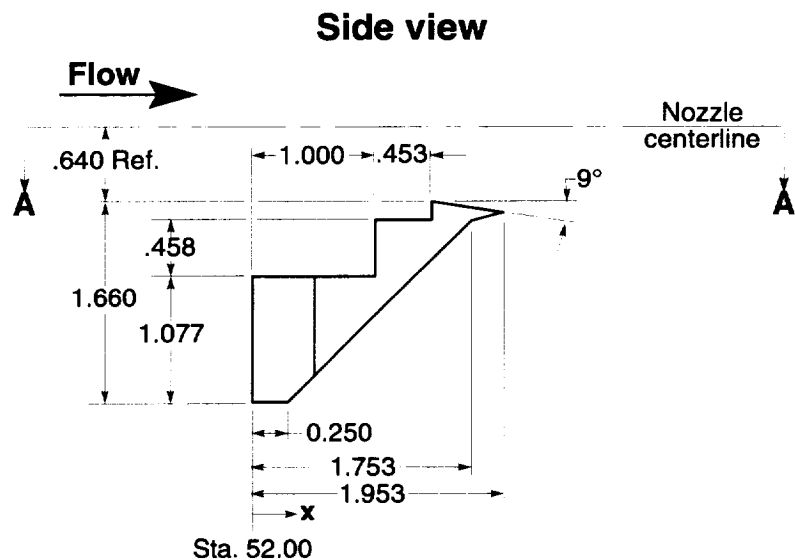
### View A-A



Static-Pressure Orifice Locations

Orifice #	x, in.	y, in.	Orifice #	x, in.	y, in.
54	1.700	0.000	59	2.700	1.350
55	1.700	0.700	60	2.700	0.700
56	1.700	1.350	61	2.700	0.000
57	1.700	2.500	62	2.327	-1.350
58	2.700	2.500	63	2.327	-2.500

Figure 9. Sketch showing details and static pressure orifice locations (denoted by circles) of nozzle upper flap. Dimensions are in inches.

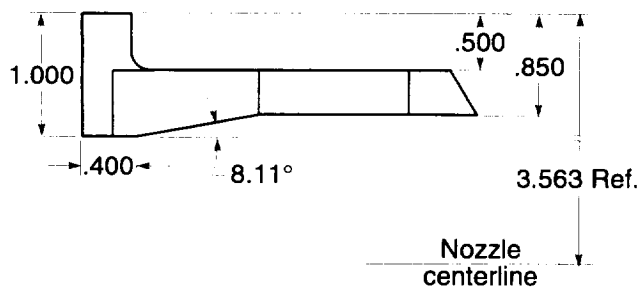


**Static-Pressure Orifice Locations**

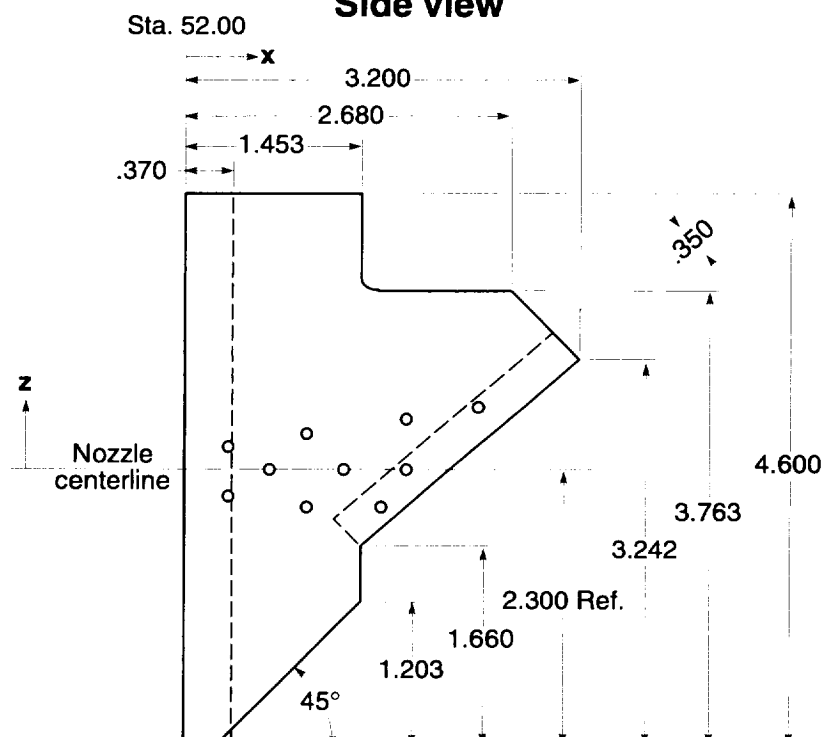
Orifice #	x, in.	y, in.
46	1.703	0.000
47	1.703	-0.700
48	1.703	-1.350
49	1.703	-2.500

Figure 10. Sketch showing details and static pressure orifice locations (denoted by circles) of nozzle lower flap. Dimensions are in inches.

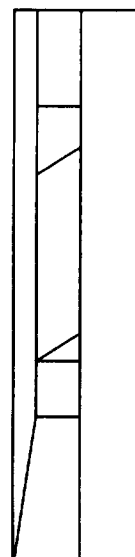
### Top view



### Side view



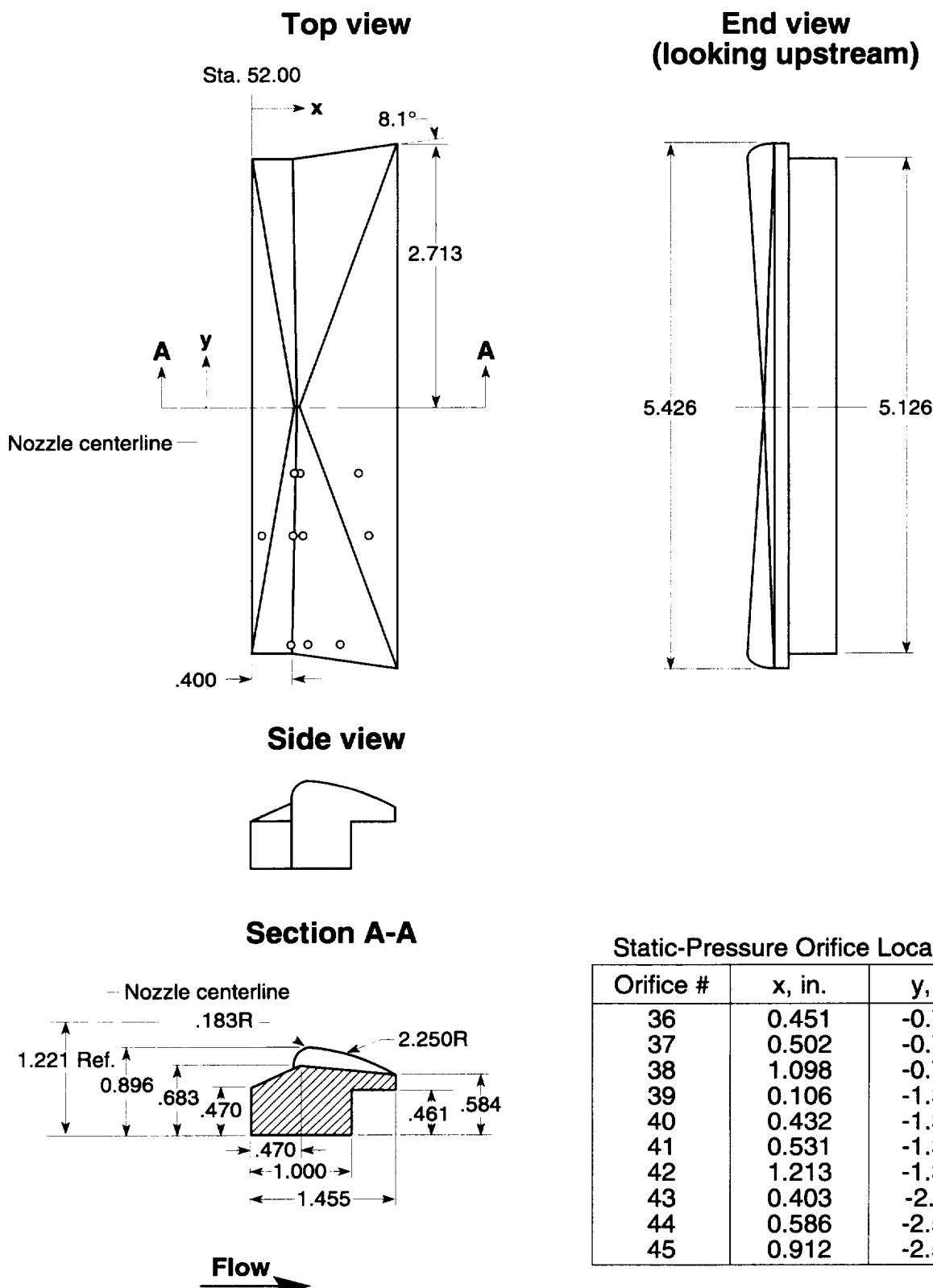
### End view



Static-Pressure Orifice Locations

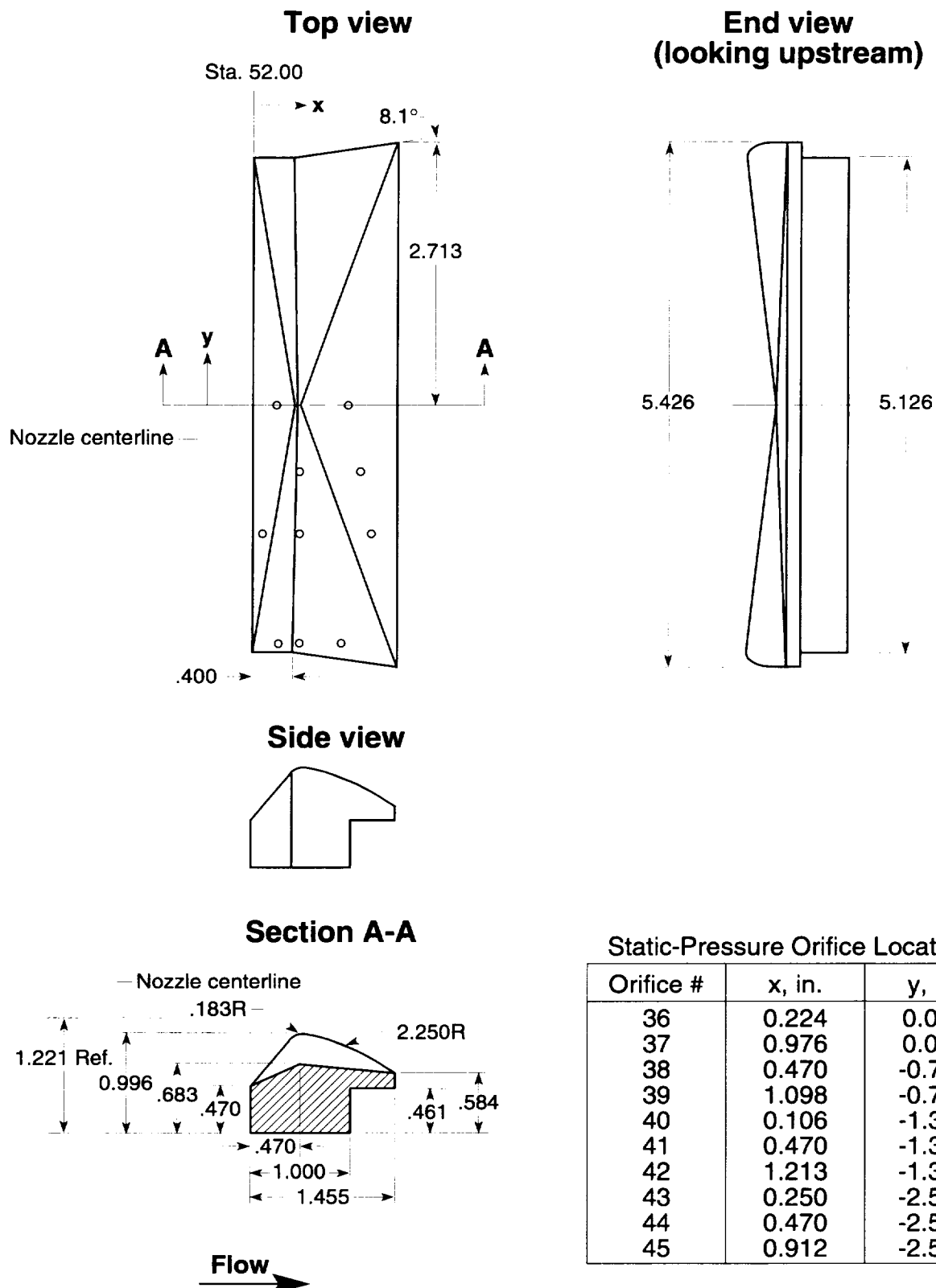
Right sidewall			Left sidewall		
Orifice #	x,in.	z,in.	Orifice #	x,in.	z,in.
26	0.370	0.200	21	0.370	0.200
27	1.000	0.300	22	1.000	0.300
28	1.800	0.427	23	2.386	0.522
29	2.386	0.522	24	1.000	-0.300
30	0.700	0.000			
31	1.300	0.000			
32	1.800	0.000			
33	0.370	-0.200			
34	1.000	-0.300			
35	1.600	-0.300			

Figure 11. Sketch showing details and static pressure orifice locations (denoted by circles) of nozzle sidewalls (right sidewall shown). Dimensions are in inches.



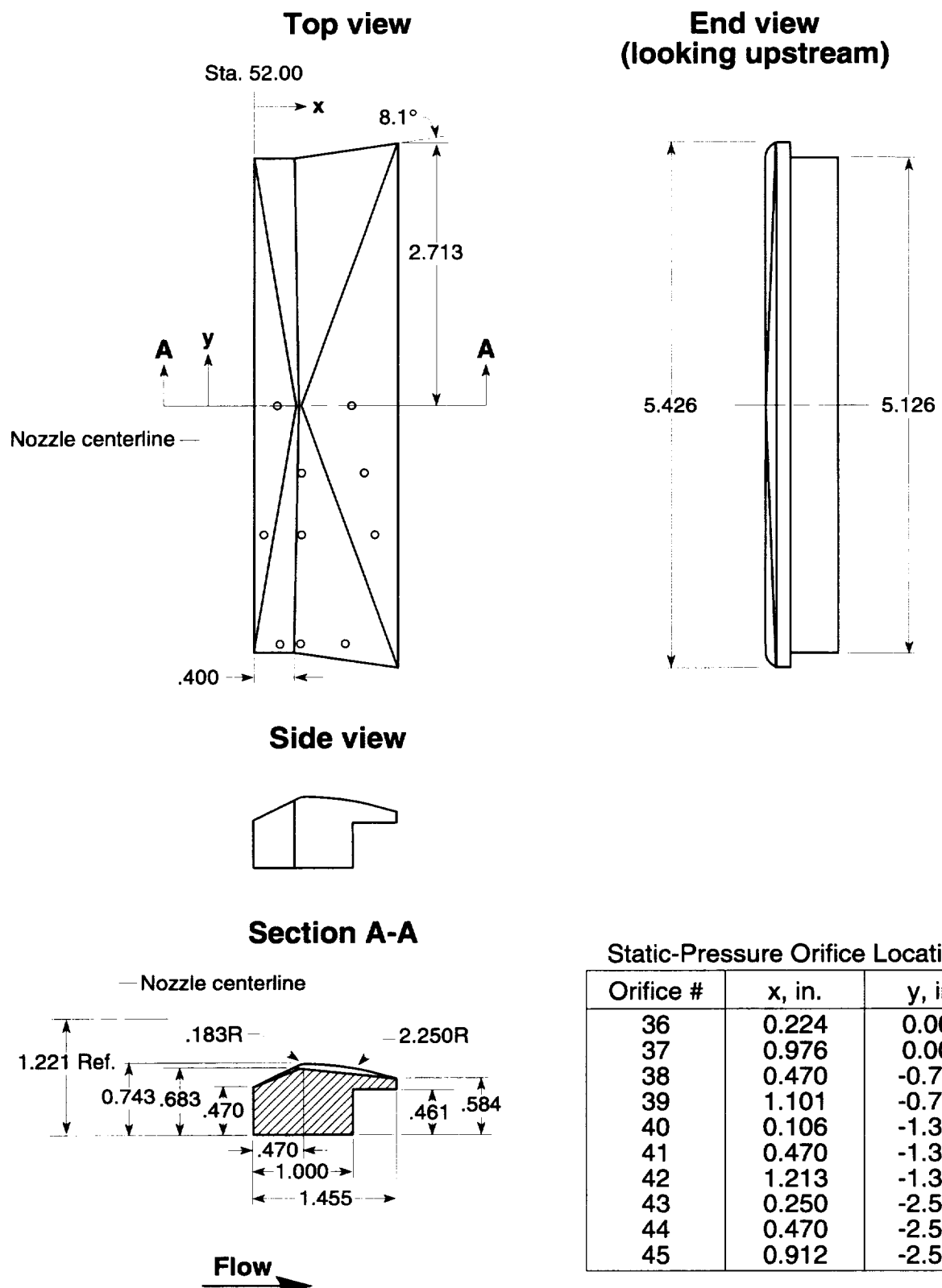
(a) Baseline dry power.

Figure 12. Sketches showing details and static pressure orifice locations (denoted by circles) of nozzle throat inserts (lower throat inserts shown). Upper throat inserts are not instrumented. Dimensions are in inches.



(b) Modified dry power.

Figure 12. Continued.



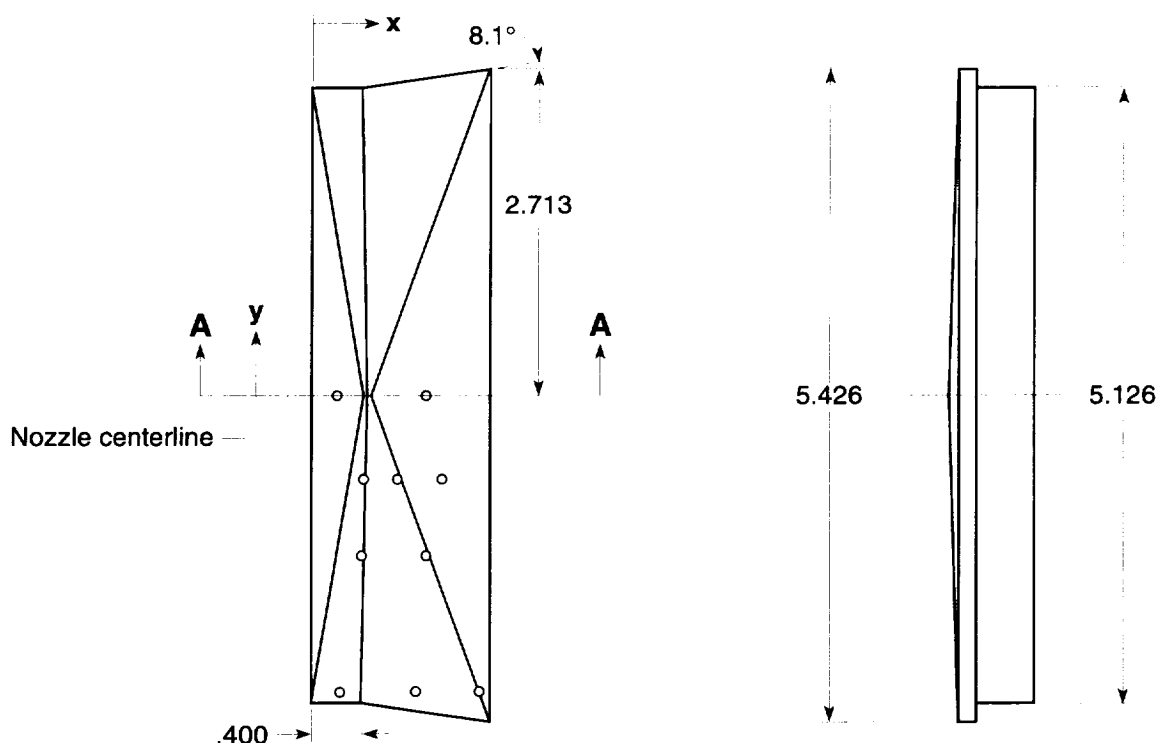
(c) Intermediate power.

Figure 12. Continued.

### Top view

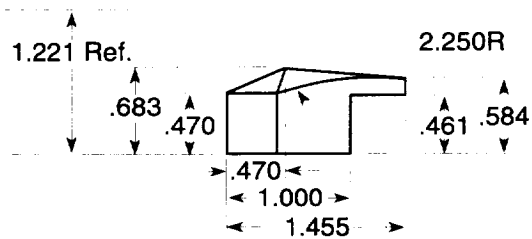
Sta. 52.00

### End view (looking upstream)



### Side view

Nozzle centerline



### Section A-A

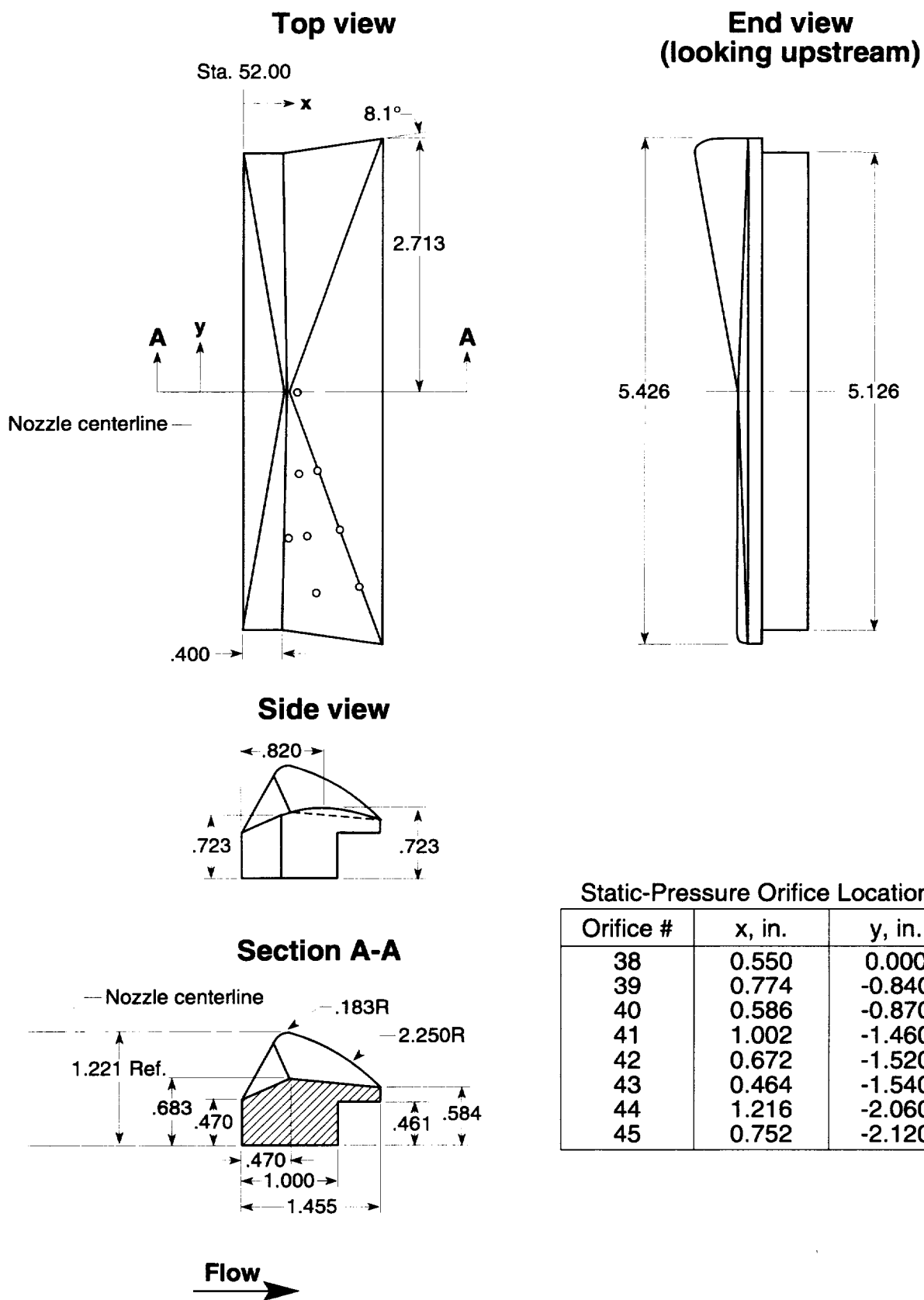


### Static-Pressure Orifice Locations

Orifice #	x, in.	y, in.
36	0.224	0.000
37	0.976	0.000
38	0.451	-0.700
39	0.720	-0.700
40	1.098	-0.700
41	0.432	-1.350
42	0.960	-1.350
43	0.250	-2.500
44	0.890	-2.500
45	1.379	-2.500

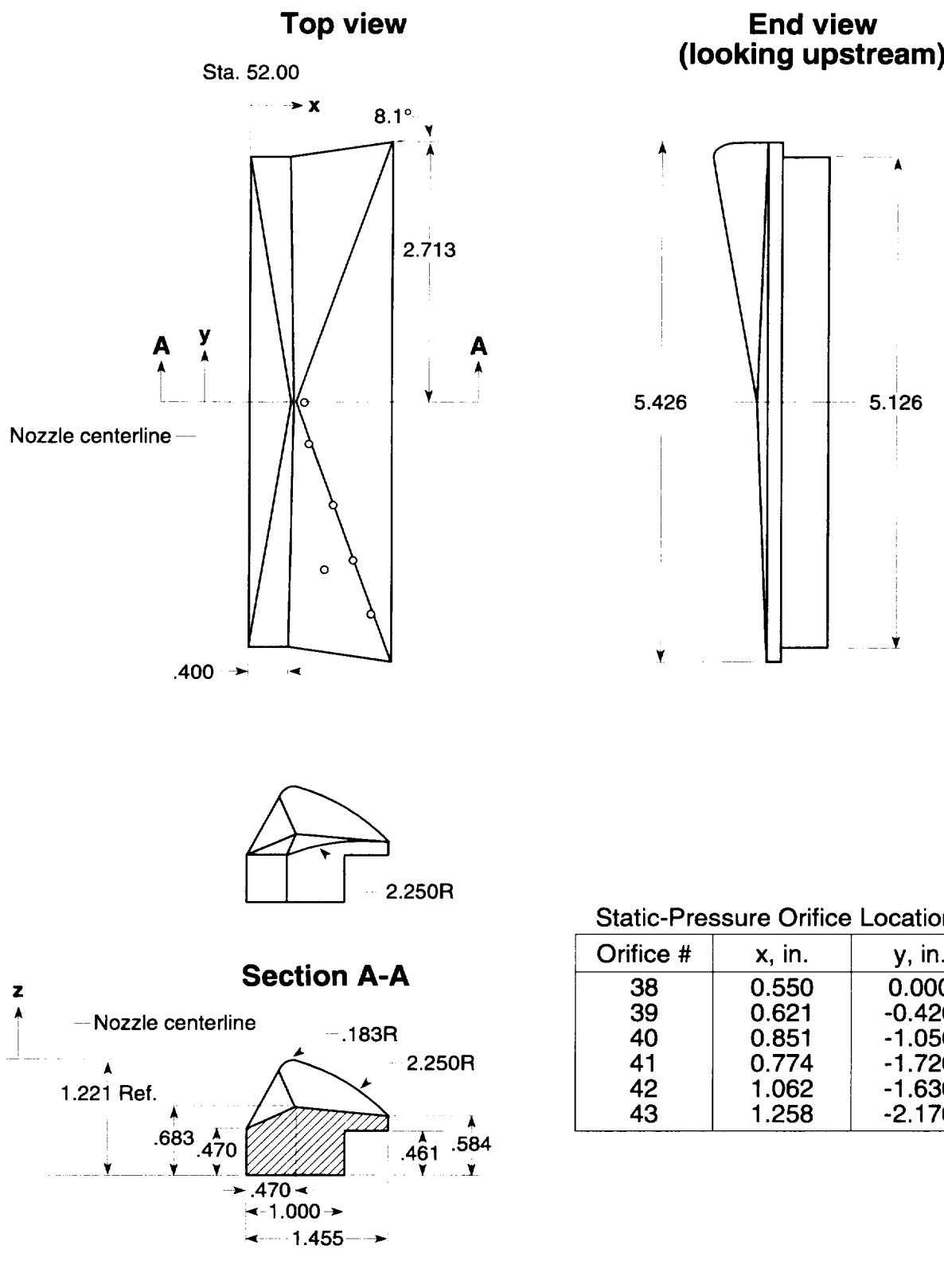
(d) Maximum A/B power.

Figure 12. Continued.



(e) 10° yaw vectored.

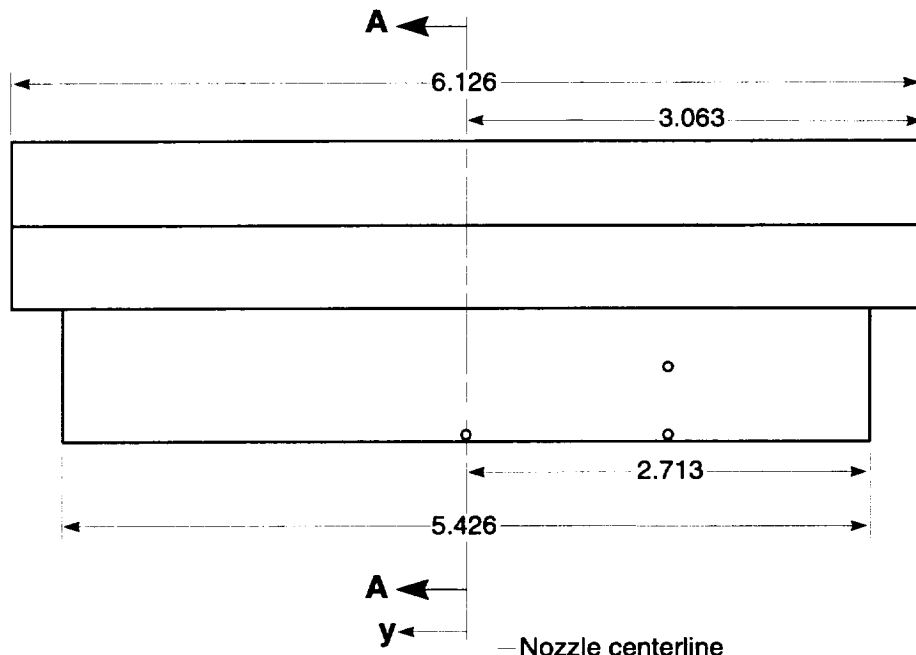
Figure 12. Continued.



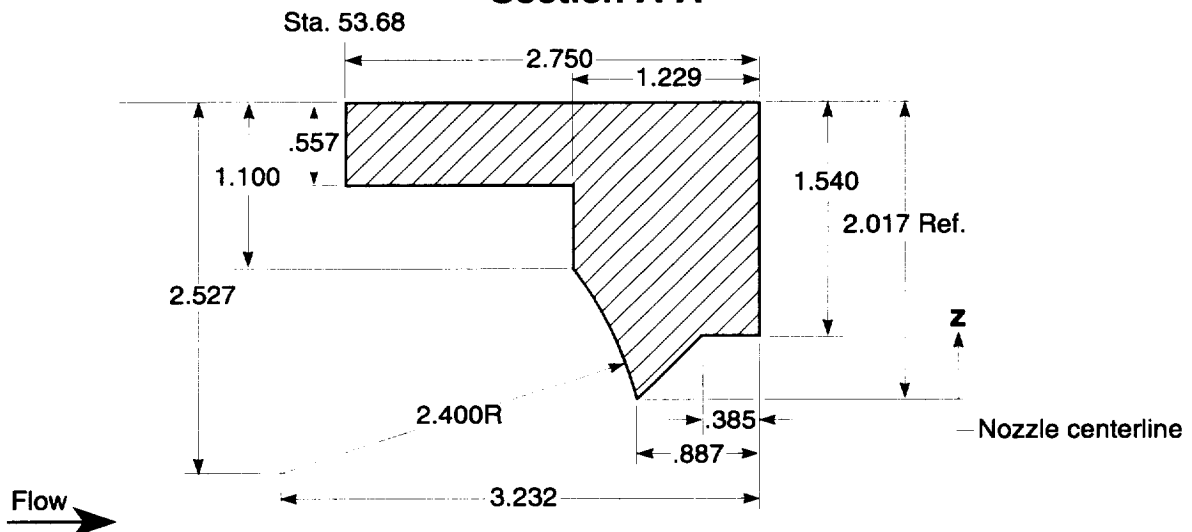
(f) 20° yaw vectored.

Figure 12. Concluded.

## **End view (looking downstream)**



## **Section A-A**



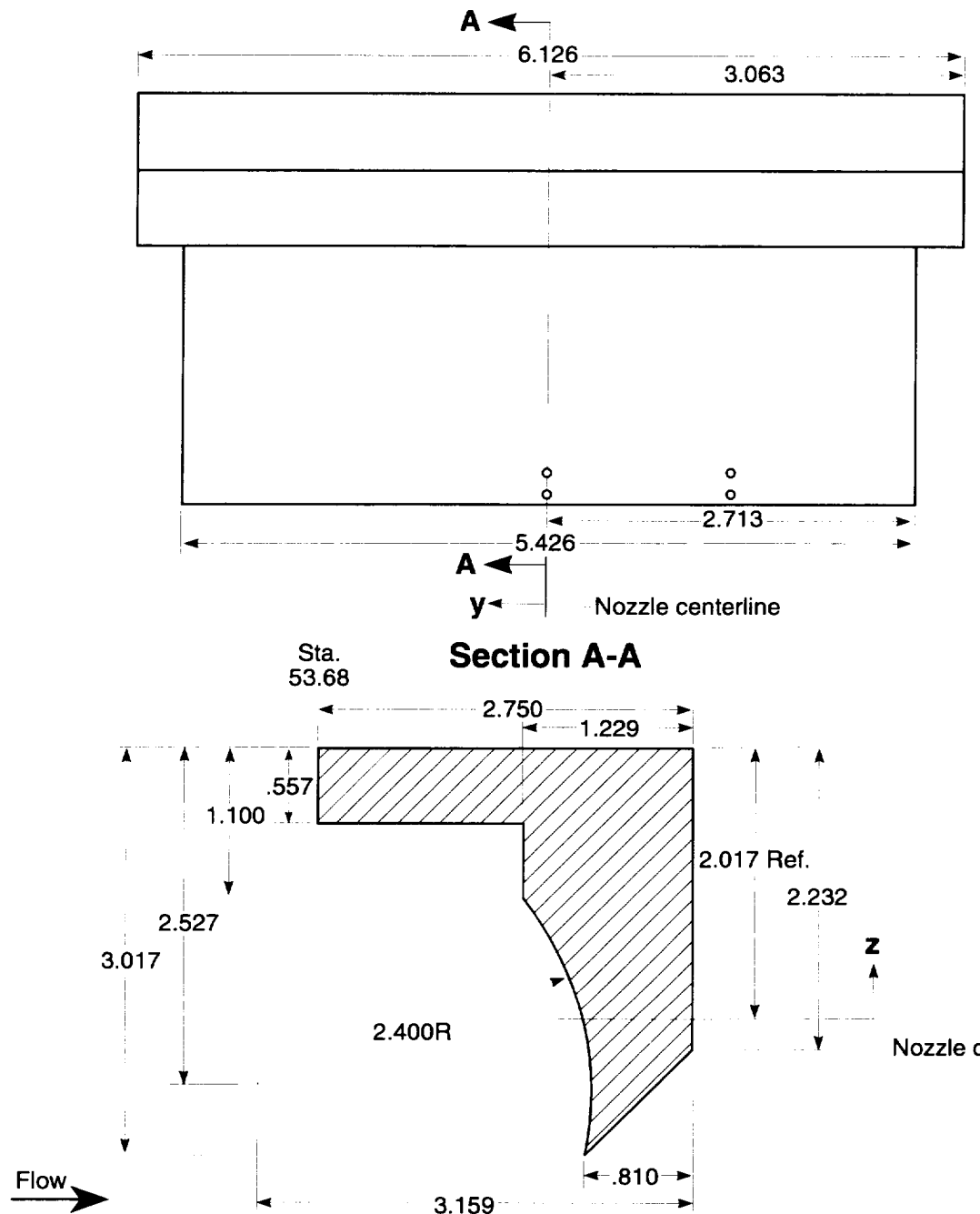
## Static-Pressure Orifice Locations

Orifice #	y, in.	z, in.
64	-1.350	0.500
65	-1.350	0.033
66	0.000	0.033

(a) 45° hood.

Figure 13. Sketches showing details and static pressure orifice locations (denoted by circles) of hoods. Dimensions are in inches.

**End view  
(looking downstream)**



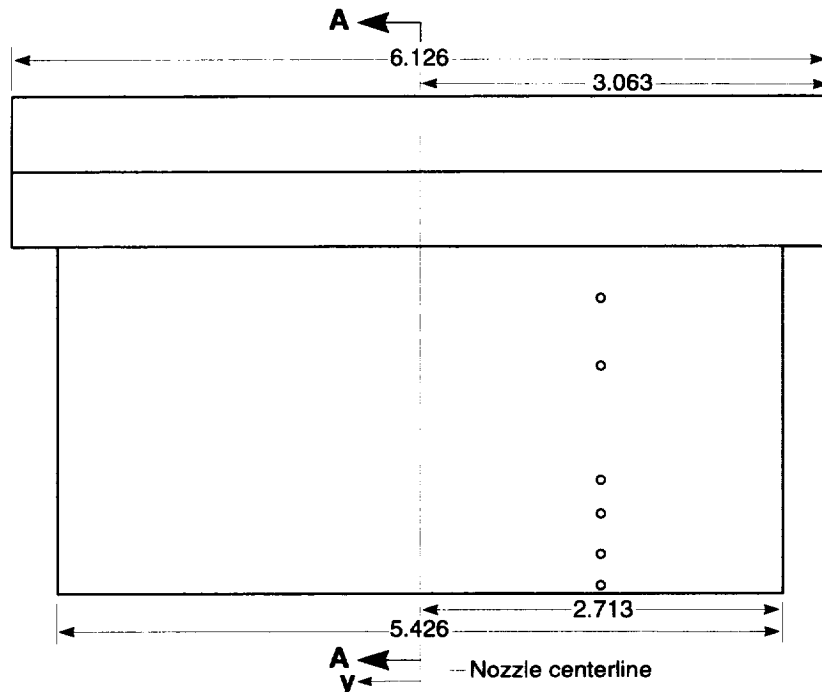
**Static-Pressure Orifice Locations**

Orifice #	y, in.	z, in.
64	-1.350	-0.800
65	-1.350	-0.967
66	0.000	-0.800
67	0.000	-0.967

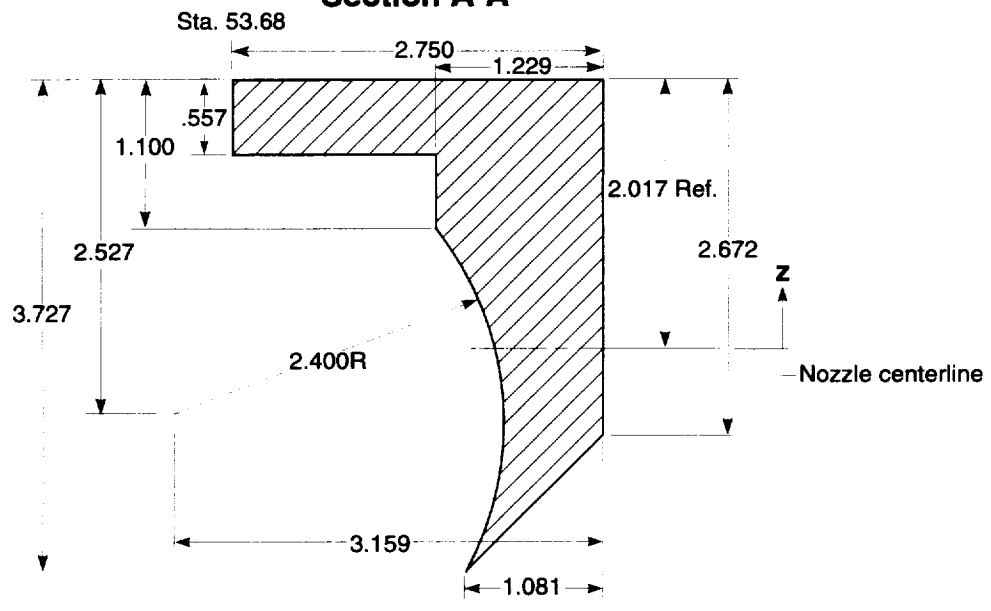
(b) 90° hood.

Figure 13. Continued.

**End view  
(looking downstream)**



**Section A-A**



**Static-Pressure Orifice Locations**

Orifice #	y, in.	z, in.	Orifice #	y, in.	z, in.
64	-1.350	0.500	67	-1.350	-1.100
65	-1.350	0.000	68	-1.350	-1.400
66	-1.350	-0.868	69	-1.350	-1.677

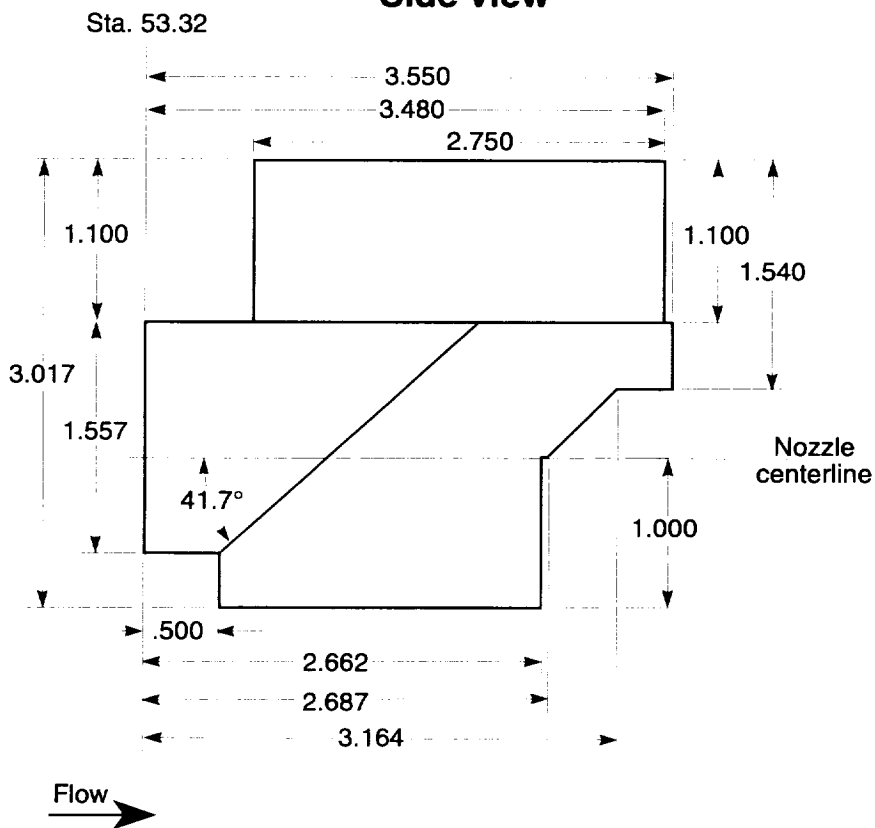
(c) 120° hood.

Figure 13. Concluded.

### Top view



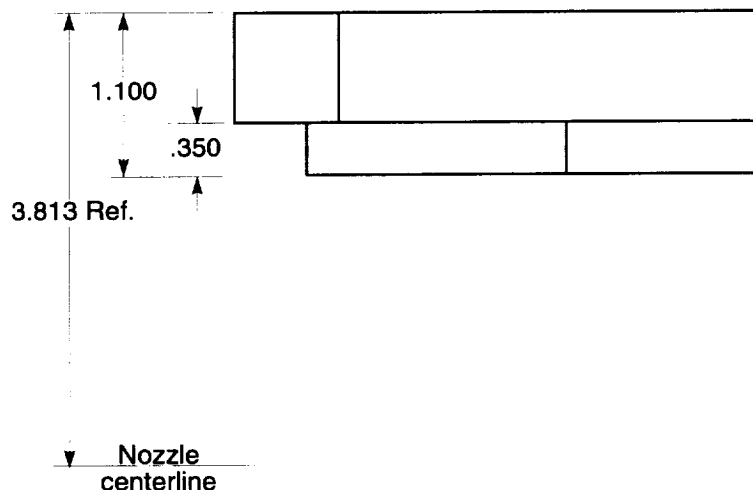
### Side view



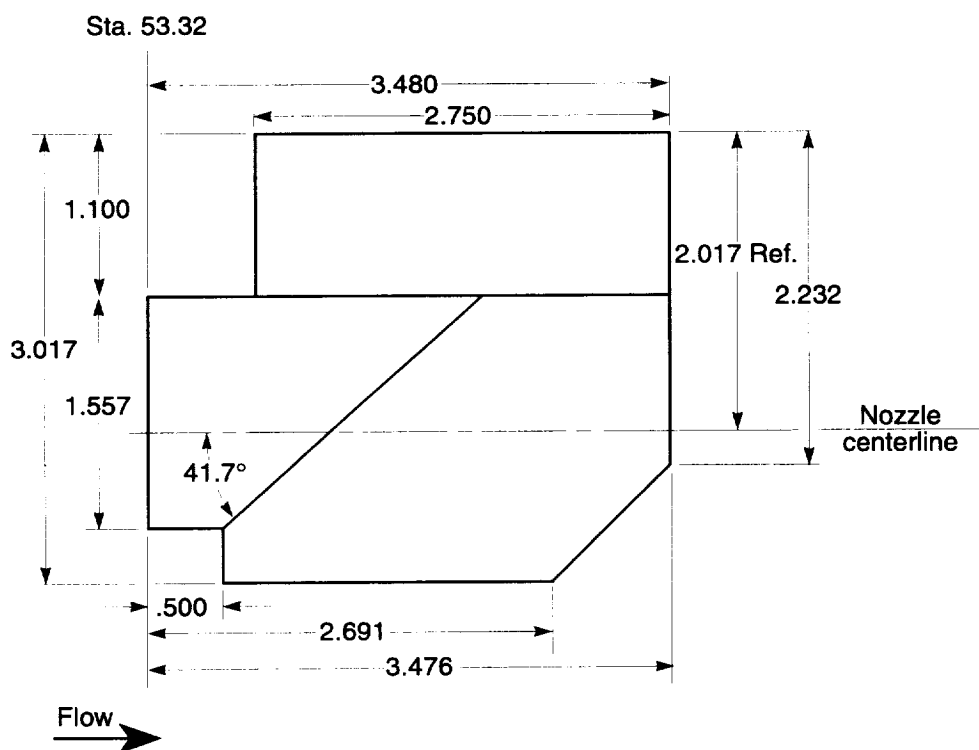
(a)  $45^\circ$  hood sidewall.

Figure 14. Sketches showing details of hood sidewalls (right sidewalls shown). Dimensions are in inches.

### Top view



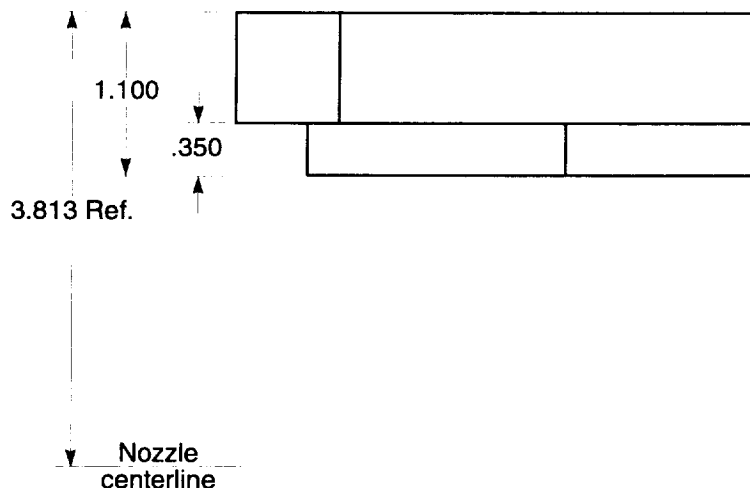
### Side view



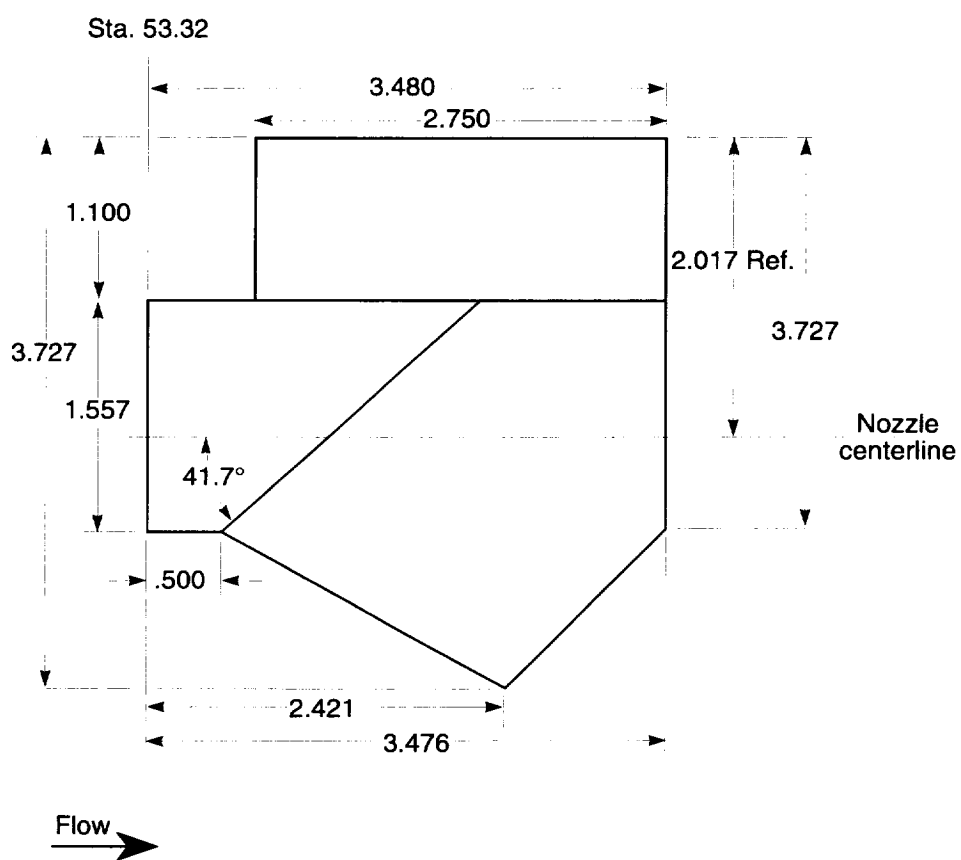
(b) 90° hood sidewall.

Figure 14. Continued.

### Top view



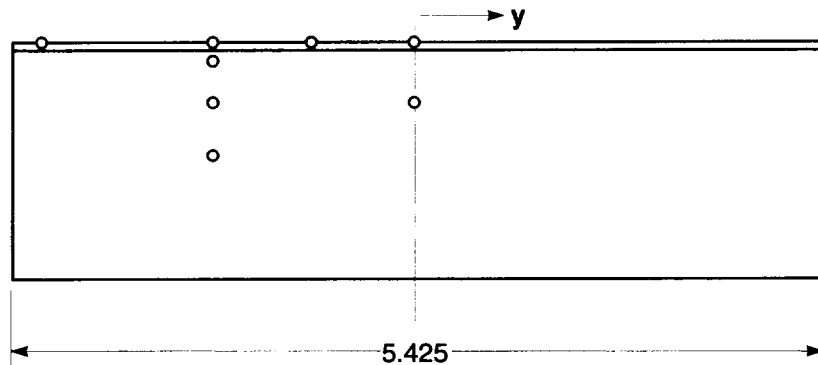
### Side view



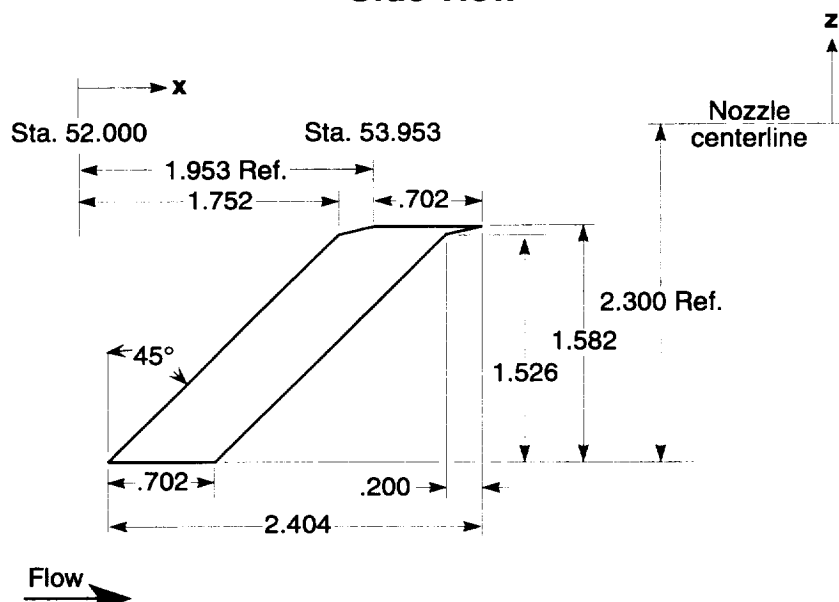
(c)  $120^\circ$  hood sidewall.

Figure 14. Concluded.

**End view  
(looking upstream)**



**Side view**



Flow →

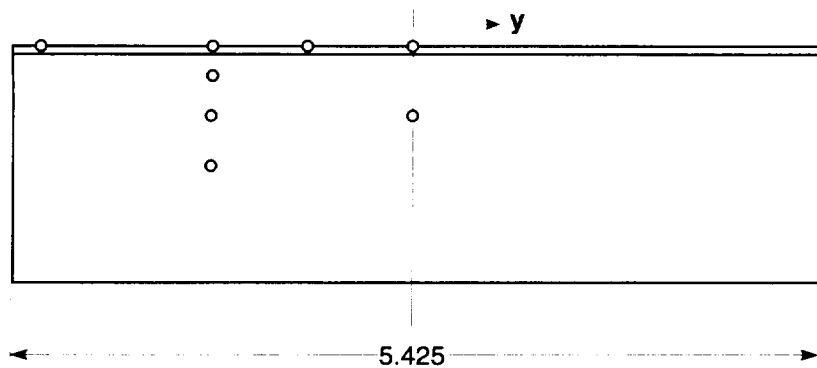
**Static-Pressure Orifice Locations**

Orifice #	x, in.	y, in.	z, in.
70	2.354	0.000	-0.718
71	2.354	-0.700	-0.718
72	2.354	-1.350	-0.718
73	2.354	-2.500	-0.718
74	2.655	-2.500	-0.718
75	2.655	-1.350	-0.718
76	2.393	-1.350	-0.860
77	2.110	-1.350	-1.143
78	1.756	-1.350	-1.497
79	2.655	-0.700	-0.718
80	2.655	0.000	-0.718
81	2.110	0.000	-1.143

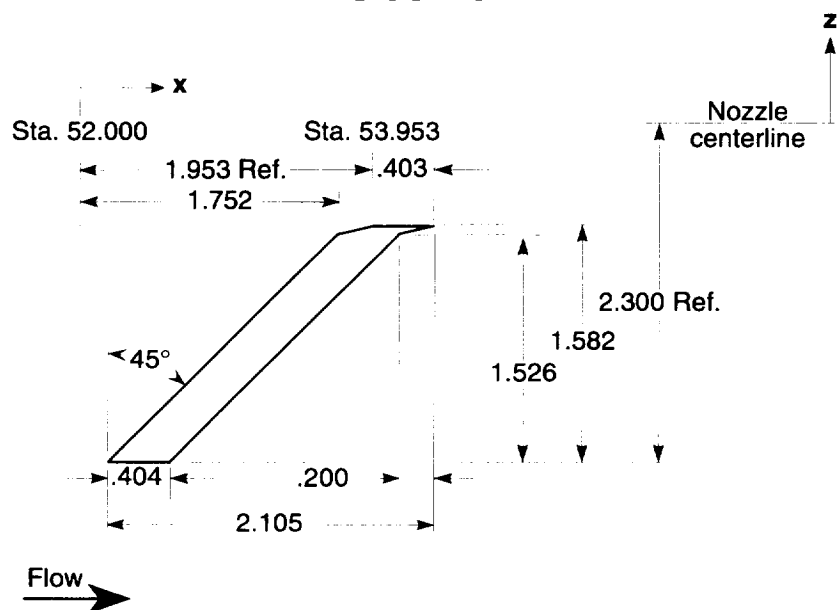
(a) Throat area control block #1.

Figure 15. Sketches showing details and static pressure orifice locations (denoted by circles) of throat area control blocks. Dimensions are in inches.

**End view  
(looking upstream)**



**Side view**



**Static-Pressure Orifice Locations**

Orifice #	x, in.	y, in.	z, in.
70	2.156	0.000	-0.718
71	2.156	-0.700	-0.718
72	2.156	-1.350	-0.718
73	2.156	-2.500	-0.718
74	2.356	-2.500	-0.718
75	2.356	-1.350	-0.718
76	2.095	-1.350	-0.860
77	1.812	-1.350	-1.143
78	1.458	-1.350	-1.497
79	2.356	-0.700	-0.718
80	2.356	0.000	-0.718
81	1.812	0.000	-1.143

(b) Throat area control block #2.

Figure 15. Concluded.

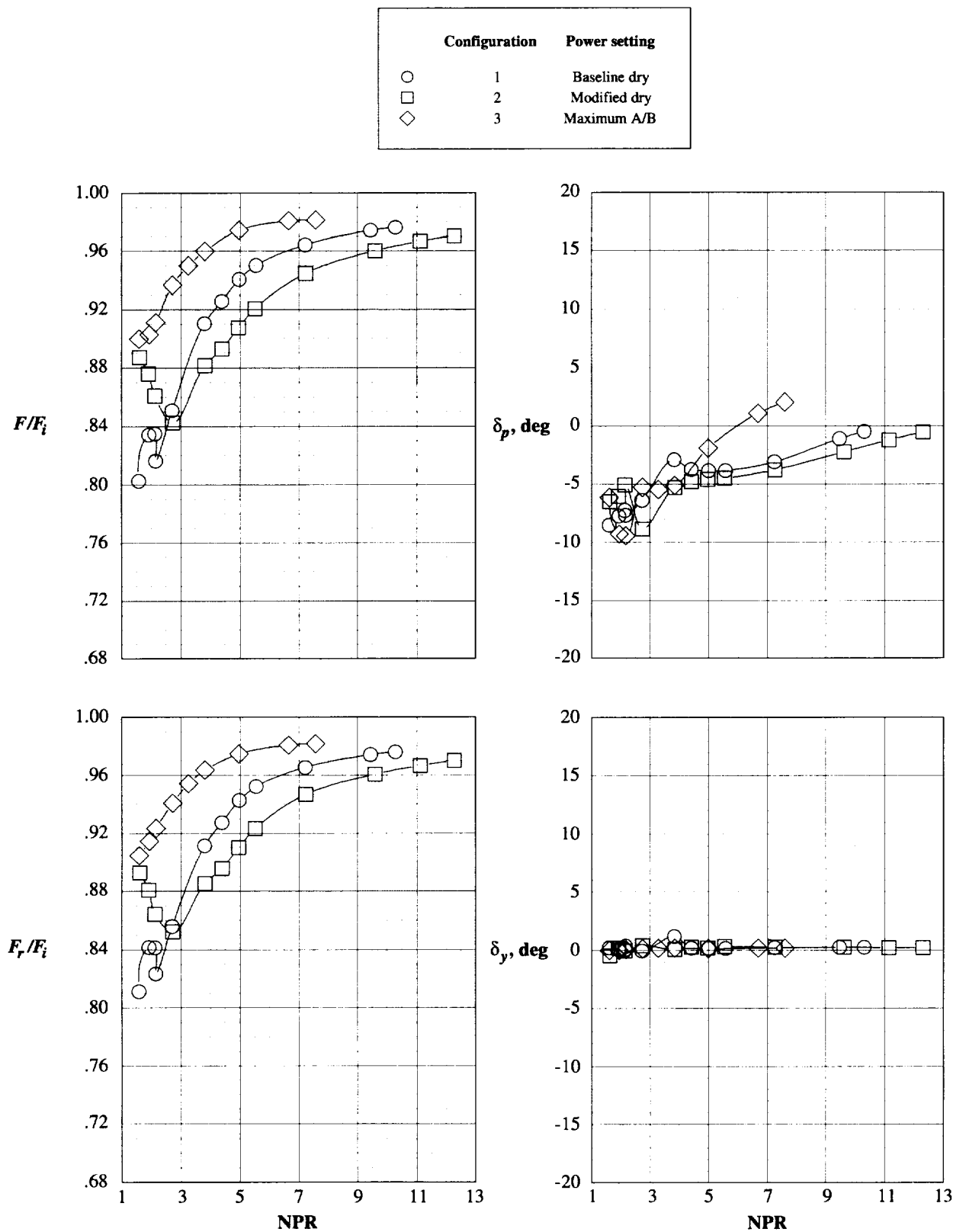
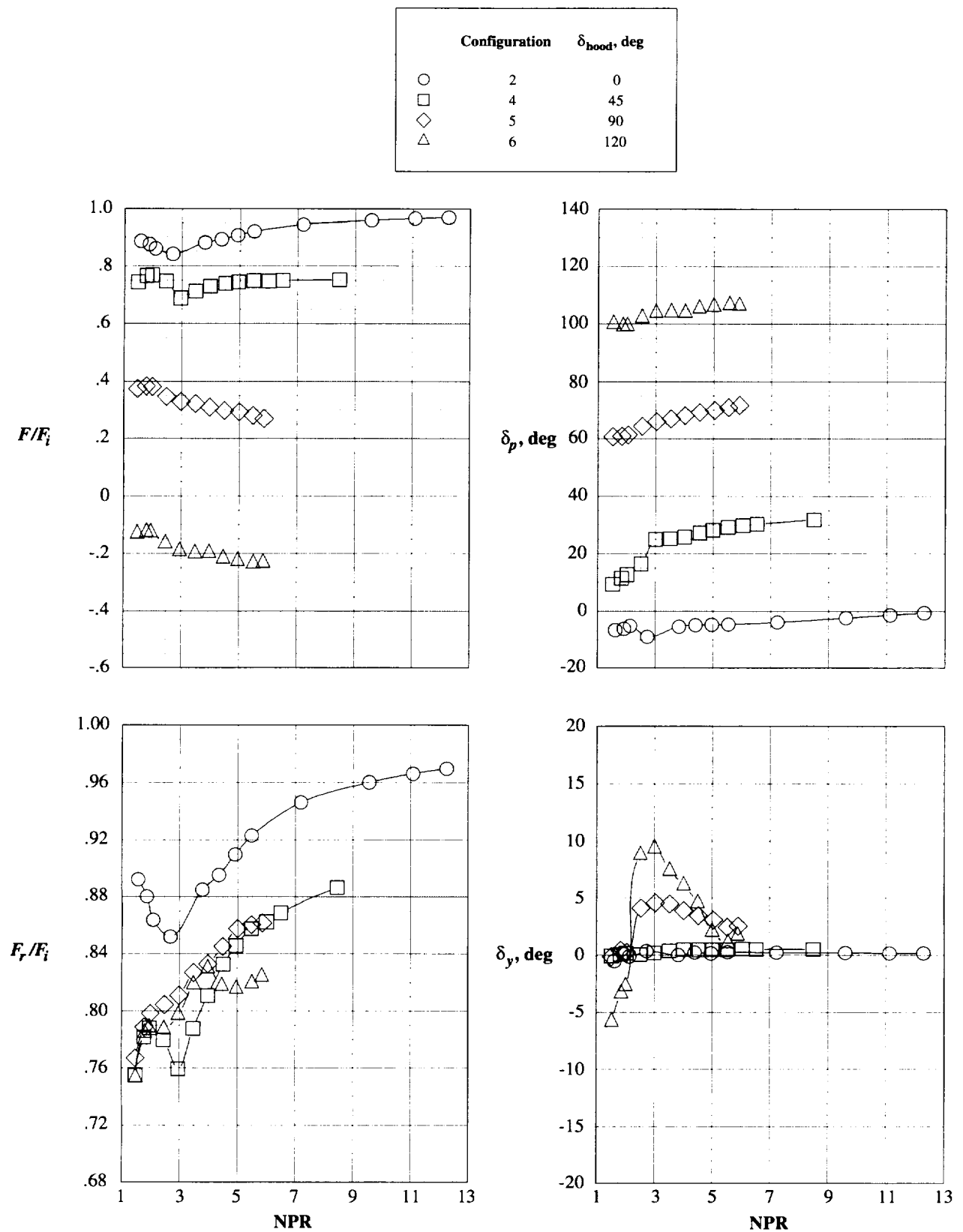
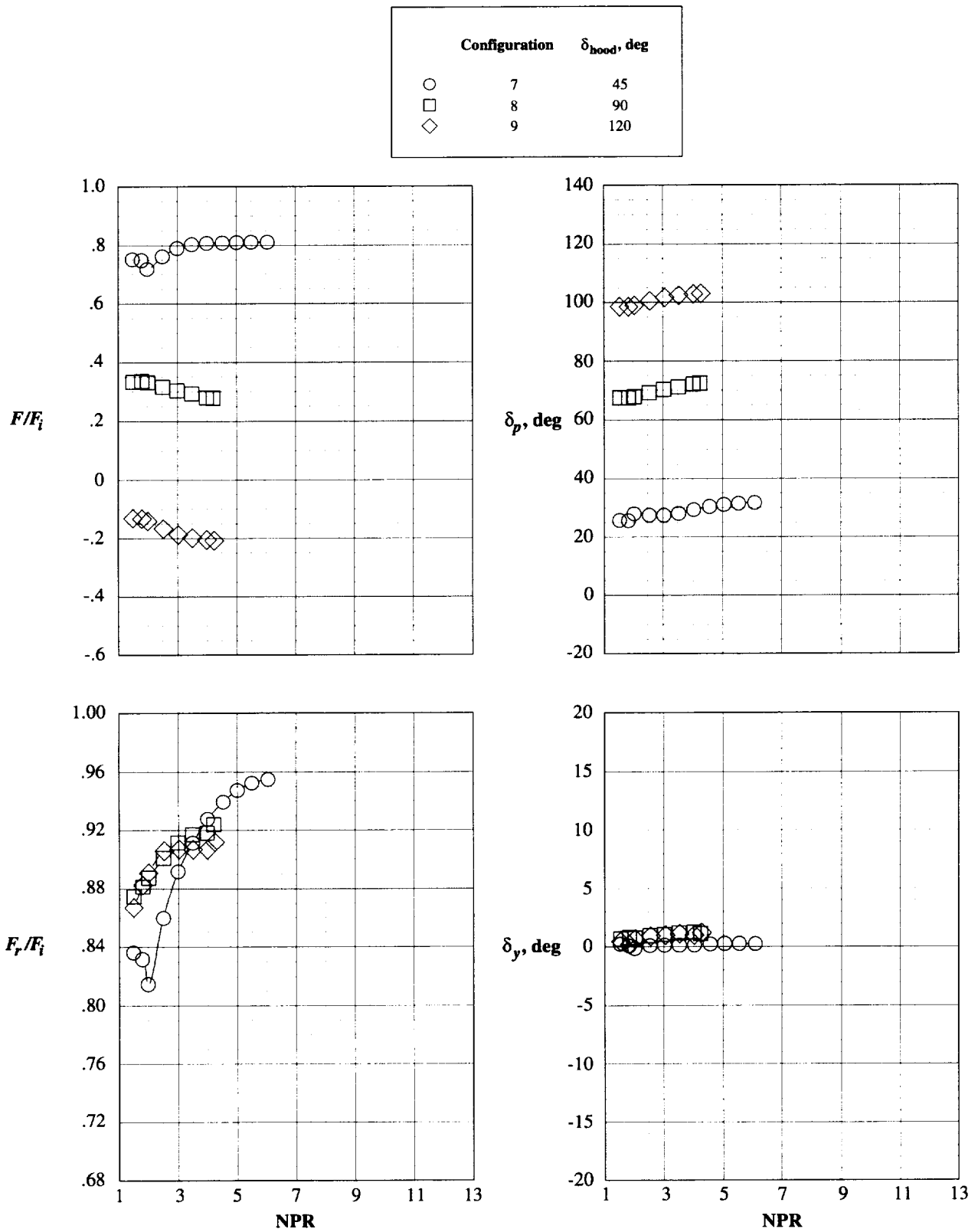


Figure 16. Effect of power setting on internal performance characteristics of cruise nozzle configurations.



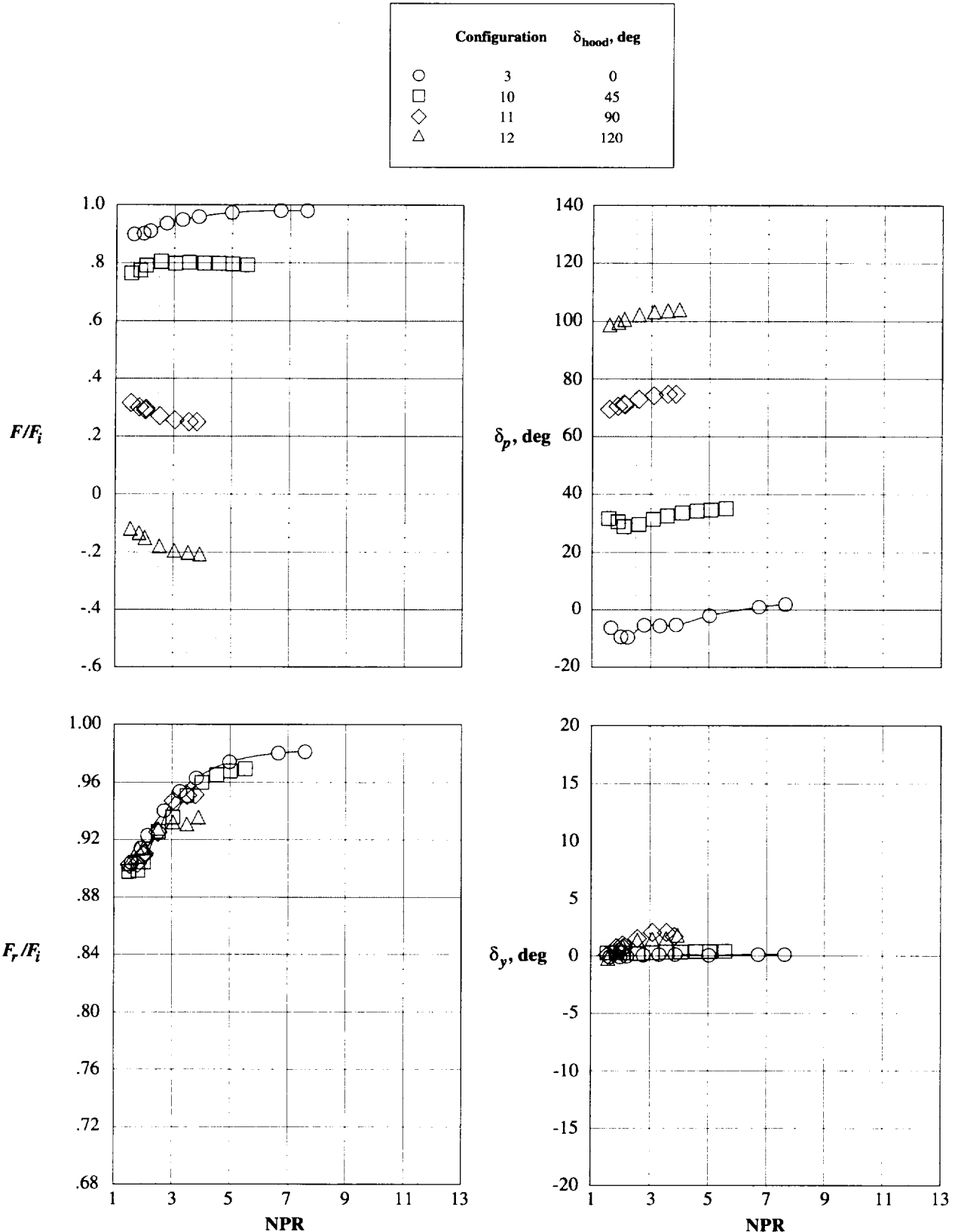
(a) Modified dry power.

Figure 17. Effect of aft-hood deflector angle on internal performance characteristics.



(b) Intermediate power.

Figure 17. Continued.

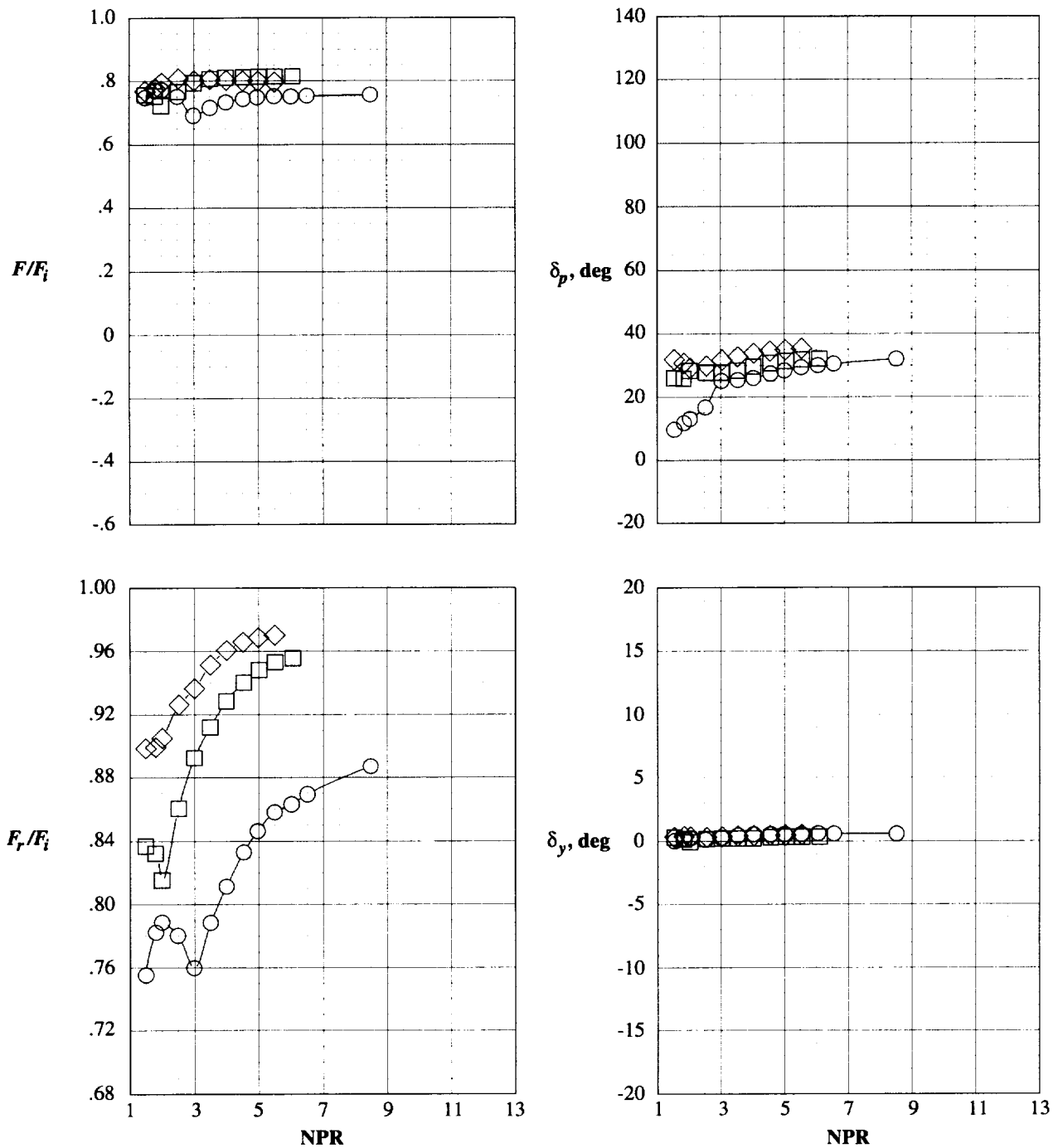


(c) Maximum A/B power.

Figure 17. Concluded.

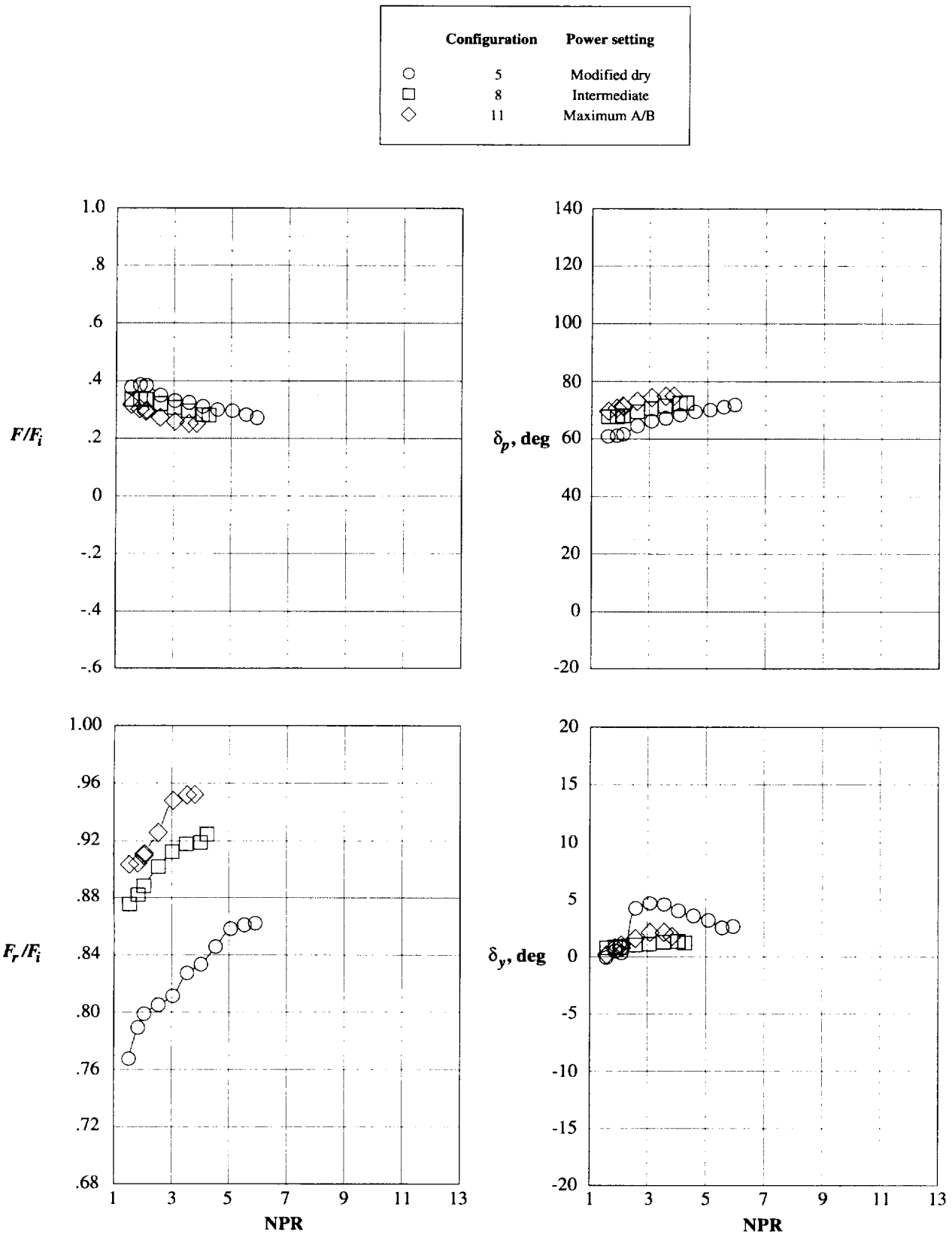
Configuration	Power setting
○	4
□	7
◇	10

Modified dry  
Intermediate  
Maximum A/B



(a)  $\delta_{\text{hood}} = 45^\circ$ .

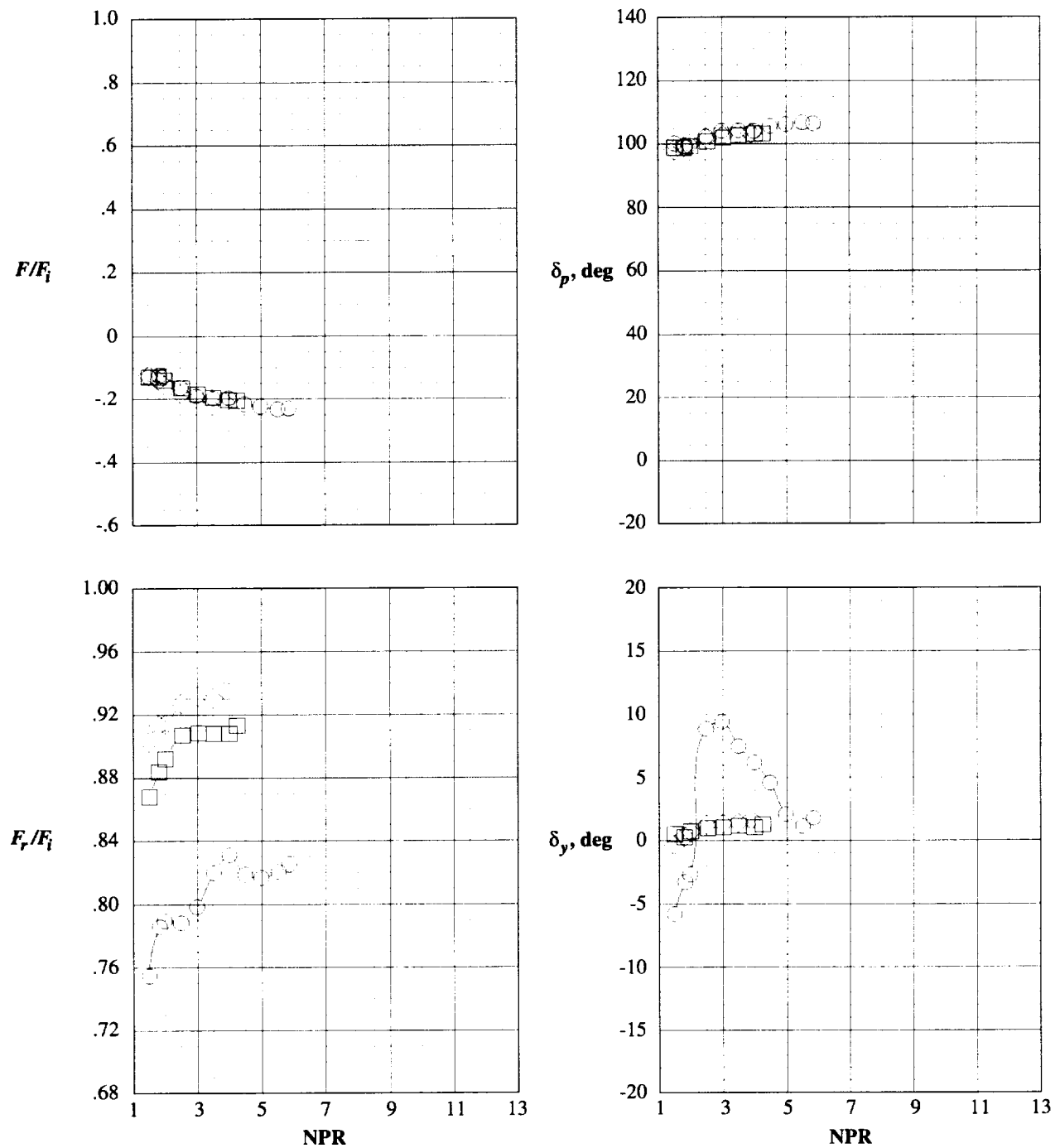
Figure 18. Effect of power setting on internal performance characteristics with aft-hood deflector deployed.



(b)  $\delta_{\text{hood}} = 90^\circ$ .

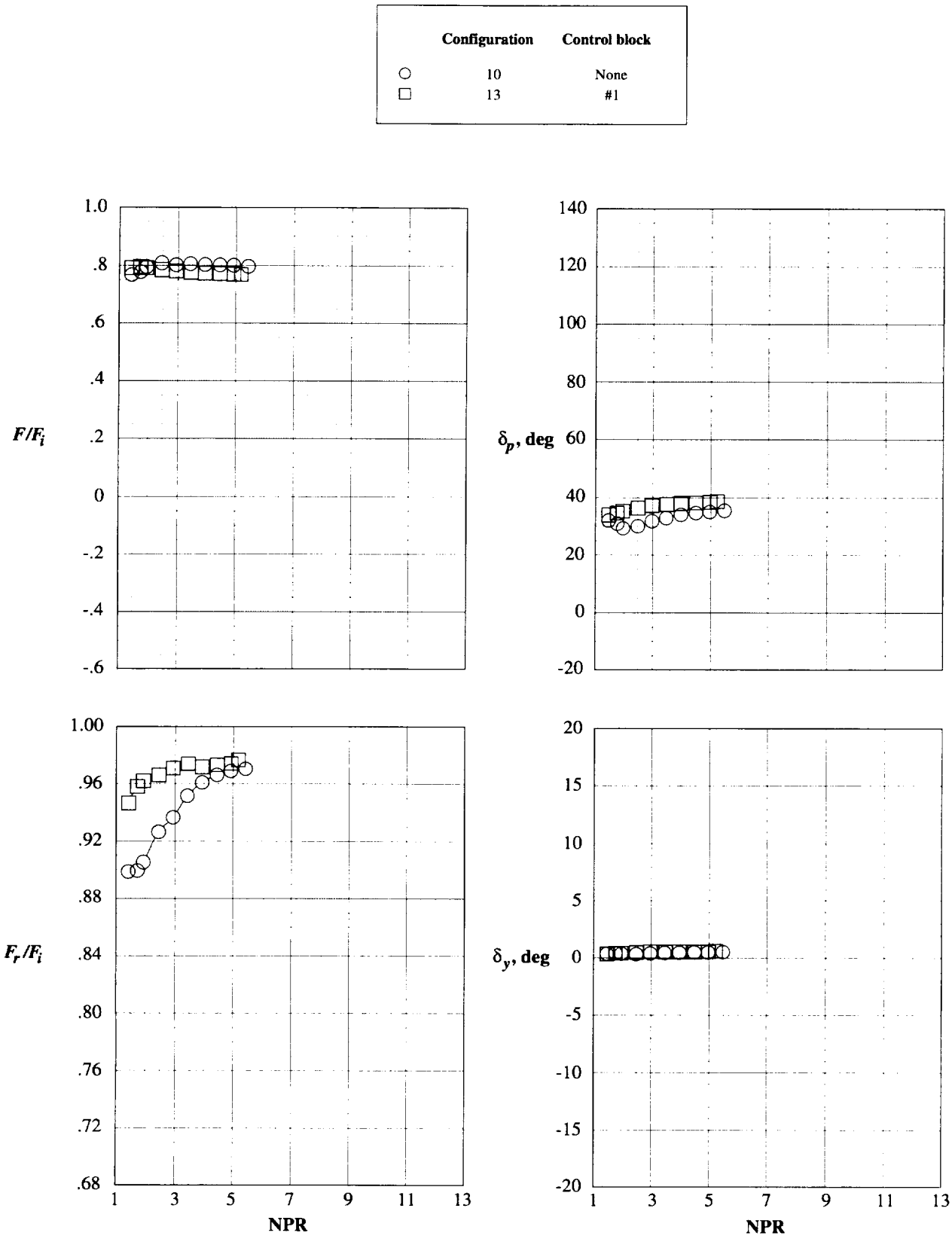
Figure 18. Continued.

Configuration	Power setting
○	6
□	9
◇	12



(c)  $\delta_{\text{hood}} = 120^\circ$ .

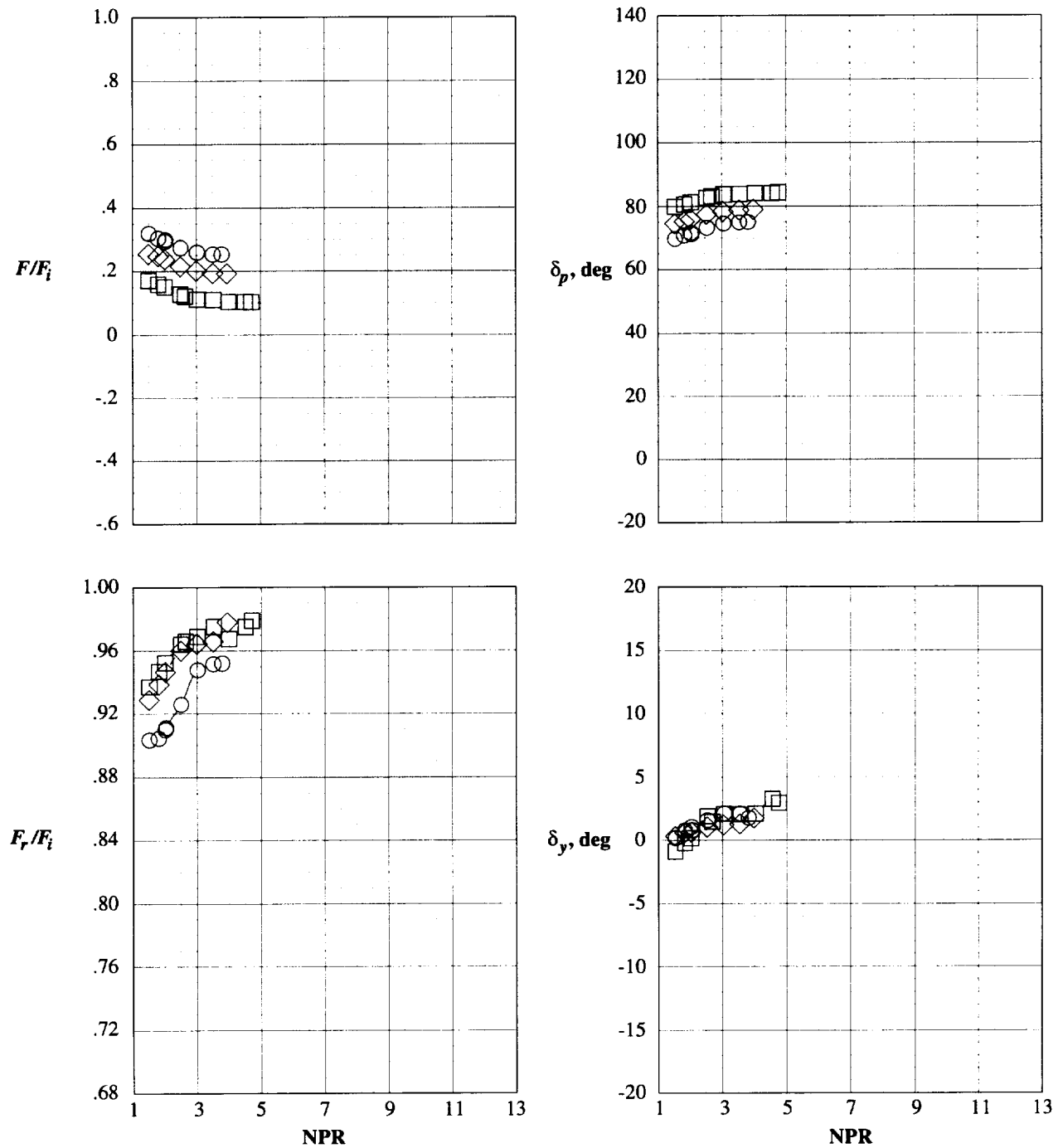
Figure 18. Concluded.



(a)  $\delta_{\text{hood}} = 45^\circ$ .

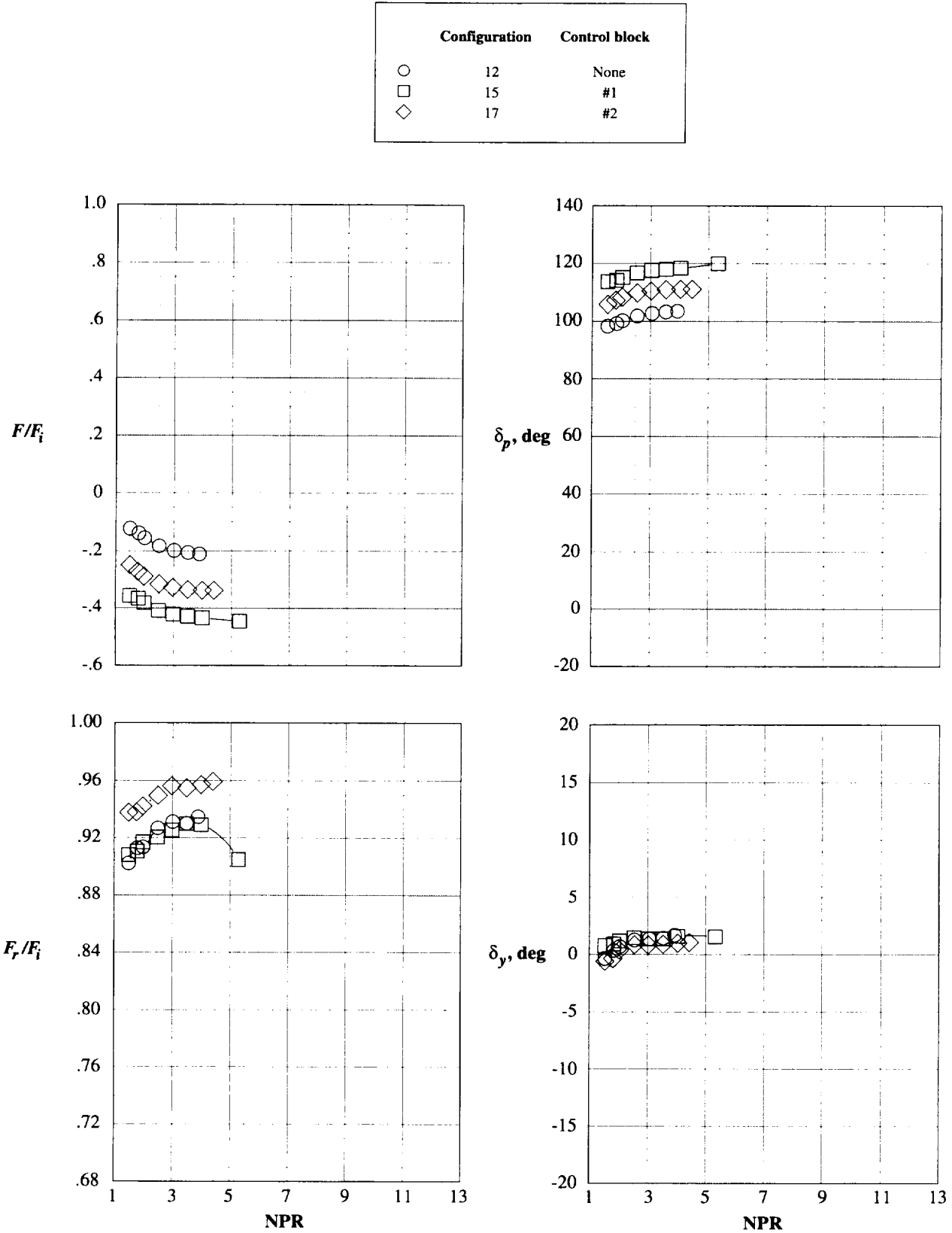
Figure 19. Effect of throat area control block on internal performance characteristics at maximum A/B power with aft-hood deflector deployed.

Configuration	Control block
○ 11	None
□ 14	#1
◇ 16	#2



(b)  $\delta_{\text{hood}} = 90^\circ$ .

Figure 19. Continued.



(c)  $\delta_{\text{hood}} = 120^\circ$ .

Figure 19. Concluded.

Configuration	Throat insert
○	1
□	18
◇	19
	Baseline dry
	10° yaw
	Maximum yaw

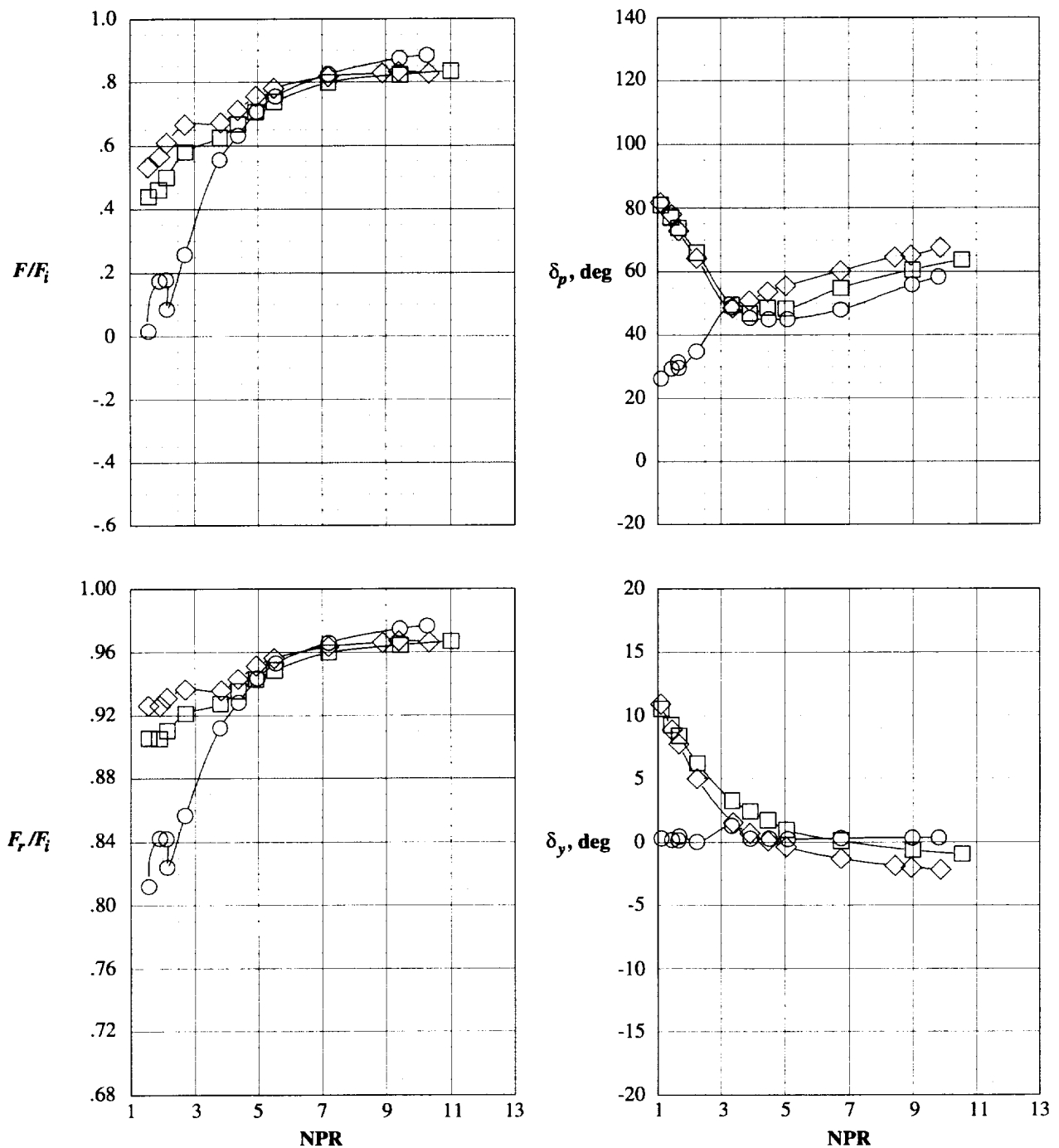


Figure 20. Effect of yaw vectored throat inserts on internal performance characteristics.



REPORT DOCUMENTATION PAGE			Form Approved OMB No. 0704-0188
<p>Public reporting burden for this collection of information is estimated to average 1 hour per response, including the time for reviewing instructions, searching existing data sources, gathering and maintaining the data needed, and completing and reviewing the collection of information. Send comments regarding this burden estimate or any other aspect of this collection of information, including suggestions for reducing this burden, to Washington Headquarters Services, Directorate for Information Operations and Reports, 1215 Jefferson Davis Highway, Suite 1204, Arlington, VA 22202-4302, and to the Office of Management and Budget, Paperwork Reduction Project (0704-0188), Washington, DC 20503.</p>			
1. AGENCY USE ONLY (Leave blank)	2. REPORT DATE	3. REPORT TYPE AND DATES COVERED	
	November 1997	Technical Memorandum	
4. TITLE AND SUBTITLE	Internal Performance of a Fixed-Shroud Nonaxisymmetric Nozzle Equipped with an Aft-Hood Exhaust Deflector		5. FUNDING NUMBERS
6. AUTHOR(S)	Scott C. Asbury		WU 522-25-31-15
7. PERFORMING ORGANIZATION NAME(S) AND ADDRESS(ES)	NASA Langley Research Center Hampton, VA 23681-2199		8. PERFORMING ORGANIZATION REPORT NUMBER
9. SPONSORING/MONITORING AGENCY NAME(S) AND ADDRESS(ES)	National Aeronautics and Space Administration Washington, DC 20546-0001		10. SPONSORING/MONITORING AGENCY REPORT NUMBER
11. SUPPLEMENTARY NOTES			
12a. DISTRIBUTION/AVAILABILITY STATEMENT		12b. DISTRIBUTION CODE	
Unclassified-Unlimited Subject Category 02      Distribution: Standard Availability: NASA CASI (301) 621-0390			
13. ABSTRACT (Maximum 200 words)			
<p>An investigation was conducted in the model preparation area of the Langley 16-Foot Transonic Tunnel to determine the internal performance of a fixed-shroud nonaxisymmetric nozzle equipped with an aft-hood exhaust deflector. Model geometric parameters investigated included nozzle power setting, aft-hood deflector angle, throat area control with the aft-hood deflector deployed, and yaw vector angle. Results indicate that cruise configurations produced peak performance in the range consistent with previous investigations of nonaxisymmetric convergent-divergent nozzles. The aft-hood deflector produced resultant pitch vector angles that were always less than the geometric aft-hood deflector angle when the nozzle throat was positioned upstream of the deflector exit. Significant losses in resultant thrust ratio occurred when the aft-hood deflector was deployed with an upstream throat location. At each aft-hood deflector angle, repositioning the throat to the deflector exit improved pitch vectoring performance and, in some cases, substantially improved resultant thrust ratio performance. Transferring the throat to the deflector exit allowed the flow to be turned upstream of the throat at subsonic Mach numbers, thereby eliminating losses associated with turning supersonic flow. Internal throat panel deflections were largely unsuccessful in generating yaw vectoring.</p>			
14. SUBJECT TERMS		15. NUMBER OF PAGES	
Exhaust Nozzles, Multiaxis Thrust Vectoring, Nonaxisymmetric Nozzles, Nozzles, STOVL		75	
17. SECURITY CLASSIFICATION OF REPORT		16. PRICE CODE	
Unclassified		A04	
18. SECURITY CLASSIFICATION OF THIS PAGE	19. SECURITY CLASSIFICATION OF ABSTRACT	20. LIMITATION OF ABSTRACT	
Unclassified	Unclassified		

NSN 7540-01-280-5500

Standard Form 298 (Rev. 2-89)  
Prescribed by ANSI Std. Z39-18  
298-102